Mechanisms and Treatment of *SCN8A* Epileptic Encephalopathy

ERIC RYAN WENGERT

B.S. Bucknell University, 2016

A Dissertation presented to the Graduate Faculty of the University of Virginia

in Candidacy for the Degree of Doctor of Philosophy

Neuroscience Graduate Program

University of Virginia

March 23, 2021

Manoj K. Patel, PhD (Dissertation Advisor) _____

Jaideep Kapur MD, PhD (Executive Committee Member) _____

Howard P. Goodkin MD, PhD _____

Mark P. Beenhakker, PhD _____

Ali D. Güler, PhD _____

Table of Contents

Summary

SCN8A epileptic encephalopathy is a devastating genetic epilepsy syndrome caused by mutations in the *SCN8A* gene which encodes the voltage-gated sodium channel isoform $Na_V1.6$. Patients experience refractory seizures, cognitive impairments, motor dysfunction, and have a substantial risk for sudden unexpected death in epilepsy (SUDEP). Gaining a mechanistic understanding of *SCN8A* encephalopathy promises to provide insight not only into basic mechanisms of epilepsy and voltage-gated sodium channel function, but also into treatment strategies for patients. On principle, a mechanistic description of *SCN8A* encephalopathy will require a quantitative characterization of 1) How mutations in *SCN8A* alter ion channel function, 2) How neuronal intrinsic excitability is changed in various neuronal populations 3) How these neurons function dynamically in circuits to produce aberrant network hypersynchrony and 4) How behavioral seizures are generated. In this dissertation thesis, I have experimentally addressed a few of these outstanding questions and by clarifying the mechanisms of *SCN8A* encephalopathy, I have indicated potential novel avenues for therapies.

Using patient-derived *SCN8A* mutations expressed in cell-culture, I have experimentally investigated how *SCN8A* mutations alter $Na_V1.6$ channel function. Additionally, I provide evidence that physiologically loss-of-function mutations in *SCN8A*, when inherited biallelically, are able to cause developmental and epileptic encephalopathy. Utilizing mouse models of *SCN8A* encephalopathy, I demonstrate aberrant neuronal excitability in various regions of the hippocampus which can be rescued by treatment of Prax330, a novel sodium channel inhibitor which is currently under investigation for treating *SCN8A* encephalopathy. To uncover a deeper understanding of seizures and SUDEP in *SCN8A* encephalopathy, we serendipitously found that mice with *SCN8A* mutations are sensitive to reflex seizures in response to high-intensity acoustic stimulation and that they have a developmentally-determined risk of seizure-induced sudden death. Using this novel model of seizures and SUDEP, our results indicate that sudden death occurs primarily due to seizure-induced respiratory arrest which can be rescued either by mechanical ventilation or activation of alpha-1 adrenergic receptor activity. Our results contribute a novel and superiorly efficient means for interrogating the mechanisms of seizure and SUDEP in mouse models of *SCN8A* encephalopathy and highlight important potential strategies for preventing SUDEP. Lastly, I characterized the contribution of specific neuronal populations to *SCN8A* encephalopathy and found important roles for both forebrain excitatory neurons as well as somatostatin-positive inhibitory interneurons underlying the mechanism of disease. As a whole, these results provide numerous important contributions to gaining a mechanistic understanding of *SCN8A* epileptic encephalopathy which is critical to developing better treatment approaches.

Publications

Jacy Wagnon, Niccolo Mancacci, Bryan Barker, **Eric Wengert**, Manoj Patel, and Miriam Meisler (2018). Partial loss-of-function of sodium channel SCN8A in familial isolated myoclonus. *Human Mutation*. 2018 May 18.

Erin Baker, Christopher Thompson, Nicole Hawkins, Jacy Wagnon, **Eric Wengert**, Manoj Patel, Alfred George, Miriam Meisler, Jennifer Kearney (2018). The novel sodium channel modulator GS458967 (GS967) is an effective treatment in a mouse model of SCN8A encephalopathy. *Epilepsia*. 2018 May 21.

Rosie Bunton-Stasyshyn*, Jacy Wagnon*, **Eric Wengert**, Bryan Barker, Alexa Faulkner, Pravin Wagley, Kritika Bhatia, Julie Jones, Marissa Maniaci, Jack Parent, Howard Goodkin, Manoj Patel, and Miriam Meisler (2019). Prominent role of forebrain excitatory neurons in SCN8A encephalopathy. *Brain*. 2019 January 2.

Eric Wengert, Anusha Saga, Payal Panchal, Bryan Barker, Ronald Gaykema, and Manoj Patel (2019). Prax330 reduces persistent and resurgent sodium channel currents and neuronal excitability in a mouse model of SCN8A encephalopathy. *Neuropharmacology*. 2019 July 3.

Eric Wengert*, Cathrine Tronhjem*, Jacy Wagnon, Katrine Johannesen, Hayley Petit, Ilona Krey, Anusha Saga, Payal Panchal, Samantha Strohm, Jorn Lange, Sussanne Kamphausen, Guido Robboli, Johannes Lemke, Elena Gardella, Manoj Patel, Miriam Meisler, and Rikke Moller (2019). Biallelic inherited *SCN8A* variants, a rare cause of developmental and epileptic encephalopathy. *Epilepsia*. 2019 October 18.

Eric Wengert and Manoj Patel (2020). The persistent sodium current and its role in epilepsy. *Epilepsy Currents*. 2020 November 25.

Ian Wenker, Frida Teran, **Eric Wengert**, Pravin Wagley, Payal Panchal, Elizabeth Blizzard, Priyanka Saraf, Jacy Wagnon, Howard Goodkin, Miriam Meisler, George Richerson, and Manoj Patel (2021). *Annals of Neurology*. 2021 February 18.

Eric Wengert. Mentor as you'd want to be mentored. *Science*. 2021 February 19

Eric Wengert*, Ian Wenker*, Elizabeth Wagner, Pravin Wagley, Ronald Gaykema, Jung-Bum Shin, and Manoj Patel (2021). Adrenergic mechanisms of seizure-induced sudden death in a mouse model of *SCN8A* encephalopathy. *Frontiers in Neuroscience*. 2021 March 4.

Eric Wengert and Manoj Patel (2021). One size doesn't fit all: Variant-specific effects in *SCN8A* epilepsy. *Epilepsy Currents*. *In Press.*

Eric Wengert, Kyle Wedgwood, Samantha Strohm, Payal Panchal, Abrar Majidi Idrissi, Ian Wenker, Pravin Wagley, Ronald Gaykema, and Manoj Patel. Somatostatin-positive interneurons contribute to seizures in a mouse model of SCN8A encephalopathy. *PNAS*. Submitted 2021 February 20

Eric Wengert, Pravin Wagley, Samantha Strohm, Nuha Reza, Ian Wenker, Ronald Gaykema, and Manoj Patel. Targeted Augmentation of Nuclear Gene Output Rescues Parvalbumin Interneuron Excitability and Reduces Seizures in a Mouse Model of Dravet Syndrome. *In Preparation.*

Jeremy Thompson, **Eric Wengert**, Pravin Wagley, Ian Wenker, and Manoj Patel (2021). Impaired potassium channel activity and glutamate synthetase expression in a mouse model of SCN8A encephalopathy. *In Preparation.*

Patents

Alpha-1 adrenergic receptor agonists to prevent seizure-induced sudden death. U.S. Provisional Pat. Ser. No. 63/136,439, filed 2021 January 12.

Fellowships/Academic Awards

NIH Ruth L. Kirschstein National Research Service Award Predoctoral Fellowship	*June 2019-May 2021*
Double-Hoo Research Award	*May 2019-April 2020*
Z Society Graduate Student Dinner (honoree)	*March 2019*
University of Virginia Robert R. Wagner Fellowship	*June 2018-May 2019*
Third-prize Outstanding Faculty Research Presentation Department of Anesthesiology Annual Celebration of Research	*May 2018*

Acknowledgements

Completing my PhD is likely the most challenging and rewarding task that I have ever completed. I have immense gratitude for everyone who has played a role in my journey. I am grateful to all involved with the Neuroscience Graduate Program at the University of Virginia for welcoming me, challenging me, and for helping me grow. I've had productive and rewarding conversations with many of you, and I am extremely proud of this program and this school.

I owe much to all of the members of the Patel lab who have influenced me on my PhD path. In particular, I would like to highlight my student mentees: Anusha Saga, Payal Panchal, Samantha Strohm, Abrar Idrissi-Majidi, and Nuha Reza. Thank you for your patience and for teaching me how to be a better mentor. Thanks also for the many times in which you helped me take myself less seriously. Additionally, I'd like to thank my lab colleagues: Ian Wenker, Bryan Barker, Jeremy Thompson, Matteo Ottolini, Pravin Wagley, Raquel Miralles, and Ronald Gaykema. I have also been aided by many collaborators across the globe including Miriam Meisler, Jacy Wagnon, Rikke Møller, Kyle Wedgwood, Jung-Bum Shin, and many others. Through conversations or help with experiments, each has made me a better scientist and it was a privilege to be on a team with each of them.

My thesis committee: Dr. Jaideep Kapur, Dr. Howard Goodkin, Dr. Mark Beenhakker, and Dr. Ali Güler have been entirely supportive, yet constructively critical of me and my scientific work. They pushed me out of my comfort zone, and my creativity and self-confidence are better because of their input. I feel honored to have been mentored by such excellent scientists.

I would like to acknowledge the patients with *SCN8A* epileptic encephalopathy and their families. They have been not only an important source of inspiration and grounding, but have further contributed creatively to my science through sharing their stories and perspectives. I am thankful to have met many of them and I hope that my work in this thesis pushes us closer toward understanding and developing better treatments for this devastating syndrome.

More than anyone else, I must thank Manoj Patel for my mentorship, instruction, funding, and for a fun environment in which to become a scientist. Without his efforts and consistent support, achievement of this milestone would not have been possible. Manoj is one of the most loyal and caring individuals I have ever met, and I plan to take many aspects of his mentorship style with me in the future.

Outside of my vocational sphere, I would like to thank my caring neighbors and the members of my church: All Souls Charlottesville. By helping to keep me grounded on the most important things- faith, family, and community, you have energized my vocational life as merely one aspect of living a good life.

I would like to thank my whole family. They have continuously, yet without external pressure, supported my lifelong quest for knowledge through education, and for that, I'm thankful. Lastly, I must thank Ellie Wengert who, more than anyone else, has seen the joys and hardships of my process of attaining a PhD. She has endured countless hours of my incessant external processing, and her gentleness and patience toward me is unwavering. Without her, my efforts in the lab would not only have been impossible, more importantly, they would not have been worthwhile.

List of Abbreviations

$Na_V1.6$—Voltage-gated sodium channel isoform encoded by the *SCN8A* gene

SUDEP- Sudden Unexpected Death in Epilepsy

I_{NaP} – Persistent sodium current

I_{NaR} – Resurgent sodium current

I_{NaT}—Transient sodium current

DEE—Developmental and Epileptic Encephalopathy

$V_{1/2}$ – Half-maximal voltage

LOF – Loss-of-function

GOF – Gain-of-function

TTX—Tetrodotoxin

EEG—Electroencephalogram

ECoG—Electrocorticogram

ID—Intellectual Disability

LEV—Levetiracetam

MRI—Magnetic Resonance Imaging

VGB—Vigabatrin

VPA—Valproic acid

TPM—Topiramate

VGSC—Voltage-gated sodium channel

ACSF—Artificial cerebrospinal fluid

ASM—Anti-seizure medication

GqDREADD – hM3Dq Designer Receptor Exclusively Activated by Designer Drug

SST— Somatostatin-positive

Chapter I. Introduction

SCN8A encephalopathy is a severe genetic epilepsy syndrome caused mutations in the *SCN8A* gene which encodes the voltage-gated sodium channel isoform $Na_V1.6$ (Estacion et al., 2014; de Kovel et al., 2014; Larsen et al., 2015; Ohba et al., 2014; Veeramah et al., 2012). Patients exhibit a devastating panoply of symptoms including refractory seizures, cognitive impairments, motor and sensory dysfunction, and importantly, a significant risk for sudden unexpected death in epilepsy (SUDEP) (de Kovel et al., 2014; Larsen et al., 2015; Ohba et al., 2014; Veeramah et al., 2012). As an epilepsy syndrome first recognized in 2012 (Veeramah et al., 2012), the basic mechanisms of *SCN8A* encephalopathy remain largely unknown. Gaining a detailed insight into the precise biophysical and neuronal mechanisms of $Na_V1.6$ dysfunction is required to more thoroughly appreciate how *SCN8A* mutations lead to epileptic encephalopathy and promises to generate novel therapeutic approaches to improve the lives of *SCN8A* encephalopathy patients.

Voltage-gated sodium channels

Voltage-gated sodium channels are highly expressed in neurons to enable action potentials, the fast and reliable intercellular signaling events that are central to the function of the nervous system (Bean, 2007). Structurally, voltage-gated sodium channels are composed of an alpha subunit (~260 kDa) and one or two associated beta subunits (~30-40 kDa) (Beneski and Catterall, 1980; Goldin et al., 1986; Isom et al., 1992). Alpha subunits each contain four homologous domains (DI-DIV) with six transmembrane segments (S1-S6) and are sufficient for ionic current flow (Goldin et al., 1986). Functionally, the S1-S4 transmembrane segments form the voltage-sensing module while the S5 and S6 segments form the pore region through which the sodium ions associate and pass through (Yarov-Yarovoy et al., 2012). Ongoing efforts in structural approaches will yield additional detailed insight into the structure-function relationship of voltage-gated sodium channels.

There are ten distinct isoforms of voltage-gated sodium channels that differ in their expression and function throughout the body. Of these ten genes, only *SCN1A*, *SCN2A*, *SCN3A*, and *SCN8A* are expressed in the central nervous system while other isoforms are expressed in other tissues that contain excitable cells (i.e. cardiomyocytes and skeletal muscle cells) (Goldin, 1999). This molecular diversity in addition to cell-type and subcellular specific expression allows for functional diversity and regulation of voltage-gated sodium channel activity. It is a major aim of current experimental efforts to precisely characterize how voltage-gated sodium channel activity determines the complex repertoire of neuronal physiology.

Functionally, voltage-gated sodium channels drive the initiation and propagation of action potentials through brief instances (~2 ms) of opening and closing (Bean, 2007). The longstanding basic paradigm of voltage-gated sodium channel function inherited from the Hodgkin-Huxley experiments describes that voltage-gated sodium channels operate by progressing through three unique conformational states—closed, open, and inactivated, by the opening and closing of two independently-functioning hypothetical gates—a voltage-sensitive activation gate and inactivation gate (Hodgkin and Huxley, 1952). Although this paradigm has proven to be scientifically fruitful, functional studies have revealed that overall voltage-gated sodium channel behavior is more complex than that predicted by Hodgkin and Huxley (Kuo and Bean, 1994; Raman and Bean, 1997; Raman et al., 1997). Indeed, voltage-gated sodium channels exhibit non-inactivating steady-state persistent and resurgent sodium currents, currents which provide additional depolarization over longer timescales than that of traditional macroscopic currents (Raman and Bean, 1997; Stafstrom et al., 1982; Wengert and Patel, 2021). Further, sodium currents also reveal slow inactivation, on the timescale of seconds, suggesting that inactivation as well as activation is dynamic with slow kinetics (Hampl et al., 2016). Additionally, a recent study, demonstrated that voltage-gated sodium channels form dimers and couple their kinetic behavior (Clatot et al., 2017). Therefore, despite substantial experimental effort to characterize voltage-gated sodium channel function, many unanswered questions regarding their general behavior remain to be addressed.

SCN8A Function

SCN8A, which encodes $Na_V1.6$, is the among the most highly expressed voltage-gated sodium channel isoform in the central nervous system (Schaller et al., 1995). $Na_V1.6$ expression is observed in both excitatory neurons and inhibitory neurons throughout many anatomical regions (Lorincz and Nusser, 2008; Makinson et al., 2017). Subcellularly, $Na_V1.6$ is localized to the axon initial segment and nodes of Ranvier, where it critically regulates initiation and propagation of action potentials (Caldwell et al., 2000; Royeck et al., 2008). Of functional significance, $Na_V1.6$ channels have been shown to be particularly

important for generating the steady-state persistent sodium current, a contributor of neuronal pacemaking in neurons of various brain regions contributing to an array of relevant behaviors (Khaliq and Bean, 2010; Yamada-Hanff and Bean, 2013).

Mechanisms of SCN8A Encephalopathy

Although epilepsy-causing *SCN8A* mutations had been hypothesized for years (Catterall, 2000, 2012), the first *SCN8A* epileptic encephalopathy patient was first reported in 2012 (Veeramah et al., 2012). The initial patient had the single point mutation Asn1768.Asp (N1768D) which resulted in substantially greater non-inactivating persistent sodium currents relative to normal $Na_V1.6$ (Veeramah et al., 2012). Numerous additional mutations have now been identified, and while some have been investigated, biophysical characterization of patient variants remains an active area of research (Barker et al., 2016; Gardella et al., 2018; Wagnon et al., 2016, 2018; Wengert et al., 2019a, 2019b). Of functional studies completed to date, patient-derived *SCN8A* mutations typically show elevated persistent sodium currents, hypersensitive voltage-dependent activation, right-shifted voltage-dependent steady-state inactivation, or impaired decay of macroscopic currents (Liu et al., 2019; Pan and Cummins, 2020; Veeramah et al., 2012; Wagnon et al., 2016; Wengert et al., 2019b; Zaman et al., 2019). Characterization of mutant channel biophysics promises to provide insight into the molecular mechanism of dysfunction in *SCN8A* encephalopathy patients.

Presumably, dysfunction in voltage-gated sodium channels disrupts proper neuronal excitability to impair circuit function which ultimately leads to epileptic network activity. In order to experimentally interrogate how *SCN8A* mutations affect neuronal function, transgenic mouse models of *SCN8A* encephalopathy have been generated by introducing single patient-derived point mutations into the mouse genome. The *Scn8a*$^{D/+}$ mouse model (which has a single allele of the N1768D point mutation expressed globally) and the *Scn8a*-conditional$^{W/+}$ mouse model (in which the mutant allele R1872W is expressed in a manner specified by Cre recombinase) are both powerful tools studying how mutations change neuronal excitability (Bunton-Stasyshyn et al., 2019; Wagnon et al., 2015). Previous studies have identified excitatory neurons in hippocampal CA1, subiculum, entorhinal cortex, and somatosensory cortex to be abnormally hyperexcitable in these mouse models of *SCN8A* encephalopathy (Baker et al., 2018; Bunton-Stasyshyn et al., 2019; Lopez-Santiago et al., 2017; Ottolini et al., 2017; Wengert et al., 2019b). Supporting prior biophysical characterization of the N1768D mutation, these studies also found elevated resurgent and/or persistent sodium currents in *Scn8a*$^{D/+}$ neurons (Lopez-Santiago et al., 2017; Ottolini et al., 2017; Wengert et al., 2019b) Relating biophysical properties of ion channel to cellular excitability remains a major effort in experimental investigation of *SCN8A* encephalopathy.

In theory, full appreciation of the mechanisms underlying *SCN8A* encephalopathy will require a complete description of how any single *SCN8A* variant results in clinically observed behaviors, most notably, seizures. This description will involve the identification of patient-derived *SCN8A* variants and characterization of their respective biophysical properties. Further, how an *SCN8A* variant influences intrinsic neuronal excitability, the generation and propagation of action potentials as the primary output of neuronal activity, relative to any input stimulus must be clarified. Because neurons function in groups which comprise dynamic circuits throughout the brain, a mechanistic understanding of *SCN8A* encephalopathy necessitates understanding how *SCN8A* mutations distinctly influence various subpopulations and alter network-level activity. Lastly, how aberrant brain network excitability results in seizure behavior and occasionally leads to seizure-induced death must be understood. This operating framework from gene to whole-animal behavior summarizes the paradigm from which I seek to understand *SCN8A* encephalopathy mechanistically, and importantly, sets some criteria by which to judge the success of any experimental investigation (Figure 1.1). A truly complete mechanistic understanding of *SCN8A* encephalopathy will be reached only when the observed phenomena at each level (ion channel, single neuron, neural circuit, whole animal, etc.) can be explained entirely in terms of the level(s) below it. In pursuit of this ambitious goal, I have provided in this thesis experimental data from each of the levels in the framework to provide additional clarity as to the precise relationship by which seemingly small changes in the *SCN8A* gene ultimately lead to such a devastating syndrome.

In Chapter II, I describe an entirely novel biophysical mechanism of *SCN8A* encephalopathy via biallelic inherited loss-of-function *SCN8A* mutations. In Chapters III and IV, I then present results concerning efforts to help treat patients with *SCN8A* encephalopathy: First, in Chapter III, I show work elucidating the biophysical and neuronal mechanisms by which Prax330, a novel sodium channel inhibitor, normalizes neuronal excitability and treats seizures in mice harboring *SCN8A* mutations.

Second in Chapter IV, I interrogate the mechanisms of SUDEP in mice with *SCN8A* mutations. I demonstrate that mice die from audiogenic seizure-induced respiratory arrest and that alpha-1 adrenergic receptors are required for breathing recovery, offering a potential pharmacological strategy for SUDEP prevention. In the final two Chapters V and VI, I seek to clarify neuronal mechanisms of *SCN8A* encephalopathy using transgenic mouse model enabling cell-type specific expression of mutant *SCN8A*. In Chapter V, I provide evidence for an important role of forebrain excitatory neurons in driving spontaneous seizures and death. Despite the fact that expression of mutant *SCN8A* in certain populations of inhibitory interneurons did not result in spontaneous seizures, in Chapter VI, I provide evidence for a contribution of somatostatin-positive interneurons to *SCN8A* encephalopathy: Abnormal excitability and depolarization block of somatostatin-positive inhibitory interneurons due mutant *SCN8A* expression was sufficient for seizures. This surprising data regarding the important role for somatostatin interneurons in *SCN8A* encephalopathy present this neuronal population as a potential target for therapeutic intervention.

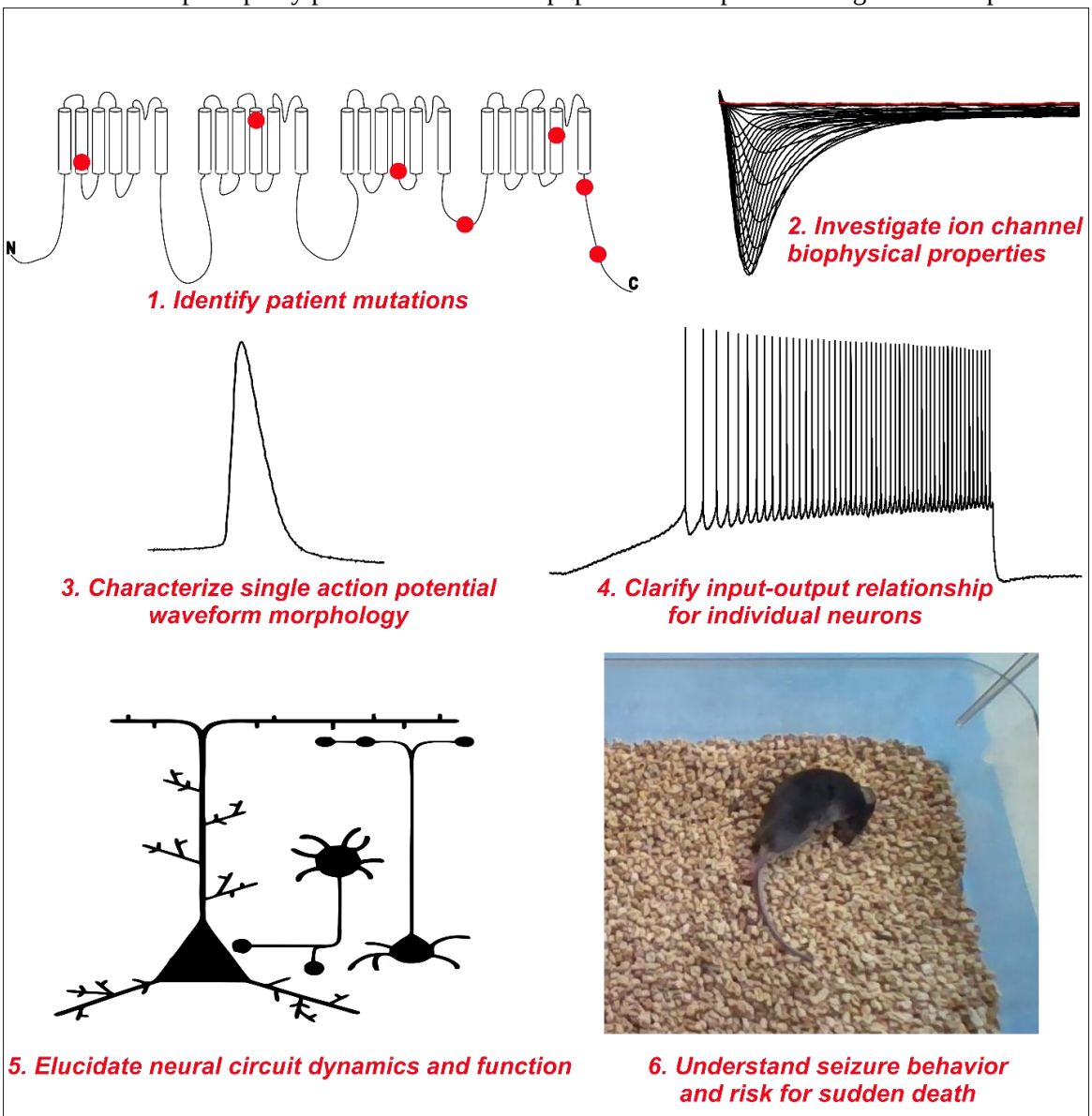

Figure 1.1: Operating framework for uncovering mechanisms *SCN8A* encephalopathy
1. Patient-derived variants (red circles) are identified in the *SCN8A* gene. 2. Voltage-clamp electrophysiology recordings of voltage-gated sodium channel currents reveal biophysical properties. 3. Current-clamp electrophysiology recordings reveal how *SCN8A* variants influence the waveform of single action potentials. 4. Simple input-output computations performed by individual neurons are clarified by electrophysiology experiments. 5. Elucidate how groups of neurons working in together in circuits orchestrate network dynamics and overall brain function.6. At the level of the whole organism (whether transgenic mice models of disease or an epileptic patient), a seizure manifests with defined behavior driven by excessive and hypersynchronous brain activity. Seizures occasionally impair vital body functions and result in sudden unexpected death in epilepsy (SUDEP). Mechanistic understanding of SCN8A encephalopathy will be achieved when each level is fully explained in terms of the level below it.

Chapter II: Biallelic inherited *SCN8A* variants, a rare cause of developmental and epileptic encephalopathy

Rationale

The phenotypic spectrum of *SCN8A* encephalopathy now includes several hundred individuals with various types of epilepsy including benign familial infantile seizures with or without paroxysmal dyskinesia, less severe epilepsies with or without comorbid intellectual disability (ID), and severe early onset developmental and epileptic encephalopathy (Anand et al., 2016; Butler et al., 2017; Gardella et al., 2016, 2018; Han et al., 2017; Johannesen et al., 2019; Larsen et al., 2015; Ohba et al., 2014; Pan and Cummins, 2020; Veeramah et al., 2012; Zaman et al., 2019). Functional studies have demonstrated that *SCN8A*-related epilepsies are typically monoallelic mutations that are physiologically gain-of-function (Pan and Cummins, 2020; Veeramah et al., 2012; Wagnon et al., 2016; Zaman et al., 2019). In this chapter, my colleagues and I report the first two human families in which two *SCN8A* mutant alleles were biallelically inherited to cause epileptic encephalopathy and severe ID in the offspring. Functional analysis demonstrated a shared mechanism of inheritance of one complete loss-of-function allele and one allele with partial loss-of-function by affected individuals in both families. Thus, these surprising results indicate an entirely novel biophysical mechanism of disease characterized by the biallelic inheritance of loss-of-function *SCN8A* variants.

Introduction

SCN8A, encoding the voltage-gated sodium channel $Na_V1.6$, was initially implicated in developmental and epileptic encephalopathy (DEE) in 2012 (Veeramah et al., 2012). Severe *SCN8A* DEE (Mendelian Inheritance in Man EIEE13) is characterized by intractable seizures with an average age at seizure onset of 4 months, cognitive deterioration, pyramidal/extrapyramidal signs, progressive cerebral atrophy, and visual impairment leading to cortical blindness (Anand et al., 2016; Butler et al., 2017; Gardella et al., 2016, 2018; Han et al., 2017; Johannesen et al., 2019; Larsen et al., 2015; Ohba et al., 2014; Pan and Cummins, 2020; Veeramah et al., 2012; Zaman et al., 2019). There are often prolonged focal seizures with prominent hypomotor and vegetative symptoms that may evolve to clonic or bilateral tonic-clonic manifestations. Epileptic myoclonus, spasm-like episodes, and recurrent convulsive status epilepticus are frequently observed. All affected individuals described to date are monoallelic (heterozygous) carriers of a gain-of-function (GOF) or loss-of-function (LOF) variant in combination with a wild-type (WT) allele.

Functional studies have demonstrated that *SCN8A*-related epilepsies are typically caused by monoallelic GOF alterations leading to neuronal hyperexcitability (Pan and Cummins, 2020; Veeramah et al., 2012; Wagnon et al., 2016; Zaman et al., 2019). A small number of heterozygous LOF variants have been found in patients with ID, autism spectrum disorder (ASD), or movement disorders who do not necessarily have epilepsy (Trudeau et al., 2006; Wagnon et al., 2017a, 2018). The less severe familial *SCN8A*-related disorders show an autosomal dominant pattern of inheritance, whereas the large majority of EIEE13 cases occur *de novo*. A similar pattern has been reported for *SCN2A*, in which GOF variants cause early onset seizures, and LOF variants tend to be associated with later onset seizures or with ID or ASD without epilepsy (Wolff et al., 2017).

In the mouse, homozygosity for partial LOF alleles of *Scn8a* results in movement disorders including ataxia, tremor, and dystonia, whereas complete LOF results in juvenile lethality with loss of ambulation (O'Brien and Meisler, 2013). In the present chapter, I and my collaborators describe the first two human families with biallelic inherited variants in *SCN8A*. The index patients are born of heterozygous parents who exhibit mild cognitive deficits, whereas the probands suffer from DEE and severe ID. Functional analysis demonstrated a shared mechanism of inheritance of one complete LOF and one partial LOF allele by affected individuals in both families

Methods

DNA Sequencing

Both families underwent targeted gene panel sequencing as part of their formal diagnostic workup at either the Institute of Human Genetics, University of Leipzig Hospital and Clinics (Family 1) or the Danish Epilepsy Centre (Family 2). The parents or legal guardians of all probands provided written informed consent, and the study was approved by the local ethics committees. In Family 1, targeted sequencing of a custom panel of 131 genes associated with epilepsy (TruSight Rapid

Capture Kit) was performed. Genomic DNA was extracted from blood using standard methods, and the library was sequenced on a MiSeq v2 300 sequencer (Illumina). In Family 2, targeted sequencing of 78 epilepsy genes was performed. Genomic DNA was extracted from blood using standard methods, and SureSelect library building was followed by sequencing on the Ion PGM system (Ion PGM 200 Sequencing Kit), as previously described (Møller et al., 2017).

Family ID	Family 1 Patient A	Family 1 Patient B	Family 2
Sex	M	F	M
Current age	4 years	2 years	27 years
Family history	Both parents: mild cognitive deficits. Two maternal uncles one maternal aunt have ID and/or epilepsy. One maternal half-brother has speech delay		Both parents have mild cognitive deficits.
Development	Severe ID	Severe ID	Profound ID
Age at szr onset	3 months	few hours after birth	7 months
Szr type at onset	focal seizure	convulsive status epilepticus	Tonic seizure + eye-roll
Szr types	Clonic, focal, or brief tonic seizures	Brief tonic, automotor seizures	Infantile febrile seizures tonic seizures, absences
EEG features	12 -mo: hypsarrhythmia 3 y: moderate background slowing: mild nonspecific EEG abnormalities	8 d: medium-weight generalized discharges; 4 m: hypsarrhythmia; 17 mo: moderate background slowing; mild nonspecific EEG abnormalities	7 y: ictal regular generalized 3-4 Hz paroxysmsof 5-10 s; 26 y: 3-4 Hzspike-waves bilaterally in posterior quadrants
Movement Disorder	No	No	Dyskinesia
Other neurological features	Hypotonia, strabismus; 19 mo: auditory neuropathy	Hypotonia, 8 mo: strabismus	Hypotonia, spastic tetraplegia
Vision impairment	6 mo: FVEP: binocular response pos: hyperopia	11 mo: hyperopia	Myopia
Additional features	Bilateral hip dysplasia, constipation hemangioma, swallowing difficulties, regurgitation, 28 m: microcephaly (-3.4 SD)	Constipation, swallowing difficulties, apnea, dysphagia; 5 mo: microcephaly (-5 SD); 13 mo PEG tube	Recurrent pneumonia, constipation, phimosis, reflux, asthma, bilateral hip dysplasia, dysphagia, scoliosis, kyphosis
MRI	4 mo and 26 mo: pineal cyst. Otherwise normal	4 mo: delayed myelination	8 y: cerebral atrophy
Allele 1	c.805G>A p.(Gly269Arg) mat	c.805G>A p.(Gly269Arg) mat	c.2464G>A p.(Gly822Arg) pat
Allele 2	c.4079C>A p.(Thr1360Asn) pat	c.4079C>A p.(Thr1360Asn) pat	c.4912C>T p.(Arg1638Cys) mat

Abbreviations: EEG, electroencephalogram; F, female: ID, intellectual disability: M, male: mat, maternal: MRI, magnetic resonance imaging: pat, paternal: PEG, percutaneous endoscopic gastrostomy: pos, positive: FVEP, flash visually-evoked potential

Table 2.1: Clinical features of affected individuals with inherited biallelic *SCN8A* variants

Variants with a mutant allele frequency < 1% in the general population (gnomAD, Broad Institute) were classified according to the ACMG guidelines (Richards et al., 2015). In silico evaluation was performed using SIFT Blink (J. Craig Venter Institute), Polyphen2 (Harvard), Combined Annotation-Dependent Depletion (CADD; University of Washington), MutationTaster (Charité), Model Predictive Control (MPC; Harvard), and the following splicing tools: SpliceSiteFinder-like, MaxEntScan, NNSPLICE, and Human Splicing Finder. In addition, database synchronization by ClinVar (National Center for Biotechnology Information) and Human Gene Mutation Database (Biobase) was performed. Sanger sequencing was carried out to confirm all variants and to perform segregation analysis.

Electrophysiology

Missense variants were introduced into the tetrodotoxin (TTX)-resistant mouse cDNA $Na_v1.6R$ by site-directed mutagenesis with QuikChange II XL (Agilent Technologies) and analyzed as previously described (Wagnon et al., 2016). The 6-kb open reading frame of each construct was resequenced to eliminate clones containing extraneous mutations. $Na_v1.6$ variants were expressed by transfection of neuron-derived ND7/23 cells (Sigma-Aldrich). Sodium currents were recorded 48 hours after transfection in the presence of 500 nM TTX to block endogenous sodium currents, using the whole-cell configuration of the patch-clamp recording technique.

Results

Clinical features of affected children and parents from two families segregating biallelic SCN8A variants

The clinical data of the three index patients are summarized in Table 2.1.

Family 1

The index patients were a sibling pair (three-year-old male and two-year-old female) born to unrelated parents (Figure 2.1A). Both parents had mild cognitive impairment/borderline intellectual functioning. They both attended special school, obtained vocational training, and were able to live independent lives. Neuropsychological evaluations were not available. Additional affected family members included a maternal half-brother of the affected sibs and two of the mother's half-brothers and one half-sister, all with mild ID and one with unclassified epilepsy. Unfortunately, none of the maternal relatives were available for genetic testing.

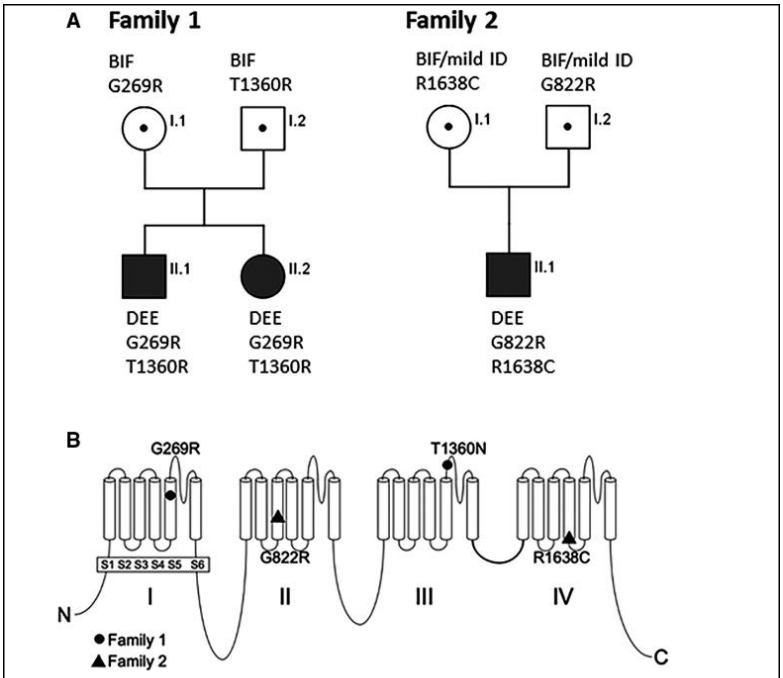

Figure 2.1. Biallelic inheritance of developmental and epilepticencephalopathy (DEE) in two families, and the protein location of the novel variants.

The male sibling was born at term after an uncomplicated preg-nancy and delivery (Apgar 10/10). Postnatally, he needed treatment of hypoglycemia and was tube fed for several days due to feeding difficulties. He presented with global developmental delay and onset of intractable daily focal seizures at 3 months of age. Treatment with levetiracetam (LEV) was initiated, which led to transient seizure reduction. However, during the course of the disease, he developed clonic and daily brief tonic seizures (lasting a few seconds). His initial electroencephalogram (EEG) showed background slowing and multifocal epileptiform discharges, which progressed to hypsarrhythmia. Treatment with sulthiame and prednisolone was tried without any effect. Magnetic resonance imaging (MRI) performed at four months of age was normal, except for a small pineal cyst. At follow-up, he presented with muscular hypotonia, severe ID, and microcephaly (−3.4 SD at 28 months). Additional features included strabismus, hyperopia, and bilateral hip dysplasia (type IIa on the right and type Ib on the left side). At 19 months of age, bilateral coxa valga was observed and confirmed by X-ray. Furthermore, he suffered from constipation and swallowing difficulties with regurgitation and vomiting after chunky food. At 19 months of age, he was diagnosed with an auditory neuropathy with almost complete hearing loss. He could turn to both sides at 30 months of age, but was not able to sit, crawl, stand, walk, or communicate. His epilepsy continued to be intractable, and currently he has one to two brief tonic seizures per week despite treatment with LEV, vigabatrin (VGB), and valproic acid (VPA). EEG at follow-up showed background slowing and mild nonspecific abnormalities.

The female sibling was born at term after a risk pregnancy due to maternal hypertension. Birth and postnatal adaptation were complicated by perinatal asphyxia and left cerebral hemor-rhage (Apgar 1/1/2). Postnatally, she presented with hypoxic ischemic encephalopathy, and when only a few hours old she developed convulsive status epilepticus. She presented with daily dyscognitive seizures and brief focal motor seizures with a tonic component. She continued to have episodes of convul-sive status epilepticus. EEG showed multifocal epileptiform discharges, which evolved to hypsarrhythmia at four months of age. At 10 months of age, she suffered from daily brief tonic seizures. She was developmentally delayed from birth, and severe ID was present at follow-up. MRI at four months of age showed delayed myelination. At five months of age, severe micro-cephaly was evident (−5 SD). At follow-up, she had adequate head control and was able to grab things, but was unable to turn or sit, and had poor eye contact. Additional features included hyperopia,

strabismus, constipation, hypotonia, apneas, and eating difficulties. Tube feeding was initiated at 13 months. She experienced a transient response to phenobarbital, and her EEG improved during treatment with prednisolone, 5 mg/kg/d for two weeks, showing only background slowing and nonspecific EEG abnormalities. VGB and sulthiame treat-ment resulted in no seizure improvement. Current treatment includes sulthiame and VPA and is accompanied by 10-15 absence seizure per day.

Gene panel testing revealed that the two affected sibs were compound heterozygotes for the *SCN8A* missense variants p.Gly269Arg (c.805G>A) located in the pore loop of do-main I and p.Thr1360Asn (c.4079C>A) in the pore loop of domain 3 (Figure 2.1B). Sanger sequencing demonstrated that both variants were inherited (Figure 2.1B).

Family 2

The proband was a 27-year-old male born to unrelated parents. Both parents had mild cognitive deficits. They were able to live independent lives with guidance and support. Both attended special school, received disability pensions, and worked in a sheltered workshop. Neuropsychological evaluations were not available, and both parents were lost for follow-up.

The patient was born at term after an uncomplicated pregnancy and delivery. He was readmitted to the hospital within the first week of life due to cyanosis, hypotonia, and apathetic behavior. At six months of age, delayed psychomotor development became evident (no eye contact, lack of head control, hypotonia), and at seven months of age, he experienced his first seizure, characterized by eye rolling and stiffness of the whole body. His EEG was reported as slightly abnormal, but no antiepileptic treatment was initiated. A computed tomography scan showed atrophy of the frontal lobes. At this approximate age, he was removed from his parents and put in foster care. In the following years, he was diagnosed with severe ID, spastic tetraplegia, myopia, and bilateral hip dysplasia. He never gained the ability to walk or communicate, and was admitted several times due to febrile seizures, asthmatic bronchitis, gastroesophageal reflux, pneumonia, and constipation. At the age of seven years, brief episodes with staring were noticed. Ictal EEG recordings showed regular diffuse 3-4–Hz epileptic discharges lasting for 5-10 seconds. Oxcarbazepine was introduced but was administered irregularly for a few days by the foster mother, only during febrile episodes. At 8.5 years, it was stopped. MRI performed at the age of eight

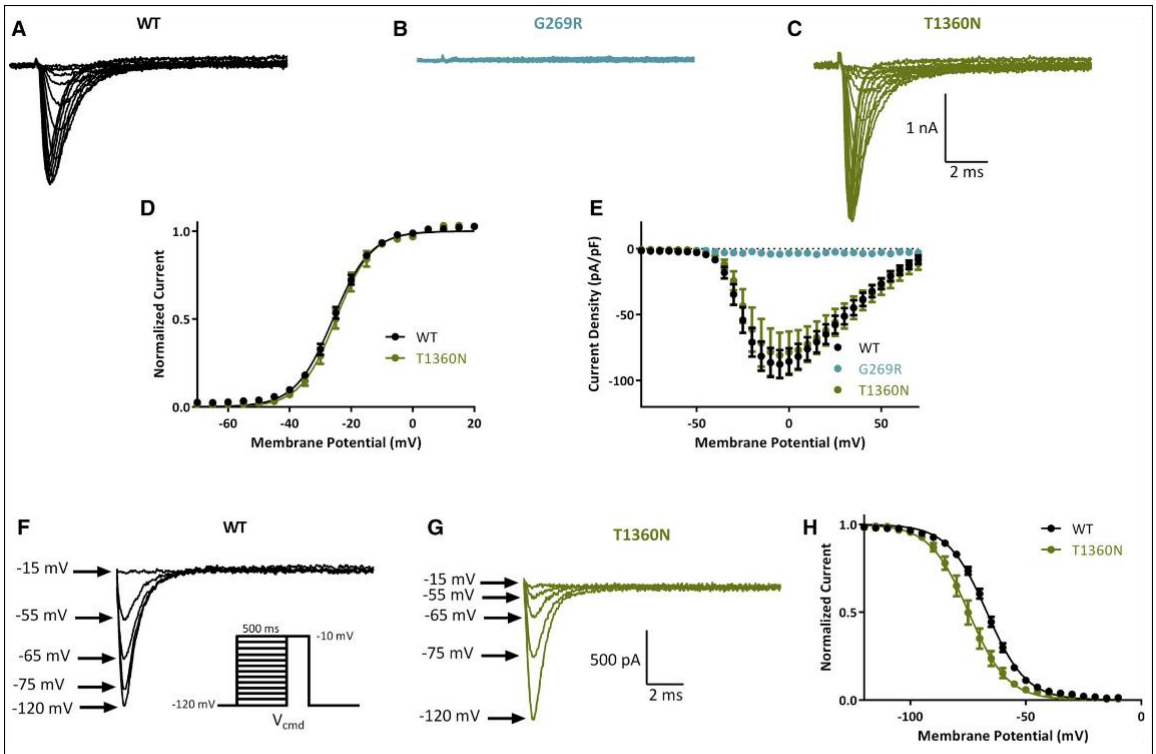

Figure 2.2: Biophysical characterization of sodium channel variants in Family 1. A-C, Representative traces of families of sodium channel currents recorded from ND7/23 cells expressing wild type (WT; A), G269R (B), and T1360N (C). D, Averaged current-voltage curves for WT (n = 37) and T1360N (n = 7). E, Voltage dependence of channel activation. F, G, Example traces of steady-state inactivation curves for WT (F) and T1360N (G). Inset shows voltage protocol for steady-state inactivation (Vcmd: voltage command). H, Voltage dependence of steady-state inactivation for WT (n = 37) and T1360N (n = 7). Data represent mean ± SEM. Smooth lines in D and H correspond to single Boltzmann equation fits to average data.

years did not show abnormalities. When he was nine years old, he was moved to a residential care institution, where he now lives. Tonic-clonic seizures, occasional dystonic/dyskinetic episodes, and eating difficulties were reported. At the age of 10 years, topiramate (TPM) and VPA were initiated, achieving seizure control for some years. He was also treated with risperidone for behavioral problems (agitation and screaming). At age 15 years, TPM was stopped. In the following years, the seizure frequency progressively increased, and at 20 years of age, he was referred to the Danish Epilepsy Center because of drug-resistant epilepsy with weekly tonic seizures and staring episodes. His interictal EEG showed sub-continuous theta-delta activity and high-amplitude spike and slow waves, bilaterally in the posterior quadrants, as well as less prominent focal slowing and infrequent spike and slow waves in the frontotemporal regions. The staring episodes were recorded on video-EEG and did not have an EEG correlate. LEV was added to VPA, with improvement of seizure duration and frequency from weekly to monthly. At latest examination, he was profoundly intellectually disabled, nonverbal, and wheel-chair bound and had spastic tetraplegia, dyskinesia, dysphagia, scoliosis, kyphosis, and severe myopia.

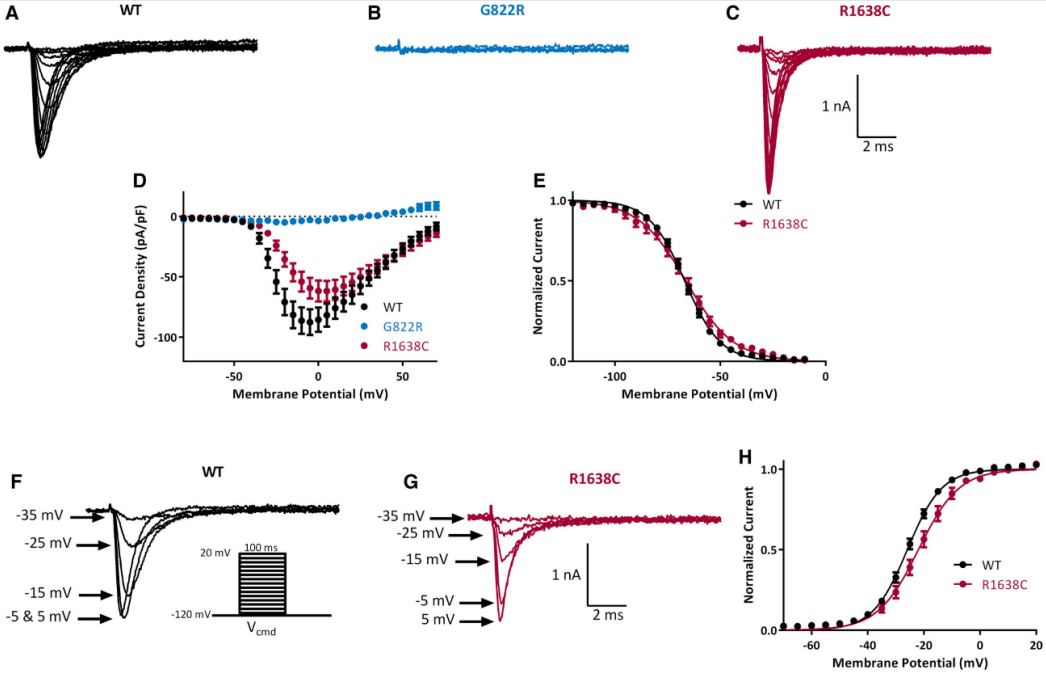

Figure 2.3: Biophysical characterization of sodium channel variants in Family 2.
Biophysical characterization of sodium channel variants in Family 2. A‐C, Representative traces of families of sodium channel currents recorded from ND7/23 cells expressing wild type (WT; A), G822R (B), and R1648C (C). D, Averaged current‐voltage curves for WT (n = 37), G822R (n = 9), and R1638C (n = 12). E, Voltage dependence of steady‐state inactivation for WT (n = 37) and R1638C (n = 12). F, G, Example traces of sodium currents recorded for WT (F) and R1638C (G) showing a reduction in current amplitude in R1638C cells compared with WT at a given activation voltage. Inset shows activation voltage protocol. H, Voltage dependence of activation for WT (n = 37) and R1638C (n = 12). Data represent mean ± SEM. Smooth lines in E and H correspond to single Boltzmann equation fits to average data

Gene panel sequencing revealed that the index patient was compound heterozygous for the *SCN8A* missense variants p.Gly822Arg (c.2464G>A) located in the middle of trans-membrane segment D2S3 and p.Arg1638Cys (c.4912C>T) at the cytoplasmic end of transmembrane segment D4S4. Sanger sequencing demonstrated that both variants were inherited (Figure 2.1B).

SCN8A is highly intolerant of variation in the general population, with a probability of LOF intolerance of 1.00 and a missense z score of 7.94 in the gnomAD database. There are only four protein truncations and 384 missense variants in the gnomAD database, 21 compared to the pre-diction of 80 truncations and 1114 missense variants. The four variants detected in the present study are absent from the gnomAD database and are predicted to be deleterious by two or more prediction programs including CADD score, MPC score, and PolyPhen.

Functional Analysis

ND7/23 cells were transfected with Nav1.6 cDNA, and sodium currents were recorded. Cells transfected with WT Nav1.6 generated current density of −90 ± 11 pA/pF (n=37; Figure 2.2A). Transfection of variant G269R from Family 1 (allele 1) did not generate any detectable current (−6 ± 1.4 pA/pF, n= 5; Figure 2.2B) and was not significantly different (P > .05) from non-transfected cells (−4 ± 0.8 pA/pF, n=5). In contrast, the variant T1360N (Family 1, allele 2) generated current density similar in magnitude to the WT channel (−82 ± 17 pA/pF, n= 7; Figure 2.2C). The voltage-dependence of activation

of T1360N channels did not differ from WT (Figure 2.2D,E; Table 2.2). However, analysis of voltage-dependent steady-state inactivation demonstrated a hyperpolarizing shift of −7.5 mV in the half maximal voltage of inactivation ($V_{1/2}$) of T1360N compared to WT (P<.01; Figure 2.2F-H, Table 2.2). The predicted effect of this mutation is to reduce channel availability.

Family 2 allele 1 (G822R) did not generate detectable sodium current (−7 ± 1 pA/pF, n = 12; Figure 2.3B,D). Family 2 allele 2 (R1638C) generated current density of −63.7 ± 2.7 pA/pF (n=12), which did not differ from WT (P>.05; Figure 2.3C,D). The $V_{1/2}$ for activation of R1638C was shifted in a depolarizing direction by +3.8 mV in comparison with the WT channels (P<.05; Figure 2.3F-H, Table 2). This is predicted to reduce the number of channel openings at any given voltage. The $V_{1/2}$ for steady-state inactivation between R1638C and WT channels did not differ (Figure 2.3E, Table 2.2). The depolarizing shift in voltage-dependent activation exhibited by R1638C is consistent with reduced neuronal activity.

	Activation		Inactivation	
	$V_{1/2}$ (mV)	k	$V_{1/2}$ (mV)	k
WT, n=37	-25.8 ± 0.8	5.37 ± 0.22	-66.9 ± 0.9	7.75 ± 0.14
Family 1, allele 2 T1360N, n=7	-26.0 ± 1.6	5.29 ± 0.47	-74.4 ± 1.6*	7.79 ± 0.35
Family 2, allele 2 R1638C, n=12	-22.0 ± 0.8**	6.65 ± 0.29*	-66.7 ± 2.0	10.4 ± 0.88***

Abbreviations: WT, wild type; $V_{1/2}$ half-maximal voltage. *P<0.05. **P<0.01. ***P<0.001 compared to WT by unpaired t-test.

Table 2.2: Activation and steady-state inactivation parameters of WT and variant $Na_v1.6$ voltage-gated sodium channel currents

Discussion

My colleagues and I describe two pedigrees (Figure 2.1) in which probands with inherited biallelic variants of *SCN8A* are severely affected with DEE. The monoallelic (heterozygous) parents have only mild cognitive deficits. In each family, one parent had a more severe allele with complete LOF and one parent had a partial LOF variant, with the probands inheriting one of each type of variant. These variants exhibit dominant expression in heterozygous carriers with mild phenotypes and a much more severe phenotype in com-pound heterozygous carriers with two variant alleles. None of the four variants had been previously described in patients, but all are predicted to likely be pathogenic and are absent from the control population in the gnomAD database. Functional tests demonstrated reduced or complete LOF of the variant channels. In the only previous report of a patient with two variants of *SCN8A*, the missense variant (p.Ile1583Thr) was probably not deleterious, and the deletion was a somatic mosaic (Berghuis et al., 2015). In two families with biallelic variants of *CACNA1A*, the probands with biallelic variants suffered from DEE whereas the heterozygous parents and siblings had milder symptoms, similar to our observations (Reinson et al., 2016; Sintas et al., 2017). In addition to demonstrating a previously unreported inheritance pattern for *SCN8A*-related disorders, these families suggest an explanation for the observation that the frequency of *SCN8A* variants previously observed is lower than that for *SCN1A* (Johannesen et al, personal communication) (Bayat et al., 2015). In contrast to *SCN1A* heterozygotes, who are often affected with Dravet syndrome, the *SCN8A* heterozygotes presented in this study were not sufficiently ill to be candidates for genetic testing. There are likely to be many more individuals with mild *SCN8A*-related phenotypes who will not be discovered until genetic testing becomes more widespread.

Electrophysiological analysis of the variants G269R and G822R identified complete absence of channel activity in transfected ND7/23 cells. G269R is located in segment 5 of domain I, and G822R is located in segment 3 of domain 2, a region that is relatively lacking in variants causing dominant DEE (Meisler et al., 2016). Both variants completely eliminate channel activity, indicating that the affected residues are essential for channel function. In contrast, the variants R1638C and T1360N retained channel activity with altered biophysical properties that are consistent with partial LOF. Depolarizing shifts of voltage-dependent activation in the R1638C mutation reduce the number of channels available to open at any membrane voltage and thereby reduce neuronal excitability. The hyperpolarized shift in channel inactivation in the T1360N channel reduces channel availability due to premature entry into inactivated channel states. The predicted result in affected compound heterozygotes is altered excitability of both excitatory and inhibitory neurons, impairing overall neuronal network function.

Both families segregate one allele with complete LOF and one allele with altered biophysical properties, both of which are predicted to result in reduced neuronal activity. In contrast, most of the *de novo* variants associated with DEE result in elevated neuronal activity (Bunton-Stasyshyn et al., 2019; Lopez-Santiago et al., 2017; Ottolini et al., 2017; Wengert et al., 2019b) The most common biophysical effect of previously described *SCN8A* variants in DEE is impaired channel inactivation and elevated persistent sodium current (Veeramah et al., 2012; Wagnon et al., 2016; Zaman et al., 2019). Even in the presence of a WT allele, variants with elevated channel activity produce a severe dominant phenotype. However, for the LOF variants, the WT allele in heterozygous carriers provides compensating channel activity and heterozygous parents exhibit only mild cognitive deficits. In the individuals affected with DEE, who are compound heterozygotes for reduced function alleles, the total channel activity is predicted to be <50% of normal, resulting in the severe phenotype of *SCN8A* encephalopathy. However, it is not clear why reduced activity of Nav1.6 results in seizures. The biallelic LOF individuals in our families have phenotypes that are indistinguishable from monoallelic GOF variants, including early onset DEE with multiple seizure types (focal, clonic, and tonic), severe ID with absent speech, axial hypotonia, central visual impairment, microcephaly, and gastrointestinal symptoms, features that are all de-scribed in patients with elevated channel activity (Gardella et al., 2018). These results indicate the possibility that $Na_V1.6$ function must be maintained in proper balance and that physiological deviation in either direction (more or less channel activity) is potentially proconvulsant. It cannot be excluded that other rare genetic variants may contribute to the observed phenotypes.

A small number of heterozygous carriers of partial or complete LOF of *SCN8A* have been described previously, with variable consequences. Myoclonus in the absence of seizures was observed in one family with four affected family members (Wagnon et al., 2018). Mild to moderate ID or ASD in the absence of seizures was observed in four families (Wagnon et al., 2017b). On the other hand, absence epilepsy was observed in a family with the heterozygous protein truncating variant p.Asn544fs39 (Johannesen et al., 2019). It is likely that variations in other genes in the genetic background contribute to this variation; the effects of modifier genes on seizure phenotypes have been well established in the mouse (Kearney et al., 2002; Martin et al., 2007). It is also possible that missense variants that appear to cause complete LOF *in vitro* may actually retain some activity in vivo that contributes to the relatively mild phenotype in the monoallelic (heterozygous) parents. Recent evidence suggests that the sodium channel alpha subunits may function as dimers (Clatot et al., 2017). In this case, LOF alleles that produce full length protein could have a dominant negative effect in heterozygotes, resulting in <50% residual activity and a more severe phenotype than that of LOF alleles encoding truncated or unstable proteins.

SCN8A is widely expressed in both excitatory and inhibitory neurons of the central nervous system and peripheral nervous system. LOF variants of *Scn8a* in the mouse result in severe movement disorders without seizures; loss of 90% of normal activity results in tremor, ataxia, and dystonias, and loss of 100% of activity results in hind limb paralysis and juvenile lethality (Kearney et al., 2002; O'Brien and Meisler, 2013). Homozygosity for complete LOF alleles may also be incompatible with human life. Reduced activity of Nav1.6 in colonic mesenteric neurons may contribute to the gastrointestinal disturbances in patients with *SCN8A* encephalopathy (Bartoo et al., 2005). Future studies examining both excitatory and inhibitory neuron populations in *SCN8A* encephalopathy could be helpful to reconcile the existence of both GOF and LOF variants in patients with DEE. The neuronal population-specific impact of mutant *SCN8A* expression is the topic of Chapters V and VI of this thesis.

Chapter III: Prax330, a Novel Sodium Channel Inhibitor, Rescues Neuronal Hyperexcitability and Reduces Seizures in a Mouse Model of *SCN8A* Encephalopathy

Rationale

Therapeutic management is difficult in many patients with *SCN8A* encephalopathy, leading to uncontrolled seizures and a risk for sudden unexpected death in epilepsy (SUDEP). Thus, there is a need for novel antiseizure medications (ASMs) that specifically target aberrant voltage-gated sodium channel activity associated with *SCN8A* gain-of-function mutations. In this chapter, I provide evidence that Prax330, previously known as GS967, inhibits persistent and resurgent sodium currents and normalizes abnormal action potential (AP) waveforms in hippocampal subiculum and CA1 neurons from *Scn8a*$^{D/+}$ mice. Additionally, I show that Prax330 is able to reduce seizure frequency and extended survival in *Scn8a*$^{D/+}$ mice. Taken together, these results indicate the pathogenicity of elevated persistent and resurgent sodium currents and put forth Prax330 as a promising novel sodium channel inhibitor to treat patients with *SCN8A* encephalopathy.

Introduction

The first characterized *SCN8A* encephalopathy mutation was p.Asn1768Asp (N1768D) (Veeramah et al., 2012). The patient presented with refractory epilepsy at six months of age, intellectual disability, ataxia, and sudden unexpected death in epilepsy (SUDEP) at 15 years. Biophysical characterization of the mutation in expression systems and neurons revealed a depolarizing shift in the voltage-dependence of steady-state inactivation, an increase in the non-inactivating persistent sodium current (I_{NaP}) after termination of the transient current (I_{NaT}), and an elevated resurgent current (I_{NaR}) (Ottolini et al., 2017; Patel et al., 2016; Veeramah et al., 2012). I_{NaP} has been implicated in setting AP threshold (Deng and Klyachko, 2016), amplifying incoming excitatory and inhibitory synaptic inputs (Hardie and Pearce, 2006; Stafstrom et al., 1985; Stuart and Sakmann, 1995), driving the burst-firing mode of AP firing (Alkadhi and Tian, 1996; Su et al., 2001; Tsuruyama et al., 2013), and orchestrating rhythmogenesis in various neuronal circuits (Dong and Ennis, 2014; Paton et al., 2006; Tazerart et al., 2008; Yamanishi et al., 2018; Zhong et al., 2007). Studies of animal models and human epilepsy tissue have reported increases in I_{NaP} (Barker et al., 2017; Chen et al., 2011; Hargus et al., 2013; Lopez-Santiago et al., 2017; Ottolini et al., 2017; Stafstrom, 2007; Tryba et al., 2011; Vreugdenhil et al., 2004). I_{NaR} also contributes to increased AP frequency and burst firing (Khaliq et al., 2003; Raman and Bean, 1997; Raman et al., 1997). It has therefore been suggested that elevation of I_{NaP} and I_{NaR}, due to expression of mutant voltage-gated sodium channels (VGSCs) or other modulation of VGSC function, may be a central mechanism contributing to neuronal hyperexcitability associated with seizure initiation (Stafstrom, 2007; Wengert and Patel, 2021).

Many clinically available ASMs that target VGSCs inhibit I_{NaP}, including phenytoin, carbamazepine, topiramate, and lamotrigine (Alexander and Huguenard, 2014; Colombo et al., 2013; Segal and Douglas, 1997; Spadoni et al., 2002; Sun et al., 2007). For this reason, development of a preferential inhibitor of I_{NaP} could lead to a more efficacious and potentially better tolerated ASMs (Stafstrom, 2007). Prax330 was initially developed as a selective I_{NaP} inhibitor to treat cardiac arrhythmia (Belardinelli et al., 2013; Koltun et al., 2016), however, due its brain permeability and half-life, development of Prax330 was repurposed as an ASM (Belardinelli et al., 2013; Koltun et al., 2016). More recently, Prax330 has been evaluated for efficacy in a number of severe genetic epilepsy syndrome models. *In vivo* studies in *Scn1a*$^{+/-}$ and *Scn2a*^{Q54} mouse models of epileptic encephalopathy revealed that Prax330 is able to potently reduce I_{NaP} and suppress spontaneous AP firing in acutely dissociated hippocampal neurons, protect against seizures, and extend survival (Anderson et al., 2014, 2017).

In order to further investigate the mechanisms by which Prax330 exhibits anticonvulsant activity in the *Scn8a*$^{D/+}$ mouse model of epileptic encephalopathy, my colleagues and I examined the effects of Prax330 on the biophysical properties of the mutant $Na_V1.6$- N1768D in ND7/23 cultured cells and on I_{NaP}, I_{NaR}, and neuronal excitability in subiculum and CA1 neurons from *Scn8a*$^{D/+}$ mice. Subiculum and CA1 hippocampal neurons were chosen because they provide the primary outputs of the hippocampus and have been previously implicated in epilepsy (Barker et al., 2017; Fujita et al., 2014; de Guzman et al., 2006; Toyoda et al., 2013; Vreugdenhil et al., 2004). In ND7/23 cells, Prax330 reduced the I_{NaP} in N1768D-expressing cells and caused a leftward shift in inactivation curves of both WT and N1768D channels. Electrophysiological recordings revealed elevated I_{NaP} and I_{NaR} currents and aberrantly large AP-burst waveforms in CA1 neurons and a subset of *Scn8a*$^{D/+}$ subiculum neurons. Prax330 (1 μM) reduced I_{NaP} and I_{NaR} and attenuated the abnormal AP-burst waveforms in

CA1 neurons and the subset of subiculum neurons without affecting those with normal AP morphology. Synaptically-evoked APs from *Scn8a*$^{D/+}$ subiculum neurons were inhibited by Prax330 (1 μM) while WT neurons were unaffected. Lastly, we show that treating mice with Prax330 reduces seizures and extends survival in *Scn8a*$^{D/+}$ mice. These findings suggest that Prax330 preferentially targets aberrant VGSCs associated with *SCN8A* mutations and may be useful in the treatment of *SCN8A* epileptic encephalopathy and other forms of genetic and acquired epilepsy.

Methods

ND7/23 Electrophysiology

The introduction of the N1768D mutation into the TTX-resistant $Na_v1.6$ cDNA was previously described (Veeramah et al, 2012). DRG-neuron derived ND7/23 cells (Sigma Aldrich) were grown in a humidified atmosphere of 5% CO_2 and 95% air at 37ºC in Dulbecco's Modified Eagle Medium (DMEM 1X) supplemented with 10% FBS, NEAA and Sodium Pyruvate. Cells were plated onto petri dishes 48 hours prior to transfection and transfected for 5 hours in non-supplemented DMEM using Lipofectamine 3000 according to manufacturer instructions (Life Technologies) with 5 μg of $Na_V1.6$ alpha subunit cDNA and 0.5 μg of the fluorescent m-Venus bioreporter. Electrophysiological recordings of fluorescent cells were made 48 hours after transfection.

Whole-cell patch-clamp electrophysiological recordings of sodium currents were carried out as described previously (Barker et al., 2016; Wagnon et al., 2016, 2018). The external recording solution contained in mM: 130 NaCl, 3 KCL, 1 $CaCl_2$, 5 $MgCl_2$, 0.1 $CdCl_2$, 10 HEPES, 30 TEA, 4 4-AP, and 500 nM TTX to block any endogenous sodium currents (pH adjusted to 7.4 using NaOH). The osmolality was confirmed to be ~305 mOsm. The intracellular recording solution contained in mM: 140 CsF, 2 $MgCl_2$, 1 EGTA, 10 HEPES, 4 Na_2ATP, 0.3 NaGTP (pH adjusted to 7.2 with CsOH and osmolality adjusted to 300 mOsm). All experiments were performed at room temperature (22-24ºC). Borosilicate recording pipettes were pulled to have resistances of 1.5-3.0 MΩ in recording solution. After achieving the whole-cell configuration, whole-cell capacitance and 75% series resistance were compensated. Currents were amplified, low-pass filtered at 2 kHz, and sampled at 33kHz. Cells were held at -120 mV. The voltage-dependent activation was measured from the current-voltage relationship determined using a 100 ms voltage step to command potentials ranging from -80 to 70 mV at 5 mV increments and conductance as a function of voltage was described by a Boltzmann fit of the data. The average I_{NaP} was taken to be the average current from 60-100 ms after the onset of the voltage step, once the current had reached steady state, and recorded as a percentage of the magnitude of the I_{NaT}. Steady-state inactivation, cells were stepped to pre-pulse potentials ranging from -120 to -10 mV for 500 ms before being stepped to -10 mV to assess channel availability. When calculating steady-state inactivation conductance as a function of voltage, the current of greatest magnitude was determined normalized to 1 and the final sweep which is a continuous step to -10 mV, which does not evoke any I_{NaT}, was set to be 0. The results are well-fit by a single Boltzmann equation as previously described (Barker et al., 2016).

Brain Slice Preparation

WT and *Scn8a*$^{D/+}$ mice greater than 8 weeks of age were euthanized using isoflurane and decapitated. The brains were rapidly removed and kept in ice-cold (~0ºC) artificial cerebrospinal fluid (ACSF) containing in mM: 125 NaCl, 2.5 KCl, 1.25 NaH_2PO_4, 2 $CaCl_2$, 1 $MgCl_2$, 0.5 L-Ascorbic acid, 10 glucose, 25 $NaHCO_3$, and 2 Pyruvate. The ACSF at all stages of the experiment was oxygenated with 95%/5% O_2/CO_2. Horizontal brain sections of 300 μM thickness were cut using a Leica VT1200 vibratome. The slices were placed in 37ºC oxygenated ACSF for ~30 minutes and then kept at room temperature.

Brain Slice Electrophysiology

Brain slices were placed in small chamber continually superfused (~1-2 mL/min) with recording solution warmed to (~32ºC). Subiculum pyramidal neurons were visually identified by infrared video microscopy (Hamamatsu, Shizouka, Japan) using a Zeiss Axioscope microscope. Whole-cell recordings were performed using an Axopatch 700B amplifier (Molecular Devices, pCLAMP 10 software) and were digitized by a Digidata 1322A digitizer (Molecular Devices). Currents were amplified, low-pass filtered at 2 kHz, and sampled at 100 kHz. Borosilicate electrodes were fabricated using a Brown-Flaming puller (Model P1000, Sutter Instruments Co) to have pipette resistances between 2-3.5 MΩ.

I_{NaP} Recordings

The I_{NaP} was recorded as previously described using a solution containing in mM: 20 NaCl, 130 TEA-Cl, 10 $NaHCO_3$, 1.6 $CaCl_2$, 2 $MgCl_2$, 0.2 $CdCl_2$, and 5 4-AP, and 15 glucose (pH adjusted to 7.4; 305 mOsm) (Ottolini et al., 2017). The pipette solution contained (in mM): 140 CsF, 2 $MgCl_2$, 1 EGTA, 10 HEPES, 4 Na_2ATP, and 0.3 NaGTP (pH adjusted to 7.3, 310 mOsm). Voltage ramps from -100 to -10 at 65 mV/sec led to inward ramp currents with a clear peak near -30 mV. Any cells with ramp currents that escaped voltage-control were discarded and not analyzed. Identical recordings in the presence 500 nM TTX were used to definitively isolate the sodium component of the ramp current. TTX-subtracted traces were used for calculation of peak inward current and the voltage of half-maximal activation ($V_{1/2}$).

I_{NaR} Recordings

The I_{NaR} was recorded as previously described using a modified recording solution containing in mM: 100 NaCl, 26 $NaHCO_3$, 19.5 TEA-Cl, 3 KCl, 2 $MgCl_2$, 2 $CaCl_2$, 2 $BaCl_2$, 0.1 $CdCl_2$, 4 4-AP, and 10 glucose (pH of 7.4; 305 mOsm) (Barker et al., 2017). The intracellular solution was the same as that for I_{NaP} recordings. Neurons were held at -100 mV, depolarized to 0 mV for 20 ms and then repolarized to voltages ranging between -100 mV and -20 mV in increments of 10 mV. The peak amplitude of I_{NaR} was calculated as the maximum TTX-sensitive current elicited (typically on the -30 mV step) with the steady-state current subtracted as done previously (Royeck et al., 2008).

Action Potential Recordings

Current clamp recordings were performed with an extracellular recording solution identical to that used in the slicing procedure. The intracellular solution contained in mM: 120 K-gluconate, 10 NaCl, 2 $MgCl_2$, 0.5 K_2EGTA, 10 HEPES, 4 Na_2ATP, 0.3 NaGTP (pH 7.2; osmolarity 290 mOsm). A ramp of depolarizing current 100 pA/sec was used to accurately measure AP threshold which was defined as the membrane potential at which the slope reached 5% of the upstroke velocity (Yamada-Hanff and Bean, 2013). AP amplitude was calculated as the range between threshold and the peak of the AP. A range of depolarizing current injections (-20 to 470 pA in increments of 10 pA) was used to calculate membrane and AP properties. To compare across all neurons, a slow injection of DC current was used to hold neurons at -65 mV throughout the recording. The rheobase was defined as the highest current step injected that did not result in AP firing. Input resistance was calculated using the initial -20 pA step. The upstroke and downstroke velocities were the maximum and minimum of the first derivative of the recorded trace. The AP duration (APD_{50}) was measured as the time duration of the AP measured at the midpoint between the threshold and the peak of the AP. The area under the curve (AUC) of the first AP was calculated relative to AP threshold for each cell. Synaptically-evoked APs were generated through stimulation of the CA1 afferents using a bipolar iridium stimulator (WPI, Sarasota, FL, USA). The stimulus duration was 400 μs and the intensity was adjusted (usually between 1 and 3.2 mA) to evoke APs on successive sweeps with a 10 second inter-sweep interval.

Drug

Prax330 was provided by Praxis Precision Medicines. For electrophysiology studies, Prax330 was solubilized in DMSO at a stock concentration of 10 mM and stored at -20^{O}C. Initial recordings were collected at baseline and then again after ~10 minutes with bath solution containing Prax330. Vehicle control recordings were done in an identical manner without Prax330.

For chronic administration studies, mice were fed Purina 5001 rodent chow compounded with Prax330 (8 mg/kg of chow; Research Diets, New Brunswick, NJ, USA). The estimated dose was 1.5 mg/kg/d based on average daily consumption of 190 g of chow/kg of body weight (http://www.researchdiets.com/resource-center-page/typical-food-intake). Previous studies showed that chronic treatment with this dose resulted in Prax330 plasma and brain concentrations of 1.0 ± 0.08 and 1.7 ± 0.1 μM, respectively (Anderson et al., 2017).

Survival

At six weeks of age, heterozygous *Scn8a*$^{D/+}$ mice were assigned to either Prax330 or control treatment groups by block randomization. Mice in the Prax330 treatment group were provided chow containing Prax330 (8 mg/kg of chow; Research Diets). Survival was monitored up to nine months of age by performing census checks 3-4 days per week. Survival was analyzed with Kaplan-Meier analysis using the Mantel-Cox log-rank test with $P<0.05$ considered statistically significant.

Video-electroencephalography

At six weeks of age, *Scn8a*$^{D/+}$ mice and WT littermates were assigned to either Prax330 or control treatment groups by block randomization. At age 70-80 days, mice were anesthetized with isoflurane and fitted with a prefabricated head mount (Pinnacle Technology, Lawrence, KS, USA). Following at least 48 hours of recovery, mice underwent continuous video-electroencephalographic (EEG) recording for 5-13 days. Additional days of continuous video-only recording were obtained (range = 3-26 days). Digitized EEG data were acquired and analyzed with Sirenia software (Pinnacle Technology). Epileptiform activity was scored offline by a blinded observer to identify electrographic seizures and behavioral correlates. The behavioral component of seizures scored by video-only were indistinguishable from those scored by epileptiform activity. Seizure frequencies were calculated for each individual animal and compared between treated and untreated *Scn8a*$^{D/+}$ mice using a Mann-Whitney test with $P<0.05$ considered statistically significant.

Electrophysiology Data Analysis

All electrophysiology data were analyzed by custom-written MATLAB scripts, or manually with ClampFit. GraphPad Prism software was used for displaying data and for all statistical calculations. All values represent means ± standard error of the mean (S.E.M.) or as individual data points. Statistical significance was determined using unpaired or paired t-test where appropriate with an alpha set to 0.05 (GraphPad Prism 6.02).

Results

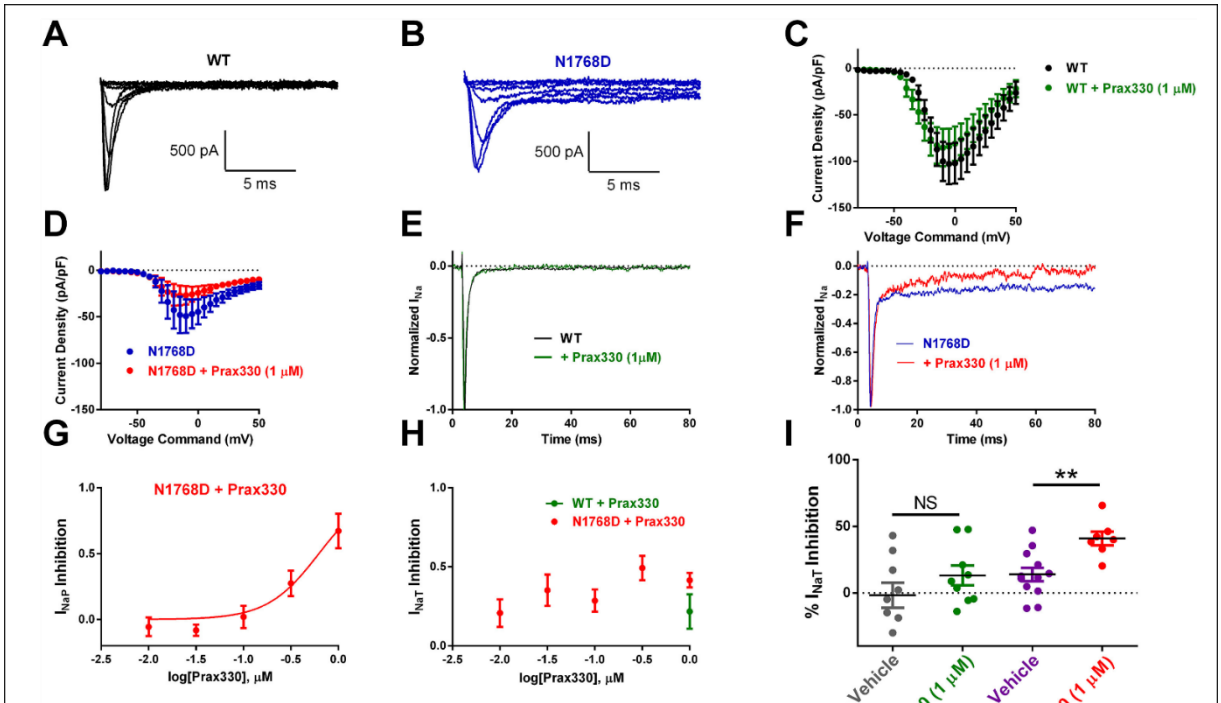

Figure 3.1: Prax330 inhibits N1768D-derived I_{NaP} in NaV1.6-expressing cells.
A-B. Families of $Na_V1.6$ channel current traces for WT- (A) and N1768D- (B) expressing ND7/23 cells. C. Current/voltage relationship for WT $Na_V1.6$ channel current density before (black) and after (green) treatment with Prax330 (1 μM). D. Current/voltage relationship for N1768D $Na_V1.6$ channel current density before (blue) and after (red) treatment with Prax330 (1 μM). E. Example normalized trace for WT before (black) and after (green) Prax330 (1 μM) treatment. F. Example normalized trace for N1768D before (blue) and after (red) treatment with Prax330 (1 μM). G. Dose-response curve for Prax330 on N1768D I_{NaP} (EC50 of 625 nM). H. Dose-response effect of Prax330 on I_{NaT}. I. Scatter plot showingeffects of vehicle (gray; n = 9) and Prax330 (1 μM; green; n = 9) on WT I_{NaT} and vehicle (purple; n = 12) or Prax330 (1 μM; red; n = 7) on N1768D INaT. Holding potential was −120 mV for all protocols. Data shown as individual values and/or mean ± SEM. **P < 0.01.

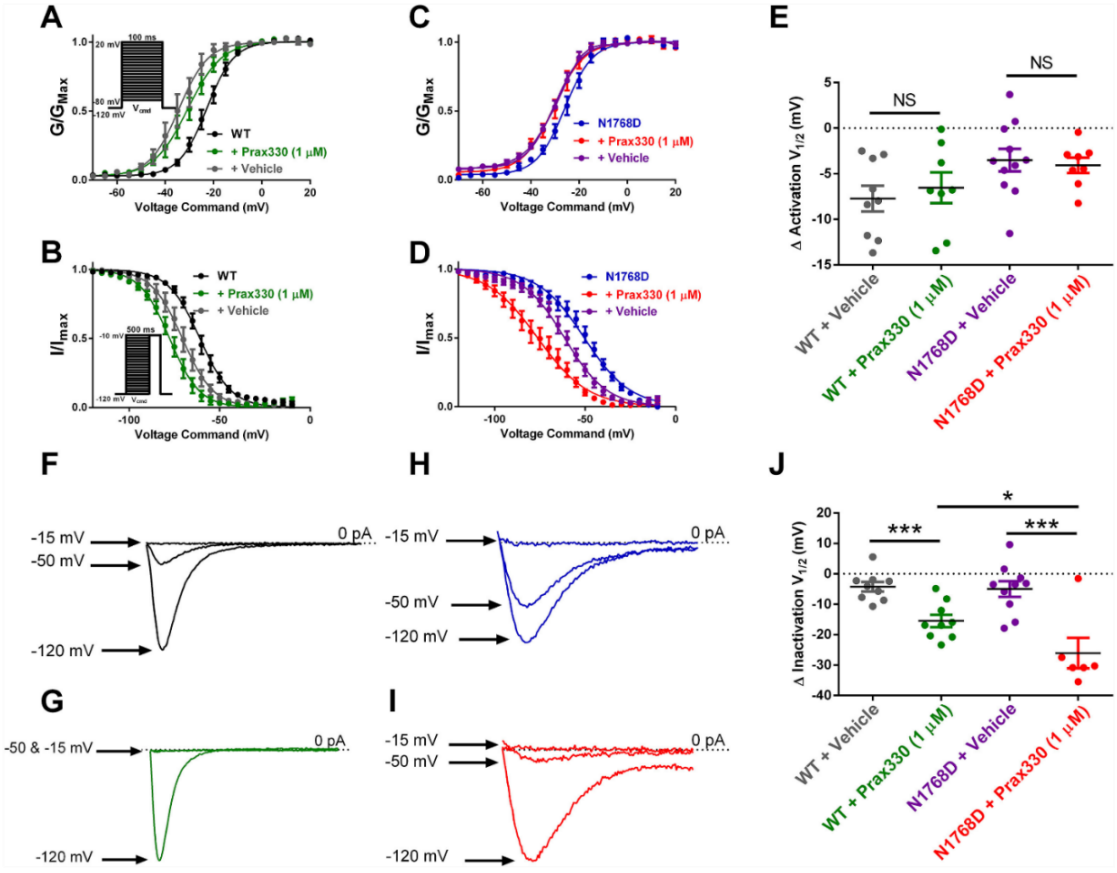

Figure 3.2: Prax330 hyperpolarizes steady-state inactivation curves in WT and N1768D $Na_V1.6$ channel currents.

A. Voltage-dependent activation curve for WT $Na_V1.6$ channel currents before (black), after treatment with Prax330 (green; 1 µM; n = 9), and vehicle control (gray; n = 9). Inset shows voltage command protocol. Cells were held at −120 mV. B. Steady-state inactivation curves for WT $Na_V1.6$ channel currents before (black) and after treatment with Prax330 (green; 1 µM; n = 9). Vehicle-treated controls are shown in gray (n = 9). Inset shows voltage command protocol. Cells were held at −120 mV C. Voltage-dependent activation for N1768D $Na_V1.6$ channel currents before (blue) and after administration of Prax330 (red; 1 µM; n = 8) or vehicle (purple; n = 11). D. Steady-State inactivation for N1768D channel currents before (blue) and after treatment with Prax330 (red; 1 µM; n = 6) or vehicle (purple; n = 10). E. Activation half-maximal voltage (V1/2) were not different between WT plus vehicle (gray; n = 9) or WT plus Prax330 (1 µM; green, n = 9), or N1768D plus vehicle (purple; n = 11), and N1768D plus Prax330 (1 µM; red, n = 8). Example traces of WT steady-state inactivation showing relative I_{NaT} after 500 m s pre-pulses to −120 mV, −50 mV, and −15 mV before (F) and after (G) treatment with Prax330 (1 µM). Example traces of N1768D steady-state inactivation showing relative I_{NaT} after 500 m s pre-pulses to −120 mV, −50 mV, and −15 mV before (H) and after (I) treatment with Prax330 (1 µM). J. Hyperpolarizing shifts in steady-state inactivation V1/2 for WT plus vehicle (gray; n = 9), WT plus Prax330 (1 µM; green; n = 9), N1768D plus vehicle (purple; n = 10), and N1768D plus Prax330 (1 µM; red; n = 6). Data shown as individual values and/or mean ± SEM. *P < 0.05, ***P < 0.001.

We first characterized the effect of Prax330 on WT and N1768D $Na_V1.6$ expressed in ND7/23 cells. Cells were held at -120 mV and stepped to potentials between -80 and 50 mV to examine the current-voltage relationship. Current densities between WT and N1768D cells were not different (WT: -103 ± 22 pA/pF (n=9), N1768D: -45 ± 14 pA/pF (n=7); Figure 3.1A-D). In agreement with previous studies (Veeramah et al., 2012), a pronounced elevation of I_{NaP} was observed in N1768D transfected cells (Figure 3.1B, F). I_{NaP} was barely detectable in WT $Na_V1.6$ transfected cells (Figure 3.1A, E). Prax330 inhibited N1768D-derived I_{NaP} in a dose-dependent manner with an approximate EC_{50} of 625 nM and a Hill slope of 1.5 (Figure 3.1G). At 1 µM, Prax330 significantly inhibited I_{NaP} by 67% (8.1 ± 1.3% of I_{NaT} before and 3.0 ± 1.1% of I_{NaT} after Prax330; $T_{(6)}$=3.61; P=0.0112; Figure 3.1F). Prax330 (1 µM) had no effect on I_{NaT} in WT cells (-103 ± 22 pA/pF at baseline to -84 ± 19 pA/pF after Prax330 treatment; n=9; Figure 3.1E, I). Prax330 did significantly reduce I_{NaT} in N1768D cells by 49 ± 10% at 300nM ($T_{(14)}$= 3.395; P=0.0044; n= 4) and by 41 ± 5% at 1 µM ($T_{(17)}$=3.48; P=0.0029; n=7) when compared to vehicle-treated time controls (Figure 3.1H, I). These findings suggest that Prax330 shows a particular efficacy toward the N1768D mutation compared to WT.

We assessed the effect of Prax330 (1 µM) on the voltage-dependence of steady-state activation and inactivation (Figure 3.2; Table 3.1). Voltage-dependent activation parameters were not different between WT and N1768D transfected cells (Table 3.1), but steady-state inactivation curves were significantly right-shifted in N1768D cells compared with WT, as previously

reported ($T_{(12)}$=4.173; P=0.0013; Fig. 3.2B,D; Table 3.1) (Veeramah et al., 2012). Left-shifts in activation curves for both WT and N1768D recorded in the presence of Prax330 (1 µM) were not different from shifts observed in vehicle-treated control recordings, indicating that Prax330 has no effect on activation parameters (Figure 3.2E; Table 3.1). In contrast, left-shifts in steady-state inactivation after Prax330 (1 µM) treatment for both WT and N1768D cells were significantly larger than that observed in vehicle controls suggesting that Prax330 (1 µM) has an affinity for inactivated channels (P<0.05; Table 3.1, Figure 3.2B-J).

Effect of Prax330 (1 µM) on WT and N1768D $Na_V1.6$ sodium currents.

	Activation		Inactivation	
	$V_{1/2}$ (mV)	k	$V_{1/2}$ (mV)	k
WT	−22.7 ± 1.5	4.9 ± 0.3	−60.9 ± 1.8	8.0 ± 0.3
+ Vehicle	−35.0 ± 2.0	5.3 ± 0.7	−67.8 ± 2.0	7.6 ± 0.3
+ Prax330 (1 µM)	−30.4 ± 2.4	5.3 ± 0.7	−77.3 ± 2.4[a]	7.7 ± 0.3
N1768D	−25.6 ± 1.4	5.6 ± 0.5	−50.8 ± 2.6[b]	12.8 ± 1.3[b]
+ Vehicle	−32.6 ± 1.0	6.4 ± 0.5	−62.0 ± 2.3	10.8 ± 0.9
+ Prax330 (1 µM)	−30.2 ± 1.7	6.0 ± 0.5	−76.9 ± 3.7[a]	12.4 ± 0.9

[a] Indicates $p < 0.05$ comparing vehicle and Prax330 application using unpaired *t*-test.

[b] Indicates $p < 0.05$ comparing WT and N1768D groups using unpaired *t*-test.

Table 3.1: Effect of Prax330 (1 µM) on WT and N1768D $Na_v1.6$ sodium currents.

Prax330 inhibits I_{NaP} and I_{NaR} in Scn8a$^{D/+}$ subiculum neurons

I_{NaP} was measured in subiculum neurons from acute brain slices obtained from *Scn8a*$^{D/+}$ mice and compared with WT littermates using slow voltage ramps from the holding potential of -100 mV to -10 mV at 65 mV/sec. Maximum I_{NaP} were significantly increased in *Scn8a*$^{D/+}$ subiculum neurons (-261 ± 20 pA; n = 24, 8 mice) compared to WT neurons (-173 ± 15 pA; $T_{(38)}$=3.167; P=0.003; n=10, 7 mice; Figure 3.3A-D). When compared to vehicle-treated controls, Prax330 (1 µM) inhibited both WT (by 48.5 ± 6.3%; n = 10, 4 mice: T=2.497; P=0.0256) and *Scn8a*$^{D/+}$ (by 56.9 ± 5.5%; n = 15, 5 mice: T=3.511; P=0.0020; Figure 3.3E). Voltage-dependent activation parameters were not different between Prax330-treated and vehicle-treated neurons (Figure 3.3F).

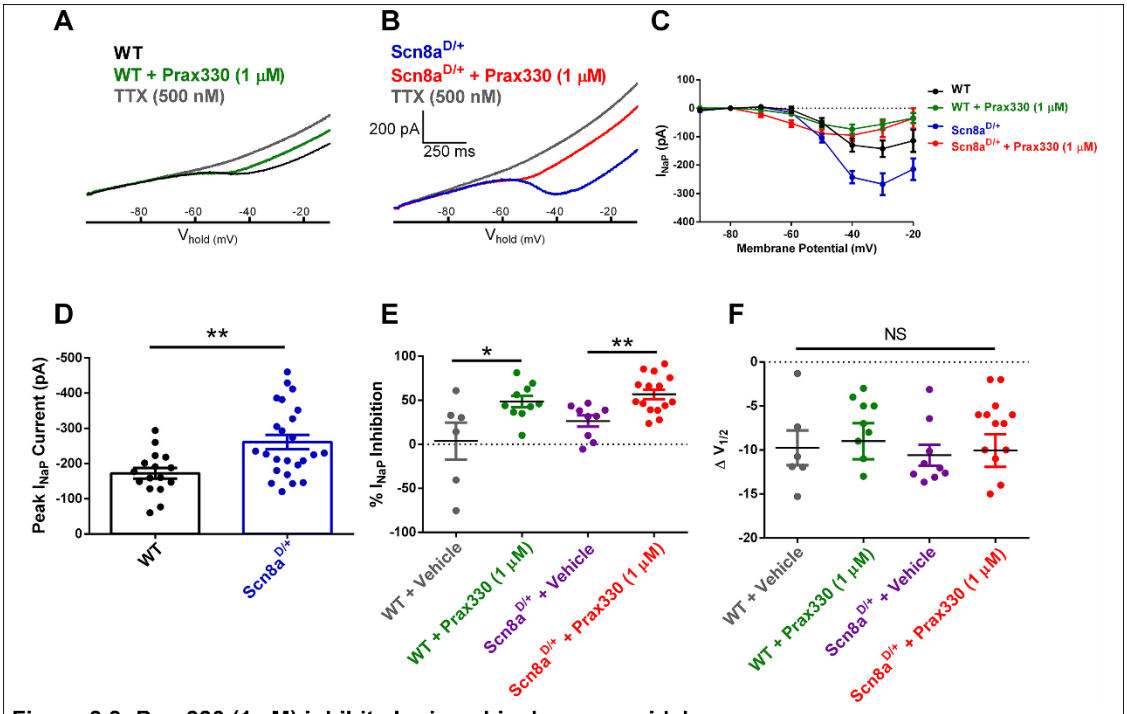

Figure 3.3: Prax330 (1 µM) inhibits I_{NaP} in subiculum pyramidal neurons.
Representative recording of I_{NaP} for WT before (black) and after (green) treatment with 1 µM Prax330 and 500 nM TTX (gray). B. Representative recording of I_{NaP} for Scn8a$^{D/+}$ before (blue) and after (red) treatment with 1 µM Prax330 and 500 nM TTX (gray). C. Current/voltage relationship of I_{NaP} for WT before (black) and after (green) Prax330 (1 µM) and current/voltage relationship of Scn8a$^{D/+}$ before (blue) and after (red) treatment with Prax330 (1 µM). D. Peak I_{NaP} current for WT (n = 16 neurons, 7 mice) and Scn8a$^{D/+}$ (n = 24 neurons, 8 mice) subiculum neurons. Scn8a$^{D/+}$ neurons have significantly larger peak I_{NaP}. E. Percent inhibition of I_{NaP} for WT plus vehicle (gray; n = 6 neurons, 3 mice), WT plus Prax330 (1 µM; green; n = 10 neurons, 4 mice), Scn8a$^{D/+}$ plus vehicle (purple; n = 9 neurons, 3 mice), and Scn8a$^{D/+}$ plus Prax330 (1 µM; red, n = 15 neurons, 5 mice). Compared to vehicle controls, Prax330 inhibited the steady-state I_{NaP} in both WT and Scn8a$^{D/+}$ subiculum neurons. F. Leftward shifts observed in activation V1/2 were not different between WT, N1768D or their respective vehicle controls; WT plus vehicle (gray), WT plus Prax330 (1 µM; green), Scn8a$^{D/+}$ plus vehicle (purple), and Scn8a$^{D/+}$ plus Prax330 (1 µM; red). Data shown as individual values and/or mean ± SEM. *P < 0.05, **P < 0.01.

I_{NaR} was also significantly elevated in *Scn8a*$^{D/+}$ brain slice subiculum neurons (−373.1 ± 41 pA; n = 20, 7 mice) compared to WT neurons (−229 ± 41 pA; n = 15, 8 mice; $T_{(33)}$ = 2.559; P = 0.0153; Fig. 3.4A, C, E). Compared to vehicle-treated controls (n = 4; 2 mice), Prax330

(1 μM) inhibited I_{NaR} by 37.6 ± 8.3% in *Scn8a*$^{D/+}$ subiculum neurons (n = 16; 5 mice, $T_{(18)} = 2.098$; p = 0.0495). In contrast, Prax330 (1 μM) had no effect on WT neurons (Fig. 3.4F), suggesting that Prax330 preferentially inhibits I_{NaR} in *Scn8a*$^{D/+}$ neurons.

Prax330 preferentially suppresses aberrant AP-bursting in Scn8a$^{D/+}$ *subiculum neurons*

Aberrant neuronal excitability in AP firing frequency and AP waveform morphology has been reported in medial entorhinal cortex and CA1 neurons from *Scn8a*$^{D/+}$ mice (Baker et al., 2018; Lopez-Santiago et al., 2017; Ottolini et al., 2017). Since subiculum neurons provide a major output from the hippocampus and have been implicated in seizure initiation in TLE (Barker et al., 2017; Fujita et al., 2014; de Guzman et al., 2006; Stafstrom, 2005; Toyoda et al., 2013), we examined subiculum neurons from *Scn8a*$^{D/+}$ mice (Figure 3.5). We found no differences in subiculum neuron AP firing frequencies between *Scn8a*$^{D/+}$ and WT mice (27.9 ± 2.4 Hz; n=18, 7 mice and 27.5 ± 1.7 Hz; n=17, 4 mice respectively). However, a subset of *Scn8a*$^{D/+}$ subiculum neurons (~ 50%) displayed a distinct, all-or-nothing AP burst that was associated with a significantly larger depolarizing event measured by taking the area under the curve (AUC) above AP threshold (1542 ± 112 mV*ms in *Scn8a*$^{D/+}$ compared to 605 ± 74 mV*ms in WT; $T_{(24)}$=7.219; P<0.0001; Fig. 3.5 A-C,E). The possible bimodal distribution for the AUC led us to separate *Scn8a*$^{D/+}$ neurons into two equal groups (n=9 cells each) based on the magnitude of AUC, *Scn8a*$^{D/+}$-low and high respectively, and examine the relative efficacy of Prax330 on the two groups (Fig. 3.5D). Interestingly, Prax330 (1μM) had no significant effect on the burst AUC for WT or *Scn8a*$^{D/+}$-low groups suggesting that *Scn8a*$^{D/+}$ neurons with physiological burst-firing resembling WT are relatively unaffected by Prax330 (Fig. 3.5 A-B, E). In contrast, *Scn8a*$^{D/+}$-high group neurons were profoundly modulated by Prax330 (1μM), resulting in a significant reduction in the AUC value (1542 ± 112 mV*ms before and 1095 ± 192 mV*ms after treatment with Prax330; $T_{(8)}$=2.327; P=0.0484; Fig 3.5. C, E). Together these results suggest that Prax330 has a greater effect on *Scn8a*$^{D/+}$ neurons with aberrant firing, potentially due to its effect on I_{NaR} and I_{NaP}, two currents that are known to contribute to burst firing and are increased in amplitude in *Scn8a*$^{D/+}$ subiculum neurons.

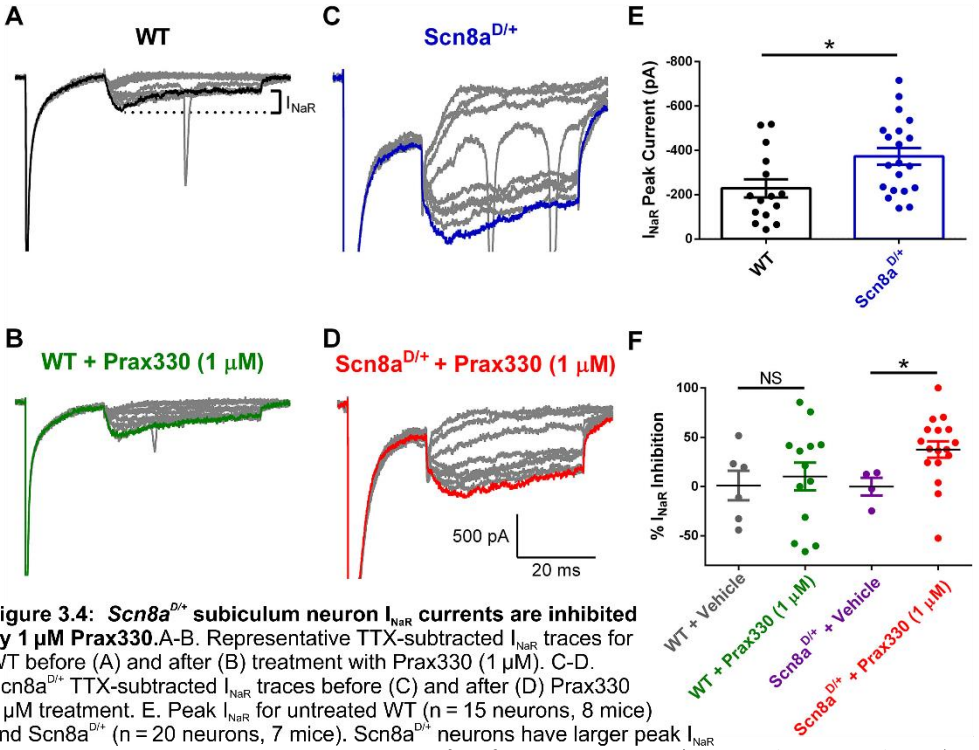

Figure 3.4: *Scn8a*$^{D/+}$ subiculum neuron I_{NaR} currents are inhibited by 1 μM Prax330. A-B. Representative TTX-subtracted I_{NaR} traces for WT before (A) and after (B) treatment with Prax330 (1 μM). C-D. Scn8a$^{D/+}$ TTX-subtracted I_{NaR} traces before (C) and after (D) Prax330 1 μM treatment. E. Peak I_{NaR} for untreated WT (n = 15 neurons, 8 mice) and Scn8a$^{D/+}$ (n = 20 neurons, 7 mice). Scn8a$^{D/+}$ neurons have larger peak I_{NaR} compared to WT neurons. F. Percent inhibition of I_{NaR} for WT plus vehicle (gray; n = 6 neurons, 3 mice), WT plus Prax330 (1 μM; green, n = 13 neurons, 5 mice), Scn8a$^{D/+}$ plus vehicle (purple; n = 4 neurons, 2 mice), and Scn8a$^{D/+}$ plus Prax330 (1 μM; red, n = 13 neurons, 5 mice). Compared to vehicle controls, Prax330 did not inhibit the steady-state I_{NaP} in WT (P > 0.05) but did inhibit I_{NaR} in Scn8a$^{D/+}$ neurons. Data shown as individual values and mean ± SEM. *P < 0.05.

Prax330 rescues hyperpolarized action potential thresholds in Scn8a$^{D/+}$ subiculum neurons

Examination of membrane properties revealed that AP thresholds were significantly hyperpolarized in *Scn8a*$^{D/+}$ (-45.6 ± 0.9 mV; n=18, 7 mice) compared to WT mice (-43.2 ± 0.7 mV; n=17 neurons, 4 mice; $T_{(33)}$=2.096; P=0.0438; Fig 3.6 A-C; Table 3.2). Notably, Prax330 (1µM) depolarized the threshold voltages in *Scn8a*$^{D/+}$ neurons to voltages observed in WT neurons, thus rescuing a critical determinant of neuronal excitability. Neither resting membrane potential (WT; -63.9 ± 0.6 mV, *Scn8a*$^{D/+}$; -62.9 ± 0.6 mV) nor membrane capacitance (WT; 37.9 ± 5.1 pF, *Scn8a*$^{D/+}$ 48.5 ± 4.7 pF) were different between WT and *Scn8a*$^{D/+}$ neurons. AP amplitude and upstroke velocity were also not different between WT and *Scn8a*$^{D/+}$neurons, but were reduced in response to Prax330 (1µM) for both genotypes, as expected for a sodium-channel blocker (Table 3.2). Surprisingly, we observed an increase in input resistance in *Scn8a*$^{D/+}$ neurons after Prax330 treatment (Table 3.2). Differences observed in rheobase, downstroke velocity, and APD_{50} between *Scn8a*$^{D/+}$ and WT neurons were not modulated by Prax330 (Table 3.2).

Effect of Prax330 (1 µM) on passive and active membrane properties in WT and *Scn8a*$^{D/+}$ subiculum neurons.

	Threshold (mV)	Input Resistance (MΩ)	Rheobase (pA)	Amplitude (mV)	Upstroke Velocity (mV/ms)	Downstroke Velocity (mV/ms)	APD50 (ms)
WT	−43.2 ± 0.8	103 ± 7	213 ± 8	93.9 ± 1.9	335 ± 26	−80 ± 2.9	1.05 ± 0.04
+ Prax330 (1 µM)	−40.1 ± 0.9[a]	112 ± 9	214 ± 14	85.6 ± 2.8[a]	277 ± 22[a]	−74 ± 4.6	1.11 ± 0.06
Scn8a$^{D/+}$	−46.2 ± 0.6[b]	153 ± 17[b]	101 ± 8	96.2 ± 2.4	336 ± 15	−56.3 ± 2.9[b]	1.37 ± 0.08[b]
+ Prax330 (1 µM)	−43.6 ± 1.2[a]	147 ± 24	128 ± 11[a]	90.9 ± 1.9[a]	278 ± 15[a]	−58.4 ± 3.6	1.40 ± 0.11

[a] Indicates p < 0.05 comparing within cell (before and after Prax330 application) using paired *t*-test.
[b] Indicates p < 0.05 comparing WT and *Scn8aD/+* groups using unpaired *t*-test.

Table 3.2: Effect of Prax330 (1 µM) on passive and active membrane properties in WT and Scn8a$^{D/+}$ subiculum neurons.

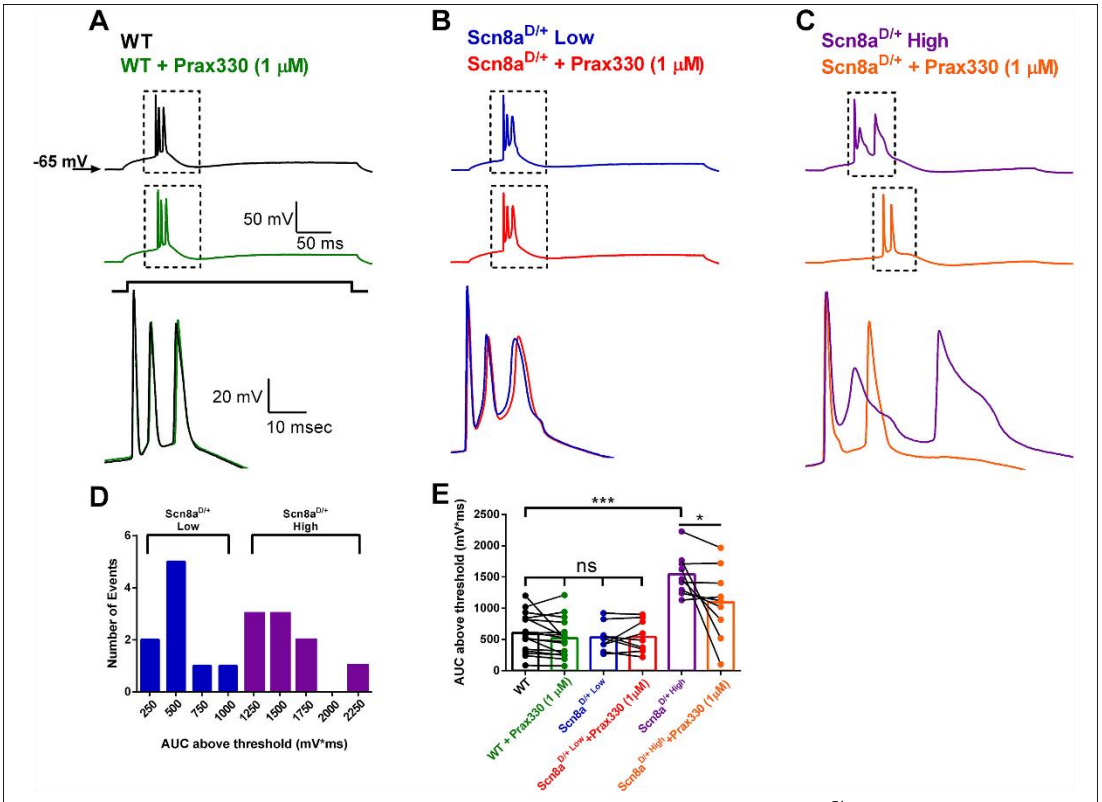

Figure 3.5: Prax330 preferentially suppresses aberrant AP-bursting in Scn8a$^{D/+}$ subiculum neurons. A. Example traces for WT before (black) and after (green) treatment with Prax330 (1 µM). B. Example traces for a low bursting Scn8a$^{D/+}$ subiculum neuron before (blue) and after (red) treatment with Prax330 (1 µM). C. Example traces for an aberrant bursting Scn8a$^{D/+}$ subiculum neuron before (purple) and after (orange) treatment with Prax330 (1 µM). Note that Prax330 (1 µM) preferentially reduces AUC in Scn8a$^{D/+}$-high bursting subiculum neurons (n = 9 neurons, 7 mice) while having little effect on low bursting subiculum neurons (n = 9 neurons, 7 mice), or WT neurons (17 neurons, 4 mice). D. Histogram of AUC data separated into Scn8a$^{D/+}$-low (blue) and Scn8a$^{D/+}$-high (purple) groups. E. Bar chart showing effects of Prax330 (1 µM) on AUC values. Data shown represent means and individual points before and after Prax330 treatment. *P < 0.05, ***P < 0.001.

Prax330 reduces synaptically-evoked action potentials in Scn8a$^{D/+}$, but not WT subiculum neurons.

The I_{NaP} strongly regulates the propensity for a neuron to initiate an AP in response to incoming synaptic excitation by amplifying synaptic inputs from dendrites (Schwindt and Crill, 1995; Stuart, 1999). Due to effects of Prax330 on I_{NaP}, we

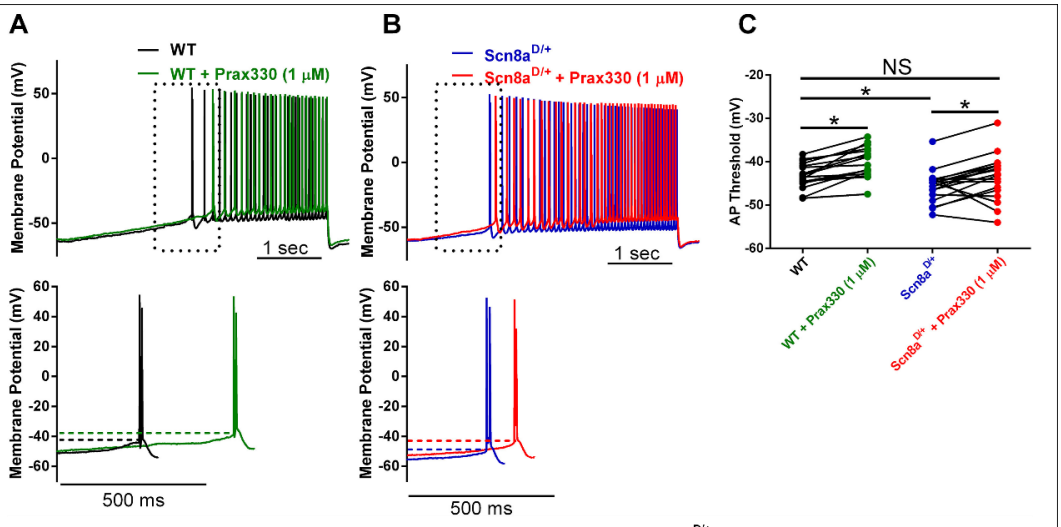

Figure 3.6: Prax330 rescues hyperpolarized AP threshold in Scn8a$^{D/+}$ subiculum neurons
A-B. Representative raw traces with APs evoked using a slow current injection ramp (100 pA/s). A. Top. WT subiculum neuron before (black) and after (green) Prax330 (1 µM) treatment. B. Top. Scn8a$^{D/+}$ subiculum neuron before (blue) and after (red) treatment with Prax330 (1 µM). Lower panels in each case show expanded trace of first action potential. Dotted lines mark action potential threshold. C. Group data for action potential (AP) threshold for WT before (black) and after (green) treatment with 1 µM Prax330 (n = 17 neurons, 4 mice) and Scn8a$^{D/+}$ before (blue) and after (red) treatment with 1 µM Prax330 (n = 18 neurons, 7 mice). Data shown represents individual points before and after Prax330 treatment. *P < 0.05.

examined the ability of Prax330 to modulate synaptically-evoked APs. In WT neurons (n= 9, 4 mice) Prax330 (1 µM) had no effect on synaptically evoked APs (Fig 3.7. A,C). In striking contrast, Prax330 (1 µM) significantly reduced the number of synaptically-evoked APs from *Scn8a*$^{D/+}$ subiculum neurons (n= 8, 4 mice; $T_{(7)}$=3.149; P=0.0162; Fig 7. B, C). This effect of Prax330 would significantly dampen the increased network excitability associated with *SCN8A* epileptic encephalopathy (Ottolini et al., 2017).

Suppression of abnormal action potential burst morphology in CA1 pyramidal neurons by Prax330.

AP waveforms from *Scn8a*$^{D/+}$ mouse CA1 pyramidal neurons exhibited prominent early after-depolarizations (EADs) that were evident during the repolarization phase of APs (Figure 3.8A-C), in agreement with previous studies (Lopez-Santiago et al., 2017). These abnormal waveforms were never observed in WT controls (Figure 3.8D). Addition of Prax330 had a profound effect on EADs, reducing their number by 41% at 500 nM and 50% at 1 µM (Figure 3.8B,C). Prax330 had no effect on AP firing frequencies from either *Scn8a*$^{D/+}$ or WT (+/+) neurons (Figure 3.8Ai-Di). Analysis of AP parameters revealed differences between *Scn8a*$^{D/+}$ and WT neurons (Table 3.3). Prax330 (1 µM) decreased AP amplitude and upstroke velocity in both *Scn8a*$^{D/+}$ and WT neurons. AP thresholds were also depolarized in *Scn8a*$^{D/+}$ neurons, but not WT (Figure 3.8E, Table 3.3). APDs were not changed (Table 3.3). Similar to our results in subiculum neurons, these findings indicate that Prx330 modulates abnormal excitability of CA1 neurons from *Scn8a*$^{D/+}$ mice.

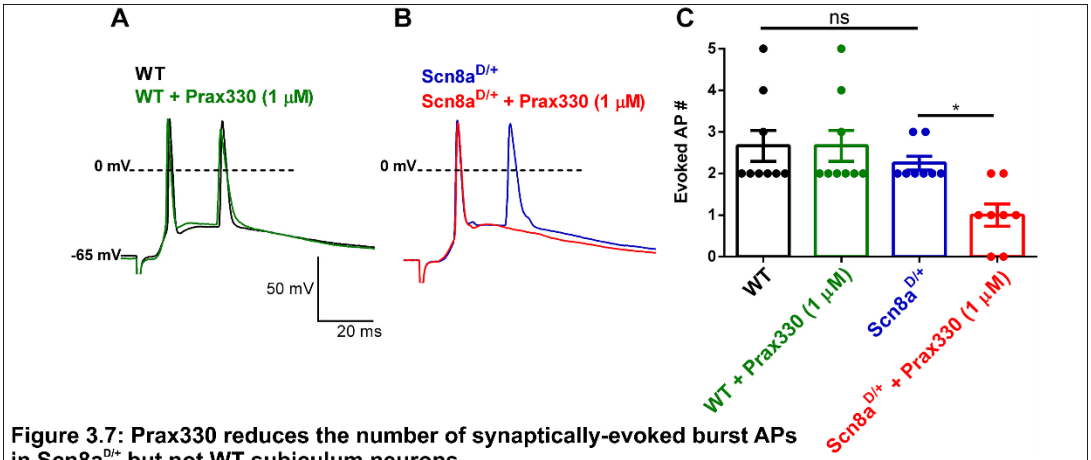

Figure 3.7: Prax330 reduces the number of synaptically-evoked burst APs in Scn8a$^{D/+}$ but not WT subiculum neurons.
A. Representative traces of WT (baseline, black; Prax330 (1 µM), green) demonstrates that Prax330 has no effect on the number of WT synaptically-evoked APs. B. Example traces of Scn8a$^{D/+}$ (baseline, blue; Prax330 (1 µM), red) demonstrates that Prax330 diminishes the number of Scn8a$^{D/+}$ synaptically-evoked APs. C. Bar chart demonstrating effects of Prax330 (1 µM) on WT and Scn8a$^{D/+}$ synaptically-evoked APs (n = 9 neurons from 4 WT mice and n = 8 neurons from 4 Scn8a$^{D/+}$ mice). Data shown represent individual points and means ± S.E.M. *P < 0.05.

Treatment with Prax330 reduces spontaneous seizures and promotes survival in Scn8a$^{D/+}$.

Previous reports showed that *Scn8a*$^{D/+}$ mice have spontaneous seizures with onset at 2 to 4 months of age, followed by death within a few days of seizure onset (Wagnon et al., 2015). To evaluate the effect of Prax330 on spontaneous seizures, mice

	Threshold (mV)	Rheobase (pA)	Input Resistance (mΩ)	Amplitude (mV)	Upstroke Velocity (mV/ms)	Downstroke Velocity (mV/ms)	AP Duration (ms)
Untreated WT	-47.4 ± 0.7	125 ± 20	169 ± 14	97.9 ± 1.0	352 ± 14	-77.5 ± 3.1	1.1 ± 0.1
WT + Prax330	-45.5 ± 1.3	116 ± 20	183 ± 15	91.3 ± 2.1*	284 ± 15**	-75.7 ± 4.2	1.1 ± 0.1
Untreated Scn8a$^{D/+}$	-43.9 ± 0.5$^{\#\#\#}$	173 ± 19$^{\#}$	149 ± 14	97.2 ± 1.4	344.4 ± 20	-54.4 ± 1.8$^{\#\#\#}$	1.4 ± 0.1$^{\#\#}$
Scn8a$^{D/+}$ + Prax330	-40.9 ± 1.1*	179 ± 26	140 ± 20	92.6 ± 2.7*	278 ± 22**	-50.4 ± 3.2	1.4 ± 0.1

Values represent mean ± SEM.
* Denotes statistical significance compared before and after Prax330 treatment using paired t-test *P<0.05, **P<0.01.
$^{\#}$Denotes statistical significance compared between WT and Scn8a$^{D/+}$ using unpaired t-test $^{\#}$P<0.05, $^{\#\#}$P<0.01, $^{\#\#\#}$P<0.001.
Table 3.3: Effect of Prax330 (1 μM) on action potential parameters in WT and Scn8a$^{D/+}$ CA1 neurons.

were continuously observed with a combination of video-EEG monitoring and continuous video monitoring for several hundred hours (Figure 3.9). Only 2 of 7 Prax330-treated mice experienced any seizures during the time of monitoring, compared with 7 of 7 untreated mice. All recorded seizures in *Scn8a*$^{D/+}$ mice initiated with a tonic phase and culminated in full tonic hindlimb extension, with the angle of hindlimbs to the torso ≥ 180°. Several of the untreated mice exhibited seizure clustering, with days of seizure freedom separating periods of high seizure frequency. Untreated *Scn8a*$^{D/+}$ mice also exhibited seizures with multiple tonic to tonic–clonic transitions. In contrast, seizures in the Prax330-treated *Scn8a*$^{D/+}$ mice had a single tonic phase that terminated with postictal suppression. Combined analysis of video-EEG and video monitoring showed that *Scn8a*$^{D/+}$ mice treated with Prax330 had significantly lower seizure frequency, with 0.3 ± 0.2 seizures/24 hours in Prax330-treated compared with 1.6 ± 0.4 seizures/24 hours in untreated mice (P<0.004, Figure 3.9A-C). No seizures were observed in WT littermate mice. These data demonstrate that Prax330 has a potent antiseizure effect in a mouse model of *SCN8A* encephalopathy.

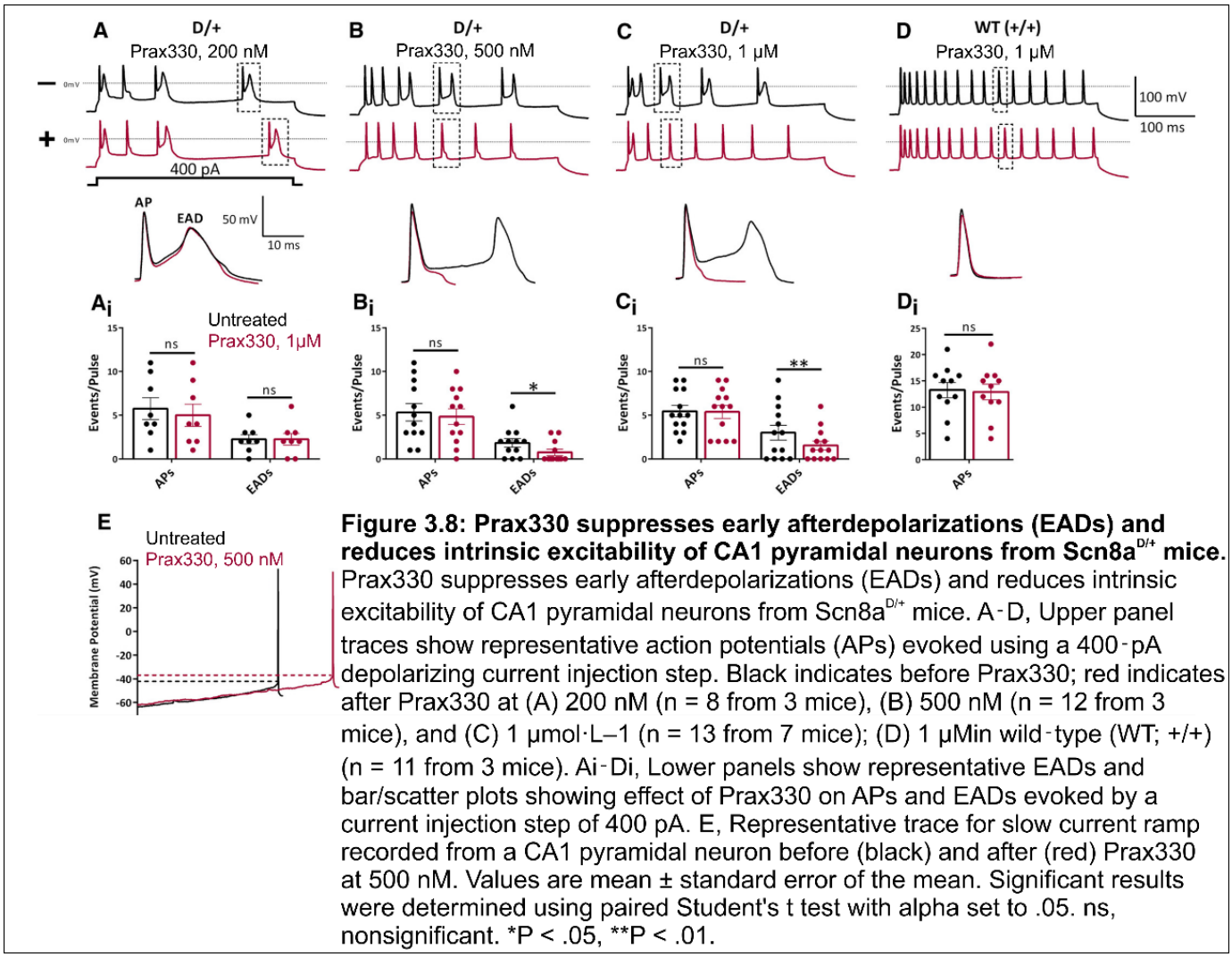

Figure 3.8: Prax330 suppresses early afterdepolarizations (EADs) and reduces intrinsic excitability of CA1 pyramidal neurons from Scn8a$^{D/+}$ mice. Prax330 suppresses early afterdepolarizations (EADs) and reduces intrinsic excitability of CA1 pyramidal neurons from Scn8a$^{D/+}$ mice. A-D, Upper panel traces show representative action potentials (APs) evoked using a 400-pA depolarizing current injection step. Black indicates before Prax330; red indicates after Prax330 at (A) 200 nM (n = 8 from 3 mice), (B) 500 nM (n = 12 from 3 mice), and (C) 1 μmol·L–1 (n = 13 from 7 mice); (D) 1 μMin wild-type (WT; +/+) (n = 11 from 3 mice). Ai-Di, Lower panels show representative EADs and bar/scatter plots showing effect of Prax330 on APs and EADs evoked by a current injection step of 400 pA. E, Representative trace for slow current ramp recorded from a CA1 pyramidal neuron before (black) and after (red) Prax330 at 500 nM. Values are mean ± standard error of the mean. Significant results were determined using paired Student's t test with alpha set to .05. ns, nonsignificant. *P < .05, **P < .01.

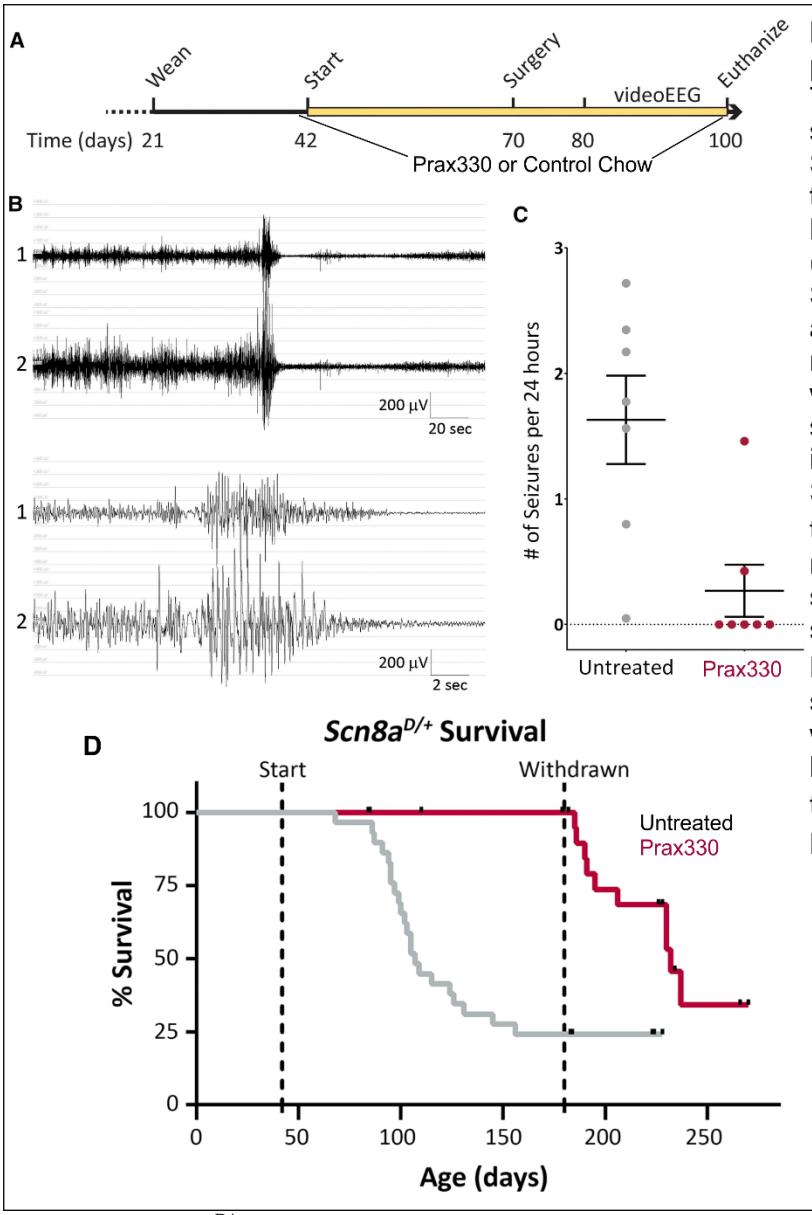

Figure 3.9: Prax330 reduces seizures and prolongs survival in Scn8a$^{D/+}$ mice. Treatment with Prax330 reduces spontaneous seizure frequency in Scn8a$^{D/+}$ mice. A, Schematic representation of timeline for treatment, surgery, and monitoring of mice. B, Representative electroencephalographic (EEG) trace of an electrographic seizure in an Scn8a$^{D/+}$ mouse. Channel 1 indicates left anterior to right anterior; channel 2 indicates right anterior to left posterior. Upper panel, 5 min window. Lower panel, expanded timescale of seizure shown in upper panel. C, Seizure incidence frequency was significantly lower in Scn8aD/+ mice treated with Prax330 compared to untreated mice ($P < .004$; Mann-Whitney test; n = 7 per group). Symbols represent mean ± standard error of the mean. D. A, Kaplan–Meier survival curves comparing untreated and Prax330-treated Scn8a$^{D/+}$ mice. Treatment was started at 6 weeks of age (first dashed line) and was withdrawn at 6 months (second dashed line). Survival was significantly different between treatment groups ($P < .001$; n = 29-32; Mantel-Cox log-rank test).

Survival of *Scn8a*$^{D/+}$ mice is limited, with <50% of mice surviving to 6 months of age (Wagnon et al., 2015). To determine whether chronic treatment with Prax330 would extend survival, *Scn8a*$^{D/+}$ mice were fed chow containing Prax330 (estimated dose = 1.5 mg/kg/d) beginning at 6 weeks and continuing until 6 months of age. This dose was previously shown to be anticonvulsant in *Scn2a*^{Q54} and *Scn1a* $^{+/-}$ mouse models and does not produce any signs of behavioral toxicity or sedation (Anderson et al., 2014, 2017). Treatment with Prax330 beginning at 6 weeks and continuing to 6 months of age completely rescued premature lethality of *Scn8a*$^{D/+}$ mice, with 100% of Prax330-treated mice (n = 32) surviving to 6 months of age, compared with only 24% of untreated mice (7/29; $P < .001$, Mantel-Cox log-rank). Removal of the Prax330 chow at 6 months of age resulted in rapid loss of protection, and 65% of the previously treated mice died within the following 3 months (Figure 3.9D). Loss of Prax330 benefit following withdrawal suggests that it acts primarily as an anticonvulsant rather than a disease-modifying treatment.

Discussion

In this chapter, I have demonstrated that 1) subiculum and CA1 neurons from a mouse knock-in model expressing the patient mutation N1768D (*Scn8a*$^{D/+}$) have pro-excitatory firing properties associated with elevated I_{NaP} and I_{NaR} channel currents compared to WT littermates, 2) Prax330, a novel VGSC inhibitor, modulates inactivation parameters of WT and N1768D $Na_V1.6$ currents, causing hyperpolarizing shifts in inactivation parameters and inhibiting I_{NaP} observed in N1768D cells, 3)

in *Scn8a*$^{D/+}$ subiculum neurons, Prax330 reduces I_{NaP} and I_{NaR} and selectively suppresseses abnormal burst-firing in both subiculum and CA1 neurons, and 4) Prax330 reduces spontaneous seizure frequency and prolongs survival in *Scn8a*$^{D/+}$ mice.

Elevated I_{NaP} has been implicated in facilitating neuronal hyperexcitability associated with epilepsy. Many gain-of-function mutations in $Na_V1.1$, $Na_V1.2$, $Na_V1.3$, and $Na_V1.6$ display an increased I_{NaP} (Blanchard et al., 2015; Holland et al., 2008; de Kovel et al., 2014; Liao et al., 2010; Lossin et al., 2002; Ottolini et al., 2017; Rhodes et al., 2004; Veeramah et al., 2012; Wagnon and Meisler, 2015; Wengert and Patel, 2021; Zaman et al., 2018). Increased I_{NaP} has been reported in animal models of temporal lobe epilepsy and in human epilepsy patients (Agrawal et al., 2003; Barker et al., 2017; Chen et al., 2011; Hargus et al., 2013; Stafstrom, 2007; Vreugdenhil et al., 2004). Increased I_{NaP} induces aberrant neuronal excitability, producing large burst AP events, leading to seizures in rodents (Alkadhi and Tian, 1996; Mantegazza et al., 1998; Otoom and Alkadhi, 2000; Otoom et al., 2006), and suppression of I_{NaP} by ASMs is considered an important mechanism of action (Stafstrom, 2007; Wengert and Patel, 2021). Consistent with these observations, preferential inhibitors of I_{NaP} have shown promise in animal models of epilepsy (Anderson et al., 2014; Romettino et al., 1991; Urbani and Belluzzi, 2000). Prax330 was originally developed as an antiarrhythmic drug due to its ability to target I_{NaP} generated by the cardiac sodium channel, $Na_v1.5$ (Belardinelli et al., 2013; Potet et al., 2016; Sicouri et al., 2013). In this study, I demonstrate that Prax330 is a potent inhibitor of neuronal I_{NaP}, with effects not only on the mutant $Na_v1.6$- N1768D channel expressed in a neuron-derived cell line, but also on subiculum neurons in acute brain slices. Since I_{NaP} is thought to provide sustained depolarization after an initiated AP and amplify synaptic inputs from distal dendrites to facilitate repetitive and/or burst-firing of APs, suppression of these currents is predicted to suppress epileptiform burst firing (Harvey et al., 2006; Schwindt and Crill, 1995; Stuart, 1999; Stuart and Sakmann, 1995; Yamada-Hanff and Bean, 2013). In agreement with this prediction, Prax330 normalized the AP-burst waveform in *Scn8a*$^{D/+}$ CA1 pyramidal neurons without an effect on WT AP firing (Baker et al., 2018). Here, I show that Prax330 is particularly effective at modulating subiculum neurons with large, abnormal AP waveforms, and has little effect on APs that did not display epileptiform morphology. I suggest that these aberrantly firing neurons likely exhibited larger I_{NaP} and/or I_{NaR} currents, accounting for their sustained depolarization and prolonged neuronal excitation. Selective inhibition of epileptiform neurons enhances the therapeutic potential of Prax330 and could reduce side effects.

The I_{NaR} is a slow inactivating depolarizing current that can contribute to increased AP frequency and burst firing by providing additional depolarization during the falling phase of an AP (Khaliq et al., 2003; Raman and Bean, 1997; Raman et al., 1997). Increases in I_{NaR} have been reported in animals models of epilepsy and are also considered therapeutic targets in epilepsy (Hargus et al., 2013; Jarecki et al., 2010; Khaliq et al., 2003; Patel et al., 2016). Here, I show that *Scn8a*$^{D/+}$ subiculum neurons have elevated I_{NaR} that are suppressed by Prax330. Recent studies indicate that inhibition of I_{NaR} is an important mechanism of action of cannabidiol, a compound with promise in treating different types of epilepsy including genetic epilepsies (Devinsky et al., 2016a, 2017; Kaplan et al., 2017; Khan et al., 2018; Patel et al., 2016). However, recent evidence suggests that cannabidiol also inhibits the transient sodium current making these studies somewhat inconclusive regarding the specific role of I_{NaR} in epilepsy (Ghovanloo et al., 2018).

I evaluated the effects of Prax330 on subiculum and CA1 neurons because they provide a major outputs from the hippocampus proper and are an important anatomical site affecting seizure initiation (Fujita et al., 2014; Toyoda et al., 2013). It has been proposed that synaptic connection from CA1 neurons to subiculum neurons is reorganized in epilepsy leading to increased excitation of subiculum neurons (Cavazos et al., 2004; de Guzman et al., 2006). Subiculum neurons from epileptic rodents have elevated I_{NaP} and I_{NaR} leading to hyperexcitability (Barker et al., 2017; de Guzman et al., 2006; Wellmer et al., 2002). Similarly, Vreugdenhil and colleagues demonstrated that I_{NaP} is elevated in a subset of subiculum neurons from human epilepsy patients (Vreugdenhil et al., 2004). Only a subset (~50 %) of the recorded neurons had elevated I_{NaP}, leading to the hypothesis of two distinct neuronal populations distinguished by I_{NaP} levels. My data are consistent, having a similar heterogeneity in *Scn8a*$^{D/+}$ subiculum neurons.

The results shown here indicate that Prax330 is able to reduce seizures and prolong survival in *Scn8a*$^{D/+}$ mice. Previous studies showed that Prax330 was efficacious in *Scn1a*$^{+/-}$, *Scn2a*^{Q54}, and *Scn8a*$^{W/+}$ mouse models of epileptic encephalopathies providing support for the notion that impaired inactivation may be a commonality across epileptic encephalopathies caused by VGSC mutations (Anderson et al., 2014, 2017; Baker et al., 2018; Bunton-Stasyshyn et al., 2019). Overall, our data encourage ongoing investigation of Prax330 for clinical use, and support other efforts to develop VGSC inhibitors that preferentially inhibit persistent and resurgent sodium currents to be used as ASMs.

Chapter IV: Adrenergic mechanisms of seizure-induced sudden death in a mouse model of *SCN8A* encephalopathy

Rationale

Gaining a mechanistic understanding of seizures in *SCN8A* encephalopathy is limited due in part to the unpredictable nature of seizures both in patients and in mouse models of *SCN8A* encephalopathy. Recently, our lab serendipitously found that the *Scn8a*$^{D/+}$ (D/+) and mouse model of *SCN8A* encephalopathy is sensitive to audiogenic seizures and seizure-induced death in response to high-intensity acoustic stimulation. In adult D/+ mice, these audiogenic seizures are nonfatal and have nearly identical behavioral, electrographical, and cardiorespiratory characteristics as spontaneous seizures. In contrast, at postnatal days 20-21, D/+ mice exhibit the same seizure behavior, but have a significantly higher incidence of seizure-induced sudden death following the audiogenic seizure. Seizure-induced death was prevented by either stimulating breathing via mechanical ventilation or by acute activation of alpha-1 adrenergic receptors. Conversely, in adult D/+ mice inhibition of alpha-1 adrenergic receptors converted normally nonfatal audiogenic seizures into fatal seizures. Taken together, our studies show that in our novel audiogenic seizure-induced death model adrenergic receptor activation is necessary and sufficient for recovery of breathing and prevention of seizure-induced death.

Introduction

Sudden unexpected death in epilepsy (SUDEP) is devastating occurrence for which patients with *SCN8A* encephalopathy have a substantial risk. Due to the unpredictable nature for instances of SUDEP however, clinical mechanisms of death remain elusive. To circumvent this issue, several rodent models have been developed in recent years to gain mechanistic insights into SUDEP. Most clinical SUDEP cases are believed to occur after generalized tonic-clonic seizures (Bird et al., 1997; Dasheiff and Dickinson, 1986; Nilsson et al., 1999; Ryvlin et al., 2013; So et al., 2000). Thus, animal models in which death occurs immediately after convulsive seizures are used to study SUDEP. Such models include the DBA/1&2, *Cacna1a*^{S218L}, *Scn1a*^{R1407X}, *RyR2*^{R176Q}, *Scn1a* KO, and *Kcna1* KO mouse models as well as inducible kainic acid and maximal electroshock seizure models. These approaches have fueled various hypotheses concerning the mechanisms of SUDEP, including brainstem spreading depolarization (Aiba and Noebels, 2015; Aiba et al., 2016; Jansen et al., 2019; Loonen et al., 2019), autonomic dysregulation and cardiac arrhythmias (Auerbach et al., 2013; Glasscock et al., 2010; Kalume et al., 2013), and respiratory arrest due to central (Buchanan et al., 2014a; Faingold et al., 2010; Kim et al., 2018; Kruse et al., 2019), or obstructive apnea (Irizarry et al., 2020; Nakase et al., 2016; Villiere et al., 2017). Of these models, only the Dravet Syndrome models (i.e. *Scn1a*^{R1407X} and *Scn1a* KO) directly represent a patient population that is susceptible to SUDEP (Escayg and Goldin, 2010; Kim et al., 2018). The genetic etiologies of *DBA*/1&2, *Cacna1a*^{S218L}, *RyR2*^{R176Q}, *Lmx1b*$^{f/f/p}$, and *Kcna1* KO mice are either unknown, identified from non-epilepsy patient populations, or are manipulations that lead to loss of an entire cell population, receptor subtypes, or ion channels, which are not known to occur in epilepsy patients.

In this chapter, my colleagues and I demonstrate the ability to evoke seizures on demand in D/+ mice using high-intensity sound. These evoked seizures are nearly identical to spontaneous seizures with respect to behavioral, electrographic, and cardiorespiratory parameters. We also serendipitously determined a developmental window in which audiogenic seizures almost always (~85%) lead to seizure-induced death. Using our audiogenic seizure model, we demonstrate that 1) the primary cause of seizure-induced death is respiratory arrest that is initiated during the tonic phase, 2) nonfatal seizures also present with transient apnea but breathing recovers after the tonic phase, 3) peri-ictal alpha-1 adrenergic receptor activity is both necessary and sufficient for survival after a tonic-clonic seizure, and 4) the mechanism of action for adrenergic stimulation is breathing recovery after initial tonic phase apnea.

Methods

Mice

All mice were housed and maintained in accordance with the Animal Care and Use Committee standards of the University of Virginia in a temperature and humidity-controlled vivarium with a standard 12-hour light/dark cycle with food and water *ad libitum*. Both male and female mice were used in roughly equal numbers, and no sex differences were observed for any of the experiments based on seizure behavior or risk of sudden death.

Genotyping

Genotyping of transgenic mice was done using standard PCR techniques with DNA acquired from tail biopsies. Genotyping of D/+ mice was performed as previously described (Wagnon et al., 2015), using the primers 5'-TGACT GCAGC TTGGA CAAGG AGC-3' and 5'-TCGATGGTGT TGGGC TTGGG TAC-3'. The resulting PCR product, a 327 bp genomic fragment of *SCN8A* containing the mutation, was then digested with HincII which generates a single fragment of 327 bp for the wild type allele and two fragments of 209 and 118 bp for the mutant allele.

Audiogenic seizure assessment

To test for audiogenic seizures mice were taken from their home cage and transferred to a clean test cage where they were allowed to acclimate for ~20 seconds before the onset of the acoustic stimulus. Similar to a method described previously (Martin et al., 2020), a sonicator (Branson 200 ultrasonic cleaner) was used to produce the audiogenic stimulus directly adjacent to the test cage. The stimulus duration lasted for 50 seconds or until the animal had a behavioral seizure.

Audiogenic seizures were recorded using a laptop webcam. Duration of seizure phases were analyzed by taking the time in seconds that the mouse spent in each of the phases: a wild-running phase characterized by fast circular running throughout the cage, a tonic phase characterized by hindlimb extension and muscle rigidity, a clonic phase typified by myoclonic jerking of the hindlimbs, and recovery exemplified when the mouse ceased myoclonic jerking and righted itself. In cases where death occurred, the end of the tonic phase was apparent at the point of hindlimb muscle relaxation. For all experiments involving rescue of seizure-induced sudden death, at least one control mouse from the experimental litter was confirmed to experience seizure-induced sudden death before conducting any rescue experiments on remaining littermates.

Surgical preparation

Custom electrocorticogram/electrocardiogram (ECoG/ECG) headsets (PlasticsOne, Inc., or Pinnacle Technology Inc.) were implanted in 6-10-week-old D/+ mice using standard aseptic surgical techniques. Anesthesia was induced with 5% and maintained with 0.5%–3% isoflurane. Adequacy of anesthesia was assessed by lack of toe-pinch reflex. A midline skin incision was made over the skull, and burr holes were made at the lateral/rostral end of both the left and right parietal bones to place EEG leads, and at the interparietal bone for a reference and ground electrodes. Two ECG leads were passed subcutaneously to the left abdomen and right shoulder and sutured into place to approximate a lead II arrangement. The headsets were attached to the skull with dental acrylic (Jet Acrylic; Lang Dental). Mice received postoperative analgesia with meloxicam (0.5-1 mg/kg, i.p.) or ketoprofen (5 mg/kg, i.p.) and 0.9 % saline (0.5 ml i.p.) and were allowed to recover a minimum of 2-5 days prior to experiments.

Recording of ECoG, ECG, and breathing for spontaneous seizures

After recovery from surgery, mice were individually housed in custom-fabricated plethysmography chambers and monitored 24 hours a day. Plethysmography chambers were built to comply with requirements for continuous housing described in the Guide for the Care and Use of Laboratory Animals (Council, 2011). The floor of the chambers had approximate dimensions of 4.5 x 4.5 inches (> 20 sq. inches) and 7 inches tall. There were ports for air in and air out, and for pressure monitoring. The chamber was supplied with a continuous flow of room air at approximately 400 ml/min via supply and exhaust air pumps (MK-1504 Aquarium Air Pump; AQUA Culture) balanced to maintain chamber pressure near atmospheric. Mice had access to a continuous supply of water and food. The surgically implanted headsets were attached to a custom low torque swivel cable, allowing mice to move freely in the chamber.

To assess breathing frequency, the pressure of the epilepsy monitoring unit chamber was measured with an analogue pressure transducer (SDP1000-L05; Sensirion). ECoG and ECG signals were amplified at 2000 and bandpass filtered between 0.3 -100 Hz and 30 - 300 Hz, respectively, with an analogue amplifier (Neurodata Model 12, Grass Instruments Co.). Biosignals were digitized with a Powerlab 16/35 and recorded using LabChart 7 software (AD Instruments, Inc.) at 1 kS/s. Video acquisition was performed by multiplexing four miniature night vision-enabled cameras and then digitizing the video feed with a Dazzle Video Capture Device (Corel, Inc.) and recording at 30 fps with LabChart 7 software in tandem with biosignals.

Recording of ECoG, ECG, and breathing for audiogenic seizures

For simultaneous ECoG, ECG, and breathing during audiogenic seizures, the same surgical procedure and experimental setup described above was used. Although mice remained in the chambers 24 hours a day, recording only took place during periods of audiogenic seizure stimulation. To induce audiogenic seizures, a 15 kHz signal was generated using Tone Generator software (NCH Software, Inc.), amplified using a Kinter K3118 stereo amplifier (Kinter USA), and converted to sound using a small 3-watt speaker lowered into the plethysmography chamber.

For recording of only breathing in pharmacological experiments, non-implanted mice were placed in the chambers immediately after injection of pharmacological agents. Stimulation of audiogenic seizures and recording of breathing were performed as described above.

Breathing and heart rate detection

Individual breaths and heart beats were identified as inspiratory deflections in the pressure transducer signal and R waves in the ECG signal, respectively, using Spike2 software (Cambridge Electronic Design, Ltd.). A breath was scored when the downward deflection went below a certain hysteresis value determined by the experimenter and rose back above a threshold of 0 mV. The minimum time between breaths was set to 0.05 s. Similarly, an R wave was identified when an upward deflection crossed a threshold value determined by the experimenter. The minimum time between R waves was set to 0.02 s. All breaths and R waves were inspected by the experimenter.

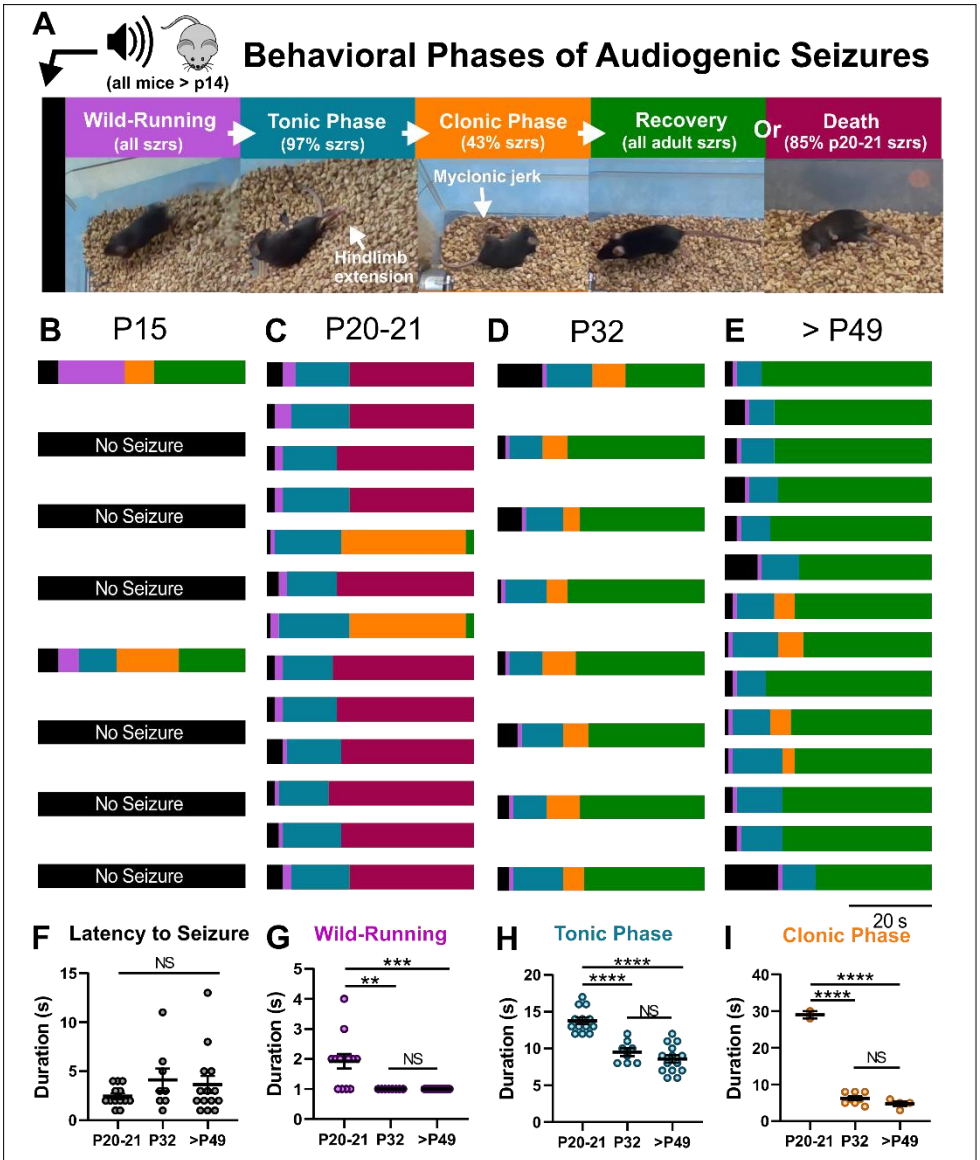

Figure 4.1: Audiogenic seizures and sudden death in D/+ mice
A. In response to high-intensity acoustic stimulation, D/+ mice exhibit wild-running (purple), a tonic phase characterized by hindlimb extension (teal), a clonic stage (orange) characterized by rapid kicking of the hindlimbs, and recovery (green) as the animal rights itself and resumes normal movement throughout the cage, or sudden death (magenta). B-E. Audiogenic seizure behavioral progression in each mouse at developmental time points P15 (B), P20-21 (C), P32 (D), and P49-P69 (E). B. Only 2 of 8 D/+ mice at P15 exhibited audiogenic seizures. C. All 13 D/+ mice at P20-21 experienced audiogenic seizures, and 11 of 13 died directly following the tonic phase. The two that recovered did so after a relatively extended clonic phase. D. At P32, all 8 D/+ mice had audiogenic seizures and recovered. E. In adult D/+ mice (P49-P69), all mice experienced seizures followed by recovery. F-I. Duration of seizure phases, latency to seizure onset (F), wild-running (G), tonic phase (H), and clonic phase (I) for D/+ mice ages P20-21 (n=13), P32 (n=8), and P49-P69 (14). **, ***, ****, and NS indicate P < 0.01, 0.001, 0.0001, > 0.2, respectively, for post hoc comparison between age groups.

Mechanical ventilation

For the mechanical ventilation of P20-21 D/+ mice during an audiogenic seizure, we quickly placed a custom-made 3 mL pipet which fit snuggly over the mouse's nose and mouth and provided regular pulses of air (~1 mL at 2 Hz). The ventilation

was terminated after the mouse initiated gasping behavior or 20 s after the animal experienced sudden death. A full video of this procedure is available (Video 4.4).

Adrenergic receptor pharmacology

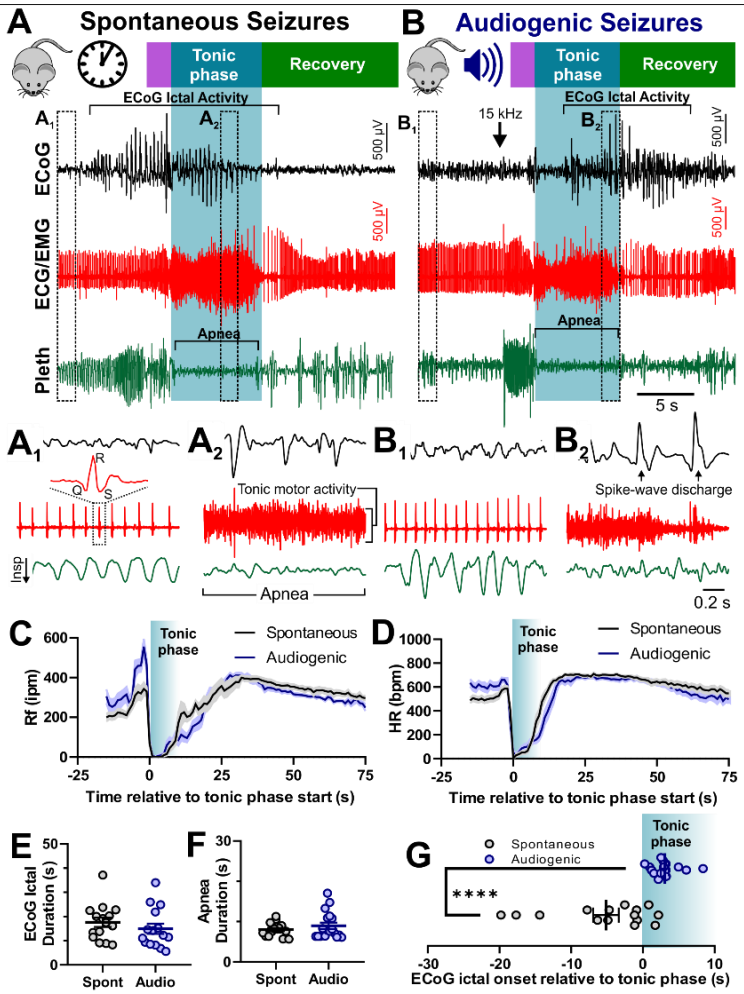

Figure 4.2: Audiogenic seizures resemble spontaneous seizures in D/+ mice
A-B. Example traces of electrocorticogram activity (ECoG), electrocardiogram activity (ECG/EMG), and breathing activity (Pleth) during example spontaneous (A) and audiogenic seizures (B). Stages of seizure behavior are indicated above the traces: Wild-running (purple), tonic phase (blue), and recovery (green). ECoG ictal activity, bradycardia, and apnea are each highlighted in brackets. Arrow indicates onset of 15 kHz acoustic stimulation (B). A1 and A2. Expanded data traces from regions indicated in A. B1 and B2. Expanded data traces from regions indicated in B. Note the high degree of tonic muscle activity and apnea in A2 and B2. C. Average breathing frequency (Rf) binned every second during spontaneous (black, n=16 seizures recorded from 4 mice) and audiogenic (blue, n=15 seizures recorded from 7 mice) seizures. D. Average heart rate (HR) binned every second during spontaneous (black, n=16 seizures recorded from 4 mice) and audiogenic (blue, n=12 seizures recorded from 7 mice) seizures. E. ECoG ictal duration for spontaneous (black, n=15 seizures recorded from 4 mice) and audiogenic (blue, n=15 seizures recorded from 6 mice) seizures. F. Apnea duration for spontaneous (black, n=16 seizures recorded from 4 mice) and audiogenic (blue, n=18 seizures recorded from 7 mice) seizures. G. Time of ictal onset relative to tonic phase. Audiogenic seizures (blue, n=15 seizures recorded from 6 mice) exhibit delayed onset of ECoG ictal activity relative to tonic phase compared to spontaneous seizures (black, n=15 seizures recorded from 4 mice) in D/+ mice. **** indicates P < 0.0001 comparison between genotypes.

All chemicals were purchased from Sigma Aldrich and were either of pharmaceutical grade or were sterile filtered prior to injection. Injections were given intraperitoneal in a volume of 50-100 µl sterile saline per mg of mouse weight (e.g. 0.1 mL for a 20 mg adult mouse). The concentration of each drug was based on the achieving the desired dosages of 2 mg/kg epinephrine HCl, 2 mg/kg norepinephrine HCl, and 3 mg/kg phenylephrine HCl, 10 mg/kg sotalol HCl, and 1 mg/kg prazosin HCl. Injection of 50-100 ul sterile saline per mg of mouse weight was used as control.

Statistical analysis

All interventions were conducted and analyzed with the experimenter blinded, except for mechanical ventilation. All data points denote biological replicates (i.e. no animal was used more than once for the same test), except for data comparing spontaneous and audiogenic seizures, which are technical replicates and the animal numbers are reported in the figure legend. All average data values are mean ± SEM. Statistics were computed using GraphPad Prism version 7 or later (GraphPad Software, Inc.) and comparisons were considered statistically significant when $P < 0.05$. Differences between two groups were assessed by unpaired, two-tailed Student's t-test when distributions passed the D'Agnostino-Pearson Omnibus normality test and Mann-Whitney non-parametric test when any distribution failed to pass the normality test. Differences between more than two groups were assessed by one-Way or two-Way ANOVA followed by Holm-Sidak's or Sidak's multiple comparison tests, respectively. For the few cases where residuals of one-Way ANOVAs failed the D'Agnostino-Pearson Omnibus normality test ($P<0.05$), we used the Kruskal-Wallis nonparametric

test followed by Dunn's multiple comparisons test. Comparison of survival proportions was done using a one-sided Fisher's exact test.

Results

Characterization of audiogenic seizure behavior in D/+ mice

We serendipitously discovered that D/+ mice are susceptible to audiogenic seizures when a sonicator (Branson 200 Ultrasonic cleaner) was turned on in close proximity to D/+ mice. Further investigation using the same acoustic stimulus revealed that D/+ mice at ages P20-21, P32, and P49-P69 exhibit stereotyped seizure behaviors; wild-running followed by a tonic phase with hindlimb extension that was, in some cases, followed by a clonic phase consisting of myoclonic leg jerking (Fig. 4.1A; Video 4.1). Only 2 of 8 D/+ mice were sensitive to audiogenic seizures at P15 (Fig. 4.1B), which we attribute to the fact that mice at this age are likely still developing their auditory system. Strikingly, all 13 D/+ mice tested at P20-21 experienced audiogenic seizures, 11 of which succumbed to sudden death immediately following the seizure (Fig. 4.1C; Video 4.2). In contrast, no deaths were observed in D/+ mice at P32 (n=8) or P49-69 (n=14) even though all mice experienced an audiogenic seizure (Fig. 4.1D-E). Further characterization of the audiogenic seizures revealed that there were no differences in latency to seizure (P=0.25; $F_{2,32}$=1.460; Fig. 4.1F) although P20-21 D/+ mice experienced seizures with longer wild-running (**P = 0.0017 and ***P<0.0002, respectively; Dunn's multiple comparisons test; Fig. 4.1G), tonic (****P < 0.0001 for both comparisons; $F_{2,32}$ = 32.99, Figure 4.1H), and clonic (****P < 0.0001 for both comparisons; $F_{2,32}$ = 211.5, Fig. 4.1I) phases compared to D/+ mice of ages P32 and P49-69. No seizures were observed in WT littermates exposed to the same acoustic stimulus (n=37; Video 4.3). It should be noted that due to the high incidence of death at P20-21, we only observed two instances of a clonic phase; thus, the statistical difference between ages in Fig. 4.1I should be interpreted with appropriate caution.

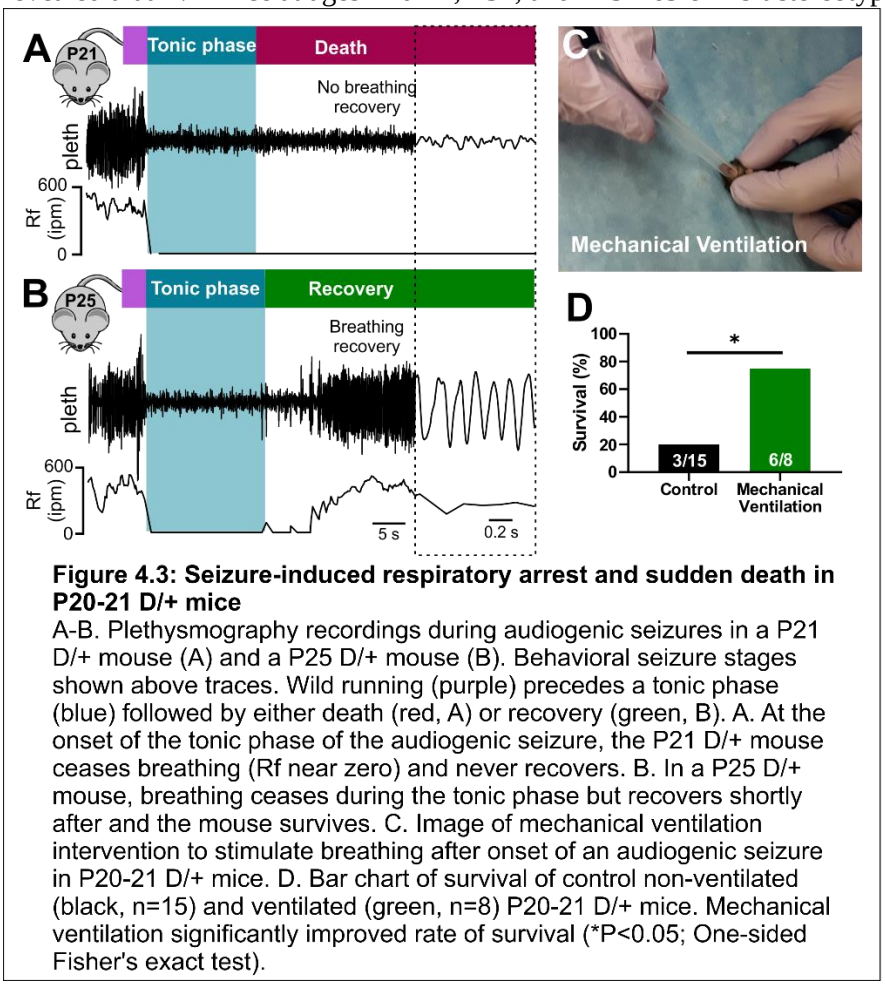

Figure 4.3: Seizure-induced respiratory arrest and sudden death in P20-21 D/+ mice
A-B. Plethysmography recordings during audiogenic seizures in a P21 D/+ mouse (A) and a P25 D/+ mouse (B). Behavioral seizure stages shown above traces. Wild running (purple) precedes a tonic phase (blue) followed by either death (red, A) or recovery (green, B). A. At the onset of the tonic phase of the audiogenic seizure, the P21 D/+ mouse ceases breathing (Rf near zero) and never recovers. B. In a P25 D/+ mouse, breathing ceases during the tonic phase but recovers shortly after and the mouse survives. C. Image of mechanical ventilation intervention to stimulate breathing after onset of an audiogenic seizure in P20-21 D/+ mice. D. Bar chart of survival of control non-ventilated (black, n=15) and ventilated (green, n=8) P20-21 D/+ mice. Mechanical ventilation significantly improved rate of survival (*P<0.05; One-sided Fisher's exact test).

Audiogenic and spontaneous seizures have similar semiology

We recorded spontaneous and audiogenic seizures from adult D/+ mice with standard rodent video/electrocorticogram (ECoG) techniques. In addition, we simultaneously recorded muscle/cardiac function and breathing frequency via electrocardiogram (ECG)/electromyogram (EMG) activity and plethysmography, respectively (Fig. 4.2). Both spontaneous and audiogenic seizures presented with a series of cortical spike-wave discharges in addition to a period noted by a large amount of tonic muscle activity, apnea, and bradycardia that coincides with the behavioral tonic phase (Fig. 4.2A-B). We found no differences in ictal or postictal breathing (Fig. 4.2C) or heart rate (Fig. 4.2D), nor ECoG spike-wave discharge (Fig. 4.2E) or apnea duration (Fig. 4.2F) between spontaneous and audiogenic seizures. We did observe a robust increase in respiratory frequency upon audio stimulation that was unsurprisingly, not observed in the spontaneous seizure type (Fig. 4.2C, -5 to 0 s). Interestingly, we found that the onset of ECoG spike-wave discharge always occurred after the initiation of the tonic phase in audiogenic seizures, whereas it typically preceded the tonic phase in spontaneous seizures (P = 0.0001,

t = 4.384, df = 28; Fig. 4.2G). These studies suggest that audiogenic and spontaneous seizures in D/+ mice are comparable, sharing highly similar, if not identical, mechanisms.

Audiogenic seizure-induced death is due to lack of breathing recovery after the tonic phase

While both cardiac and respiratory arrest have been suggested as mechanisms of SUDEP, the primary mechanism of death remains debated (Devinsky et al., 2016b; Massey et al., 2014). To examine breathing activity during terminal seizures, we conducted plethysmography recordings of P20-21 D/+ mice during audiogenic seizures (Figure 4.3). Audiogenic seizure-induced death observed in P20-21 D/+ mice occurred when apnea was initiated during the tonic phase and breathing failed to recover (Fig. 4.3A). In mice only a few days older (P25), breathing resumed immediately after the tonic phase and all mice tested survived (n = 7; Fig. 4.3B). This data supports the notion that at a critical time point of P20-21, a lack of breathing recovery causes seizure-induced death.

Stimulation of breathing via mechanical ventilation has been shown to rescue seizure-induced respiratory arrest in other mouse models of SUDEP (Faingold et al., 2010; Kim et al., 2018). Our novel ability to evoke seizures on command allowed us to assess whether this intervention could also rescue P20-21 D/+ mice. We performed mechanical ventilation (approximately 1 mL at 2 Hz delivered manually) to mice immediately after the onset of the tonic phase (Fig. 4.3C; Video 4.4). While only three of 15 non-ventilated mice survived, six of the eight mice that were ventilated survived (*P<0.05; One-sided Fisher's exact test; Fig. 4.3D), demonstrating that respiratory arrest is the primary cause of seizure-induced death in P20-21 D/+ mice.

Exogenous adrenergic receptor stimulation is sufficient for recovery breathing and survival of audiogenic seizures in adult D/+ mice.

Activation of adrenergic receptors has been shown to stimulate respiration in animals and humans (Whelan and Young, 1953; Zhang et al., 2017; Zhao et al., 2017). To determine if acute activation of adrenergic receptors could stimulate breathing and prevent audiogenic seizure-induced death, we injected P20-21 D/+ mice with either 2 mg/kg norepinephrine (NE) or an equal volume of sterile saline via intraperitoneal injection (i.p.) 1-min prior to audiogenic seizure stimulation (Figure 4A). Saline injection had no effect on survival and was not different from non-injected mice (n=13; P = 0.6; One-sided Fisher's exact test; Fig 4.4E). In contrast, injection of NE resulted in breathing recovery and increased survival (10 of 13 mice) compared to saline injection (3 of 13 mice) (*P<0.05; One-sided Fisher's exact test; Fig. 4.4E; Video 4.5). Despite relatively low sample size, 2 mg/kg epinephrine (Epi) rescued only one of the five mice indicating that it did not strongly improve survival as observed with NE (Fig. 4.4E). Based on the fact that NE primarily stimulates the alpha adrenergic receptors (Motiejunaite et al., 2020), we decided to test whether selective alpha-1 receptor agonism might prevent seizure-induced death. Injection of 3 mg/kg phenylephrine (PE) promoted postictal breathing

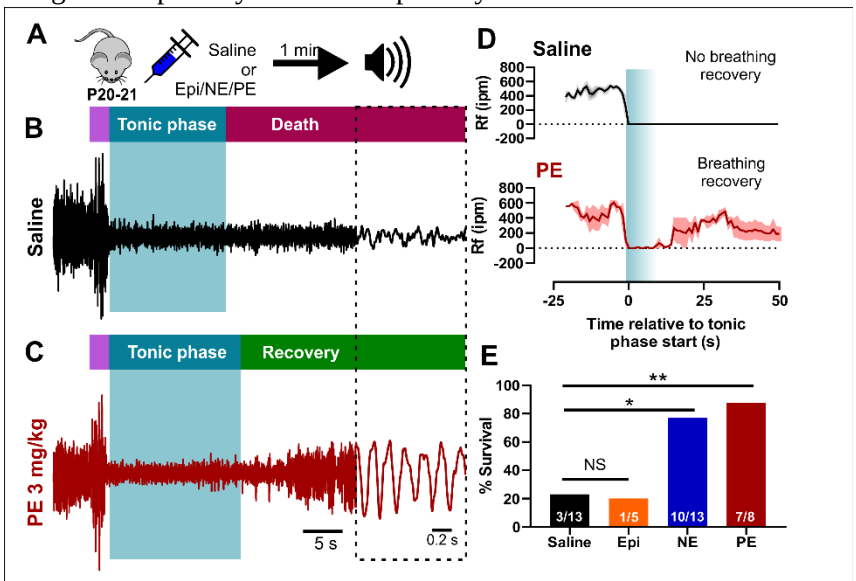

Figure 4.4: Acute activation of alpha-1 adrenergic receptors rescues seizure-induced sudden death in P20-21 D/+ mice
A. P20-21 D/+ mice were injected (i.p.) with saline, 2 mg/kg epinephrine (Epi), 2 mg/kg norepinephrine (NE), or 3 mg/kg phenylephrine (PE) 1-minute before stimulating an audiogenic seizure. B-C. Example plethysmography recordings of breathing during audiogenic seizures in P20-21 D/+ mice injected with saline control (black; B) or PE (red; C) 1 minute before acoustic stimulation. In the saline-treated mouse, breathing ceased during the tonic phase and never recovered leading to death. In the PE-treated mouse, breathing also ceased during the tonic phase but recovered and the mouse survived. D. Average breathing rates binned every second for saline-treated (black, n=5) and PE-treated (n=3, red) P20-21 D/+ mice. E. Bar chart of survival of control saline-treated mice (black; n=13), Epi-treated mice (orange; n=5), NE-treated mice (blue; n=13), and PE-treated mice (red; n=8) reveals significantly elevated rates of survival in NE (*P<0.05) and PE-treated (**P<0.01) mice. Statistical comparisons made using a one-sided Fisher's exact test.

recovery and survival in 7 out of 8 mice (**P<0.01; One-sided Fisher's exact test; Fig. 4.4A-E; Video 4.6), which suggests alpha-1 adrenergic receptor activity is sufficient to promote postictal recovery of breathing and survival of audiogenic seizures in P20-21 D/+ mice.

Endogenous adrenergic receptor function is required for recovery breathing and survival of audiogenic seizures in adult D/+ mice.

In order to test the necessity of adrenergic receptor function for breathing recovery and survival, we inhibited adrenergic receptor subtypes in adult D/+ mice which experience only non-fatal audiogenic seizures. We injected (i.p.) adult D/+ mice 15 minutes prior to audiogenic seizure stimulation with either 1 mg/kg prazosin (alpha-1 receptor antagonist), 10 mg/kg sotalol (beta receptor antagonist), a combination of the two, or saline as a control (Fig. 4.5A). As expected, all 10 saline-injected adult D/+ mice had audiogenic seizures followed by recovery of breathing and survival (Fig. 4.5B, D & E). We also observed that 12 out of 12 sotalol-treated mice survived, whereas only three of 11 prazosin-treated mice survived (**P<0.01 compared to saline-injected controls; ***P<0.001 compared to sotalol; Fig. 3.5E; Video 4.7). Interestingly, all 14 D/+ mice treated with the combination of prazosin and sotalol died immediately following an audiogenic seizure (***P<0.001; Fig. 4.5C-E). Plethysmography recordings for prazosin/sotalol-treated adult D/+ mice revealed absence of breathing recovery (Fig. 4.5C-D) similar to that of P20-21 D/+ mice (Fig. 4.3A-B and Fig. 4.4A-B). These results suggest that activity of alpha-1 adrenergic receptors is required for the normal recovery of breathing and survival following audiogenic seizures of adult D/+ mice.

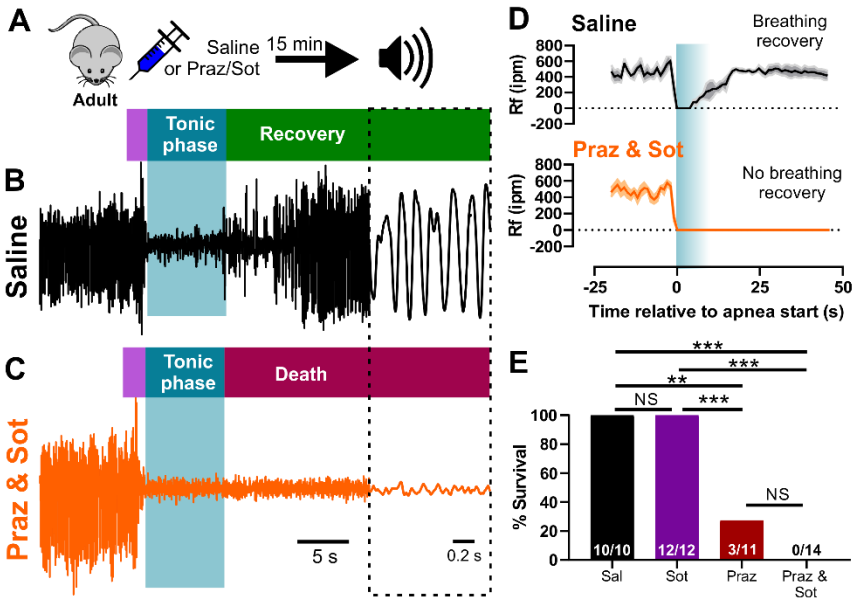

Figure 4.5: Inhibition of adrenergic receptors leads to seizure-induced respiratory arrest and sudden death in adult D/+ mice.
A. Adult D/+ mice were injected (i.p.) with saline, prazosin (1mg/kg) and/or sotalol (10 mg/kg) 15 minutes before stimulation of an audiogenic seizure. B-C. Example plethysmography recordings of breathing during audiogenic seizures in D/+ mice treated with saline (black; B) or prazosin and sotalol (orange; C) ~15 minutes before acoustic stimulation. Breathing recovers in the saline-treated adult mouse. However, breathing never recovers in the combined prazosin and sotalol-treated adult mouse after the audiogenic seizure. D. Average breathing rates for saline-treated (black; n=4) and prazosin/sotalol-treated mice (orange; n=5). E. Bar chart of survival of adult D/+ mice treated with saline (black; n=10), sotalol (purple; n=12), prazosin (red; n=11), and prazosin/sotalol (no color; n=14). Prazosin alone significantly reduced survival rate compared to saline injection (***P<0.001; n=11), with a similarly strong effect observed in mice treated with both prazosin and sotalol (***P<0.001; n=14). Statistical comparisons made using one-sided Fisher's exact tests.

Prevention of seizure-induced death with mechanical ventilation does not require adrenergic receptor function

Our results suggest that adrenergic receptor activity prevents death primarily via stimulation of breathing. We reasoned that even in the absence of functional adrenergic receptor signaling, any procedure to stimulate breathing would be able to rescue D/+ mice from seizure-induced death. To test this, we performed two sets of experiments: First, we injected (i.p.) mice with the combination of 10 mg/kg sotalol and 1 mg/kg prazosin 15 minutes prior to audiogenic seizure stimulation of adult D/+ mice, and either mechanically ventilated immediately after the start of the tonic phase or performed no intervention as a control (Fig. 4.6A). Although the adrenergic antagonist cocktail caused audiogenic seizure-induced death in adult D/+ mice (0 out 14 survived; Fig. 4.5E), all mice that received mechanical ventilation in addition to the adrenergic cocktail recovered breathing and survived (8 out of 8 survived; ***P=0.001; Fig. 4.6B).

Second, we either injected (i.p.) P20-21 D/+ mice with the same adrenergic antagonist cocktail or gave no injection prior to audiogenic seizure-stimulation, and mechanically ventilated both groups immediately after the start of the tonic phase (Fig. 4.6C). Even with relatively small sample size (n=6 mice), adrenergic receptor blockade in P20-21 D/+ mice did not prevent the ability of mechanical ventilation to promote survival in any mice tested (6 of 6 survived; Fig. 4.6C-D). This evidence supports the notion that adrenergic receptors function, likely indirectly, to stimulate breathing recovery after the tonic phase. However, any process that can directly stimulate breathing recovery will promote survival, even in the absence of adrenergic receptor function.

Discussion

In this report, we present the novel finding that mice expressing the patient-derived N1768D *SCN8A* mutation (D/+) have audiogenic seizures that are nearly identical to spontaneous seizures. Furthermore, at the specific time point of P20-21, these audiogenic seizures result in sudden death, which can be rescued by mechanical ventilation immediately after the onset of an audiogenic seizure, indicating that breathing cessation is the primary cause of death. We report that blockade of adrenergic receptors with prazosin results in seizure-induced death in adult mice, while activation of adrenergic receptors with phenylephrine rescues seizure-induced death in P20-21 mice. These results indicate that adrenergic receptor activity, most likely the alpha-1 subtype, is critical for breathing recovery after tonic seizures and represents a potential therapeutic intervention for SUDEP.

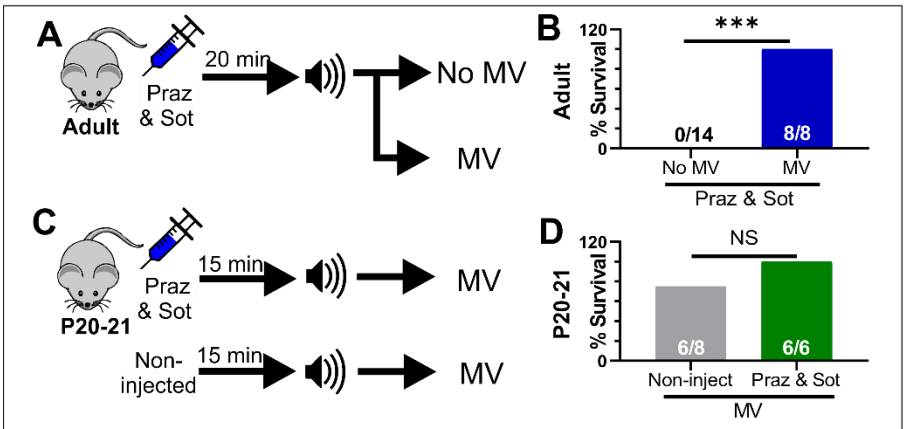

Figure 4.6: Mechanical ventilation does not require adrenergic receptor function to prevent seizure-induced sudden death.
A. Adult mice were injected (i.p.) with prazosin (1 mg/kg) and sotalol (10 mg/kg) 15 minutes before simulation of an audiogenic seizure. Some mice were either mechanical ventilated (MV) or not (No MV). B. MV increased survival (8 of 8 adult D/+ mice) compared to No MV (***P<0.001). C. P20-21 D/+ mice were either non-injected or injected with a combination of prazosin (1 mg/kg) and sotalol (10 mg/kg) 15 minutes prior to stimulation of an audiogenic seizure. All mice received mechanical ventilation (MV). D. 6 of 8 P20-21 D/+ mice that received MV only survived and were not statistically different from mice injected with a combination of prazosin (1 mg/kg) and sotalol (10 mg/kg) 15 minutes prior to stimulation of an audiogenic seizure that also received MV (6 of 6 mice). Statistical comparisons were made using one-sided Fisher's exact tests.

D/+ mice have audiogenic seizures.

SCN8A encephalopathy is a severe genetic epilepsy syndrome and neurodevelopmental disorder characterized by refractory seizures, cognitive and motor dysfunction, and a substantial risk for SUDEP (Blanchard et al., 2015; Estacion et al., 2014; Gardella et al., 2018; de Kovel et al., 2014; Larsen et al., 2015; Ohba et al., 2014; Veeramah et al., 2012; Zaman et al., 2019). *Scn8a* alleles containing patient-derived mutations form $Na_V1.6$ voltage-gated sodium channels that create aberrant neuronal excitability in various cortical neurons including hippocampal CA1 (Baker et al., 2018; Bunton-Stasyshyn et al., 2019; Lopez-Santiago et al., 2017), entorhinal cortex (Ottolini et al., 2017), subiculum (Wengert et al., 2019b), and layer V somatosensory cortex (Bunton-Stasyshyn et al., 2019). Our findings that *SCN8A* mice experience audiogenic seizures and seizure-induced sudden death suggest that additional regions, such as the inferior colliculus and amygdala which have been previously implicated in audiogenic seizures and sudden death (Coffey et al., 1996; Dlouhy et al., 2015; Faingold et al., 2017, 1992; Kommajosyula et al., 2017; Marincovich et al., 2019; Millan et al., 1986; Ribak, 2017; Wada et al., 1970), may also be functionally impacted by *SCN8A* mutations. In particular, prior studies have revealed intrinsic hyperexcitability in inferior colliculus neurons from rats susceptible to audiogenic seizures (Li et al., 1994). Interestingly, another study investigating a mouse expressing the R1627H *SCN8A* mutation found hearing impairment, abnormally elevated activity in inferior colliculus, and audiogenic seizures in response to acoustic stimulation (Makinson et al., 2016). Our results encourage future examination of various additional brain regions in models of *SCN8A* encephalopathy to more precisely identify the neuronal mechanisms responsible for the audiogenic seizures and sudden death.

Risk of death from audiogenic seizures in the D/+ mice was strongly age-dependent: Sudden death due to audiogenic seizure occurred with high probability in P20-21 mice, but was never observed in adult mice. This is in contrast to the mortality rate from spontaneous seizures in D/+ mice, where premature death can occur starting around eight weeks of age and reaches

50% mortality by one year (Wagnon et al., 2015). The age-dependent differences in seizure phenotype and risk for sudden death are likely attributable to developmental changes in hearing, *SCN8A* expression, adrenergic receptor expression (possibly the alpha-1 subtype), as well as additional unknown factors. Gain-of-function mutations in *SCN8A* could lead to altered wiring of auditory neural circuits that favor initiation of audiogenic seizures. In support of this notion, mice harboring loss-of-function *SCN8A* mutations did not exhibit audiogenic seizures despite the presence of hearing impairment, thus it is unlikely that hearing impairment alone is sufficient for audiogenic seizures (Mackenzie et al., 2009). Additionally, endogenous alpha-1 adrenergic receptor function at P20-21 may be insufficient to rescue breathing and prevent seizure-induced sudden death. The fact that we do not observe spontaneous death at P20-21 in D/+ mice suggests that although they are capable of having audiogenic seizures at this age, they likely do not experience spontaneous seizures, consistent with previous reports (Wagnon et al., 2015). As to the low mortality of audiogenic seizures in adult D/+ mice, we have observed that D/+ mice have many nonfatal spontaneous seizures prior to death (unpublished observations). However, in the present study, we never induced audiogenic seizures more than three times in a single adult D/+ mouse. Thus, the likelihood of death from any single audiogenic versus spontaneous seizure is likely not different between spontaneous and audiogenic seizures. Future studies as to how developmentally-determined alpha-1 adrenergic signaling relates to seizure-induced sudden death are needed to further clarify the mechanism(s) of death in P20-21 D/+ mice. Our results demonstrating that norepinephrine and phenylephrine administration improves survival suggest that endogenous release of these alpha-1 adrenergic receptor-targeting monoamines at P20-21 is impaired in D/+ mice.

Similar to previous reports of other mouse models susceptible to audiogenic seizures, our recordings of auditory brainstem responses revealed that D/+ mice have impaired hearing (Heffner et al., 2019; Koay et al., 2002; Mackenzie et al., 2009; Willott and Bross, 1996; Willott et al., 1995). To date, there have been no reports of *SCN8A* encephalopathy patients that exhibit hearing abnormalities and audiogenic seizures. Further audiological evaluation of patients with *SCN8A* mutations is warranted to shed light on the importance of hearing impairment and seizures.

To our knowledge this is the first model of *SCN8A* encephalopathy which exhibits spontaneous seizures and the reliable induction of both non-fatal and fatal seizures. Since seizure-induced death can be reliably induced, our model allows for a more in-depth examination of the cascade of events that lead to either fatal or non-fatal seizures, increasing the versatility of this clinically relevant model of epilepsy. Importantly, audiogenic seizures highly resemble spontaneous seizures in D/+ mice with respect to ECoG activity, heart rate, and breathing. The differences observed in relative timing of ECoG ictal activity and onset of tonic phase might indicate different focal regions between audiogenic and spontaneous seizures. Nonetheless, our data support the notion that audiogenic seizures can be utilized as a model to understand mechanisms of seizure semiology and seizure-induced death.

Respiratory arrest contributes to seizure-induced death.

There is increasing evidence that respiratory arrest is the primary cause of death in SUDEP. Most witnessed cases of SUDEP are preceded by convulsive seizures (Hesdorffer et al., 2011; Nashef et al., 2012; Ryvlin et al., 2013), and oxygen desaturation due to breathing complications is common during and after convulsive seizures (Bateman et al., 2008; Lacuey et al., 2018; Vilella et al., 2019a, 2019b). SUDEP events where cardiorespiratory parameters are adequately recorded are understandably limited; however, in these few cases patients experienced respiratory arrest prior to terminal asystole (Ryvlin et al., 2013), suggesting the primacy of respiratory failure. Data obtained from mouse models of SUDEP support this notion. Death is due to respiratory arrest for the stimulated seizures of *Lmx1b*$^{f/f/p}$ and DBA/1&2 mice, (Buchanan et al., 2014b; Faingold et al., 2010; Irizarry et al., 2020), and the spontaneous seizure-induced deaths in *Cacna1a*^{S218L} mice and *Scn1a*^{R1407X}, a mouse model of Dravet Syndrome (Jansen et al., 2019; Kim et al., 2018; Loonen et al., 2019). Breathing dysfunction is also reported for seizures induced under urethane anesthesia using *Kcna1* KO, *RyR2*^{R176Q}, *Cacna1a*^{S218L} mice, and Sprague-Dawley rats (Aiba and Noebels, 2015; Aiba et al., 2016; Loonen et al., 2019).

It has been previously reported that D/+ mice have cardiac arrhythmias and experience bradycardia prior to death (Frasier et al., 2016); however, breathing was not recorded in these studies and the sequence of events during seizure-induced death was not presented. Due to the young age of the mice in our audiogenic model of seizure-induced death we did not record cardiac function. Thus, bradycardia, or other cardiac abnormalities, could still play a role in the mortality of D/+ mice. However, the observation that mechanical ventilation prevents seizure-induced death suggests that breathing cessation is clearly an important factor in death.

Tonic phase apnea and failure of breathing recovery.

Many studies concerned with breathing cessation as a mechanism of SUDEP refer to seizure-induced respiratory arrest (S-IRA). Often, S-IRA is synonymous with seizure-induced death; drugs that prevent death also prevent S-IRA (Faingold et al., 2010; Irizarry et al., 2020; Zeng et al., 2015; Zhang et al., 2017). In D/+ mice, we find that S-IRA occurs during all audiogenic seizures and coincides with the behavioral and electrographic tonic phase, which we refer to as tonic phase apnea. D/+ mice only experienced seizure-induced death when breathing did not recover immediately after the tonic phase. This discrepancy could be attributed to the fact that for most audiogenic seizure-induce death experiments, respiratory activity is assessed by visualization, which could make it difficult to ascertain breathing, or the lack thereof, during convulsions. Another factor could be that tonic seizures in DBA1/2J mice, which are used in the majority of preclinical SUDEP research, almost always produce death, making S-IRA and death coincident with one another (Martin et al., 2020). Considering tonic seizures are associated with apnea in humans (Gastaut et al., 1963; Wyllie, 2015), it is likely that most, if not all, tonic seizures in mouse models produce apnea.

It is unclear whether tonic phase apnea is necessary for postictal apnea and death, as there is no method to selectively prevent the tonic phase from occurring. However, it has been shown that DBA1/2J and 129/SvTer mice die from tonic, but not clonic, seizures (Martin et al., 2020), implying the tonic phase is important and perhaps necessary for seizure-induced death. Thus, determining cellular and molecular underpinnings of both tonic phase apnea and failure of breathing recovery will be important foci for future SUDEP research.

Adrenergic signaling and seizure survival.

Mechanisms of seizure-induced death are poorly understood. Many proposed mechanisms involve impaired brainstem neural activity occurring due to synaptic seizure spread or spreading depolarization that impairs function of respiratory centers in the medulla producing central (Aiba and Noebels, 2015; Aiba et al., 2016; Jansen et al., 2019; Loonen et al., 2019; Patodia et al., 2018; Salam et al., 2017) or obstructive (Nakase et al., 2016; Villiere et al., 2017; Weissbrod et al., 2011) apnea. Seizure spread to non-medullary sites, such as the amygdala also suppresses breathing and is proposed to cause breathing cessation (Dlouhy et al., 2015; Marincovich et al., 2019; Nobis et al., 2019).

A body of work demonstrates the impairment of neuromodulator systems and their utility to rescue death in mouse models of SUDEP (Buchanan et al., 2014b; Devinsky et al., 2016b; Faingold et al., 2011, 2016; Feng and Faingold, 2017; Kruse et al., 2019; Patodia et al., 2018; Zeng et al., 2015; Zhan et al., 2016; Zhang et al., 2017; Zhao et al., 2017). Much of this work centers on the serotonergic system. Chronic administration of agents that increase serotonin levels can reduce the incidence of seizure-induced death (Faingold et al., 2011; Feng and Faingold, 2017; Zeng et al., 2015). In addition, genetic lesion of serotonergic raphe neurons elevates susceptibility of death after maximal electroshock seizures (Zhan et al., 2016), and optogenetic stimulation of the dorsal raphe reduces occurrence of seizure-induced death in DBA1 mice (Zhang et al., 2018). Noradrenaline has recently been shown to have a similar affect (Zhang et al., 2017; Zhao et al., 2017), and it appears that the ability of selective serotonin reuptake inhibitors (SSRIs) to prevent seizure-induced death is dependent on functional adrenergic signaling (Kruse et al., 2019).

We also demonstrate that functional adrenergic signaling is necessary for survival of seizures in adult D/+ mice, and this was largely dependent on functional alpha-1 receptors, and perhaps to a lesser extent, beta receptors. In addition, we show that exogenous stimulation of adrenergic receptors, most likely of the alpha-1 variety, is sufficient to prevent seizure-induced death in P20-21 D/+ mice. We intentionally utilized relatively high doses of epinephrine, norepinephrine, and phenylephrine in this study (Fleming et al., 2013; Gehrmann et al., 2000; Im et al., 1998; Suita et al., 2015). Our finding that epinephrine did not prevent sudden death was surprising, however, when taken together with phenylephrine's ability to prevent death and prazosin's ability to produce it, our results suggest a critical role for alpha-1 receptors in seizure survival, similar to findings using maximal electroshock seizure-induced death (Kruse et al., 2019). For this reason, we hypothesize that activation of alpha-1 adrenergic receptors is a general requirement for survival after convulsive seizures and that acute augmentation of alpha-1 receptors could also reduce risk of seizure-induced sudden death in other seizures models. Further investigation into the mechanism underlying this difference between epinephrine and either norepinephrine or phenylephrine is warranted.

Precisely how adrenergic receptors promote breathing recovery and survival is still unclear. Previous studies have shown that intracerebroventricular injection of the norepinephrine reuptake inhibitor atomoxetine or alpha-1 receptor agonist phenylephrine prevents death from the audiogenic seizures of DBA1 mice (Zhao et al., 2017) or maximal electroshock

seizures (Kruse et al., 2019), respectively. This could implicate a role in arousal neural circuitry, as a major function of noradrenergic signaling in the central nervous system is to increase arousal state (Broese et al., 2012). In our experiments, norepinephrine and phenylephrine were given intraperitoneally. Considering monoamine analogues do not cross the blood brain barrier (Hardebo and Owman, 1980; Olesen, 1972), our data suggests that peripheral alpha-1 adrenergic receptor activity is responsible for rescuing breathing in D/+ mice. Peripheral stimulation of alpha-1 receptors has little effect on heart rate but does increase peripheral resistance, which is crucial for maintaining blood flow to the heart and brain during life-threatening conditions of hypoxia and hemorrhage (Bond, 1985; Schultz et al., 2007). It is feasible that in the already compromised state of a severe convulsive seizure, multiple systems would be needed to coordinate full recovery.

Conclusion

Taken together, our results highlight the D/+ mouse model of *SCN8A* encephalopathy as a powerful novel model for mechanistic investigation of SUDEP. We demonstrated the utility of this model by providing new evidence that respiratory arrest is the primary cause of death, and that interventional approaches to stimulate breathing including the augmentation of adrenergic receptor activity might be valuable for preventing SUDEP.

Chapter V: Prominent role of forebrain excitatory neurons in *SCN8A* encephalopathy

Rationale

As demonstrated in previous chapters, mouse models of *SCN8A* encephalopathy have been useful in characterizing how mutant *SCN8A* alters the excitability of various neuronal populations to drive behavioral manifestations of *SCN8A* encephalopathy including seizures and sudden death. However, due to global expression of the mutant allele, the $Scn8a^{D/+}$ mouse model is limited in its utility for interrogating the contribution of particular neuronal subpopulations to the disease. In this chapter, I along with my colleagues, report a novel mouse model of *SCN8A* encephalopathy in which expression of the patient-derived mutation R1872W is contingent upon expression of Cre-recombinase, enabling cell-type specific expression of the *SCN8A* mutation. Global expression of the R1872W allele resulted in a severe epilepsy phenotype including convulsive seizures and lethality by two weeks of age. Neural-cell-specific activation of the R1872W mutation by Nestin-Cre also resulted in early onset seizures and death. Interestingly, restriction of R1872W expression to forebrain excitatory neurons recapitulated seizures and juvenile lethality between 1 and 2 months of age indicating that these neurons are likely prominent in driving the seizure phenotype in patients. The sodium channel modulator Prax330 prolonged survival of mice with global expression of R1872W and also inhibited abnormal persistent sodium currents in cells expressing the R1872W variant. These findings provide insight into the pathogenic mechanism of this gain-of-function mutation of *SCN8A* and identify forebrain excitatory neurons as critical targets for therapeutic intervention.

Introduction

Epileptic encephalopathies are severe seizure disorders accompanied by cognitive, behavioral and movement disturbances (Berg et al., 2010). The first *SCN8A* mutation identified in epileptic encephalopathy was the *de novo* missense variant p.Asn1768Asp (N1768D) (Veeramah et al., 2012). More than 150 additional *de novo* missense mutations have now been reported (EIEE13, MIM#614558) (Larsen et al., 2015; Meisler et al., 2016). *SCN8A* encodes the voltage gated sodium channel $Na_v1.6$, which is responsible for the initiation and propagation of neuronal action potentials. $Na_v1.6$ is concentrated at the axon initial segment and nodes of Ranvier in neurons of the central and peripheral nervous system. Patient mutations of *SCN8A* are localized to the evolutionarily conserved transmembrane segments, intracellular inactivation gate loop, and C-terminal domain (Wagnon and Meisler, 2015). Most of the characterized patient mutations result in gain-of-function changes in biophysical properties resulting in elevated channel activity, either due to premature channel opening or impaired channel inactivation (Barker et al., 2016; Blanchard et al., 2015; Estacion et al., 2014; de Kovel et al., 2014; Patel et al., 2016; Veeramah et al., 2012; Wagnon et al., 2016). Loss-of-function mutations of *SCN8A* typically result in isolated intellectual disability, myoclonus, and movement disorders (Wagnon et al., 2017a, 2018) although I demonstrated in Chapter II that biallelic inherited loss-of-function *SCN8A* mutations also result in epileptic encephalopathy(Wengert et al., 2019a).

Clinical features of *SCN8A* encephalopathy include multiple seizure types with onset between prenatal and 18 months (average 4 months) (Larsen et al., 2015; Meisler et al., 2016). Seizures are refractory to therapy and often require multi-drug treatment. Impaired cognitive function and developmental arrest or regression after seizure onset are common. Intellectual disability ranges from mild to severe. Language is commonly impaired with many affected individuals having little or no speech. Approximately half of all diagnosed children are non-ambulatory. Those who do learn to sit or walk often have a movement disorder and progressive loss of ambulation. There is also an increased risk of SUDEP, with reported rates of 5 to 10% (Johannesen et al., 2018; Meisler et al., 2016).

The first mouse model of *SCN8A* encephalopathy was generated by knock-in of the patient mutation p.Asn1768Asp (Jones and Meisler, 2014; Veeramah et al., 2012; Wagnon et al., 2015). Heterozygous $Scn8a^{D/+}$ mice recapitulated spontaneous seizures and sudden death with 50% penetrance. Video-EEG recordings identified convulsive seizures concordant with ictal activity, as well as epileptiform discharges coincident with myoclonic jerks. Mild deficits in motor coordination and social discrimination were also observed. Affected mice have seizure onset at 2–4 months and rapid progression to death (Sprissler et al., 2017; Wagnon et al., 2015). Persistent and resurgent sodium currents drive hyperexcitability in various neuronal populations (Baker et al., 2018; Lopez-Santiago et al., 2017; Ottolini et al., 2017; Wengert et al., 2019b).

To develop a conditional model of *SCN8A* encephalopathy that includes the more severe clinical features, we selected the recurrent mutation p.Arg1872Trp (R1872W). This mutation is located in a conserved region of the C-terminus that contributes to stability of the inactivated channel through ionic interaction of the positively charged arginine 1872 with

negatively charged residues in the inactivation gate (Nguyen and Goldin, 2010). Replacement of arginine 1872 with uncharged amino acids, including tryptophan, results in impaired channel inactivation and elevated current density (Wagnon et al., 2016). More than 24 independent *de novo* substitutions at residue 1872 have been reported. Clinical data for four individuals with the R1872W mutation reveal seizure onset between 10 days and 4 months of age, status epilepticus in three individuals, and severe motor disabilities including hypertonia, hypotonia, tremor, spasticity and non-ambulation (Gardella et al., 2018; Larsen et al., 2015; Ohba et al., 2014). Sudden unexpected death in epilepsy (SUDEP) was reported for one child at 5 years of age.

We now describe the generation of a conditionally inducible mouse model (*Scn8a*$^{cond/+}$) and initial characterization of the underlying pathophysiology of seizures. Global activation of the R1872W mutation (*Scn8a*$^{cond/+}$, EIIa-Cre) resulted in a more severe disease than in the original N1768D mouse, including earlier onset of seizures and shorter duration before lethality. Electrophysiological recordings revealed hyperexcitability of cortical and hippocampal pyramidal neurons. Interestingly, expression of the R1872W mutation in forebrain excitatory neurons (*Scn8a*$^{cond/+}$, Emx1-Cre) was sufficient for neuronal hyperexcitability, spontaneous seizures, and premature death indicating a prominent role for these neuronal populations in driving seizures in *SCN8A* encephalopathy.

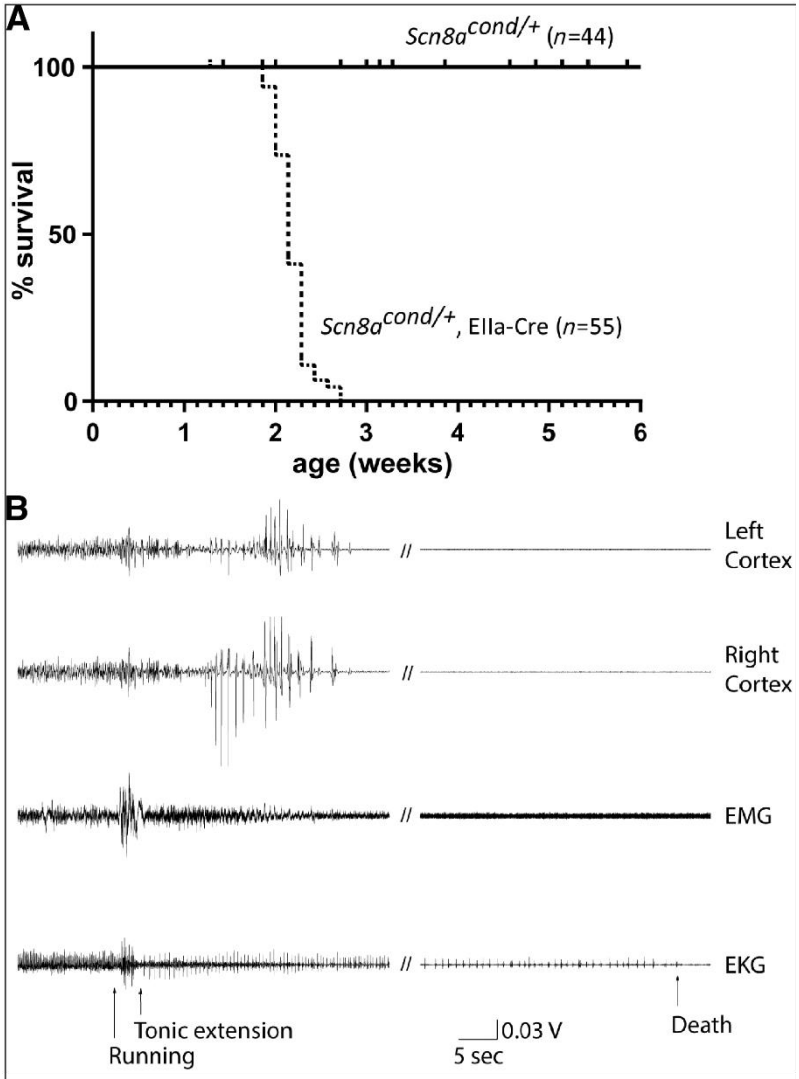

Figure 5.1: Scn8a$^{cond/+}$, EIIa-Cre mice exhibit spontaneous seizures and death.
(A) Scn8a$^{cond/+}$,EIIa-Cre exhibited sudden lethality at the end of the second week of life, with median survival of 15 days. Cre-negative littermates exhibited normal life span. (B) EEG recording of a fatal seizure in an Scn8a$^{cond/+}$, EIIa-Cre mouse on P15. The recording was obtained from bipolar insulated stainless-steel electrodes in the left parietal cortex (top trace) and right parietal cortex (second trace). The EMG artefact in the third trace reflects the period of running evolving to tonic extension. Death occurred 3 min 20 s after the onset of running. The bottom trace was obtained from an electrode placed subcutaneously in the right thorax and demonstrates sudden slowing of the heart rate from 756 bpm prior to the running fit to 156 bpm immediately afterwards.

Methods

Mice

All mice were housed and cared for in accordance with NIH guidelines in a 12/12-h light/dark cycle with standard mouse chow and water available *ad libitum*. Experiments were approved by the Committee on the Use and Care of Animals at the University of Michigan and the University of Virginia. Mice homozygous for the conditional allele (*Scn8a*$^{cond/cond}$) were crossed with the Cre lines *EIIa-Cre* (Jax 003724), *Emx1-Cre* (Jax 005628), *Gad2-Cre* (Jax 028867), *Dlx5a-Cre* (Jax 008199), and *Nes-Cre* (Jax 003771).

EEG Recordings

Electrodes were implanted in pre-weaning *Scn8a*$^{cond/+}$, EIIa-Cre mice at postnatal Days 7–15 (P7–P15) and *Scn8a*$^{cond/+}$, Emx1-Cre mice at P21 as previously described (Zanelli et al., 2014). Mice were recorded for 2–4 h twice a day starting on P9–P14. Recordings were visually inspected for the presence of defined electrographic seizures (Zanelli et al., 2014). Mice were implanted and recorded as previously described (Wagnon et al., 2015).

Electrophysiology Recordings

All electrophysiological procedures in this chapter were completed as described previously (Chapter III) (Wengert et al., 2019b).

Results

Global expression of the R1872W mutation results in seizures and premature death

Scn8a$^{cond/+}$, EIIa-Cre mice with heterozygous expression of the R1872W mutant voltage-gated sodium channel were indistinguishable from wild-type littermates for the first two weeks of postnatal life, with normal righting reflex and visible motor activity. However, beginning at P14, severe spontaneous seizures were observed with a median survival to P15 (Figure 5.1A). To monitor seizure onset, EEG electrodes were implanted in *Scn8a*$^{cond/+}$, EIIa-Cre mice at P7 to P15, and video-EEG monitoring was carried out for 2 hours/day. The seizures began with an abrupt onset of running that lasted for one to three seconds, immediately followed by loss of upright posture and brief tonic extension. The movement artefact recorded during running was followed after 4.0 ± 0.6 seconds (n=8) by an electrographic seizure or repetitive spike trains that lasted for 20 ± 3.0 seconds followed by post-ictal suppression (Figure 5.1B). The age at death for the implanted animals was P16 ± 0.4 days (n=8) which did not differ from non-implanted mice. In five of eight mice, death occurred immediately after the recording of a single seizure.

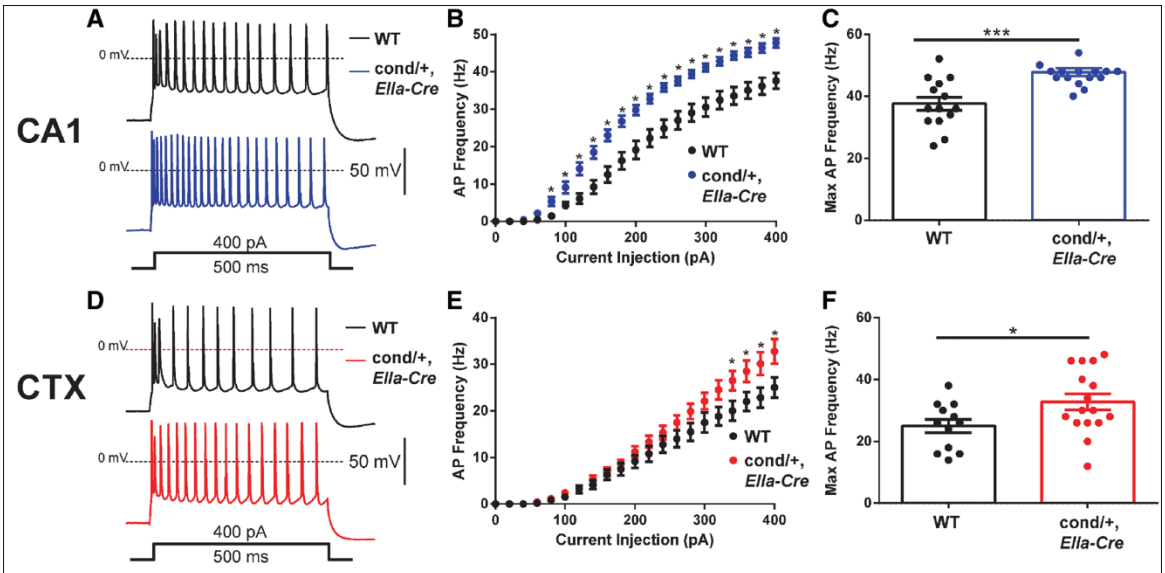

Figure 5.2. Neuronal hyperactivity in Scn8a$^{cond/+}$,EIIa-Cre mice. (A and B) Representative slice recordings from control (14 cells from four mice) and Scn8a$^{cond/+}$,EIIa-Cre CA1 neurons (16 cells from five mice). (C) Action potential firing frequency at 400 pA current injection. (D and E) Representative slice recordings from control (12 cells from four mice) and Scn8a$^{cond/+}$,EIIa-Cre layer V cortical neurons (16 cells from five mice). (F) Action potential firing frequency at 400 pA current injection. Data shown represent means ± standard error of the mean (SEM) *P < 0.05, ***P < 0.001.

Hyperexcitability of cortical neurons in Scn8a$^{cond/+}$*, EIIa -Cre mice*

To investigate neuronal activity underlying the seizures in *Scn8a*$^{cond/+}$, EIIa-Cre mice, we carried out brain slice recordings from hippocampal CA1 and cerebral cortical neurons. CA1 neurons from *Scn8a*$^{cond/+}$, EIIa-Cre mice were hyperexcitable over a range of current injection steps (Figure 5.2A-C). At a current injection of 400 pA, the action potential frequency was increased in both mutant CA1 neurons (47.8 ± 1.2 Hz; n=16 neurons from 5 mice, ***P<0.001) and mutant layer V cortical neurons (32.8 ± 2.6 Hz; n=16 neurons from five mice, P<0.05) compared with wild-type CA1 (37.6 ± 2.2 Hz; n=14 cells from four mice) and cortical neurons

	Vm, mV	Threshold, mV	Rheobase, pA	Upstroke velocity, mV/ms	Downstroke velocity, mV/ms	Amplitude, mV	APD50, ms	Input resistance, MΩ
WT (n=14, 4)	−67.0 ± 0.9	−42.4 ± 1.0	84.33 ± 9.6	328 ± 35	−57.8 ± 1.9	88.6 ± 2.5	1.39 ± 0.06	252 ± 28
Scn8a$^{cond/+}$,EIIa-cre (n=16, 5)	−67.1 ± 1.1	−43.5 ± 1.1	51.3 ± 5.8*	435 ± 25*	−55.8 ± 1.6	94.1 ± 0.9*	1.47 ± 0.04	320 ± 29*

Recordings were carried out on multiple cells from each animal (*n* = cells, animals). There was no current injection into the resting cells.
*Statistical significance at $P < 0.05$, Student's *t*-test.

Table 5.1. Membrane and action potential properties of CA1 neurons.

(25.0 ± 2.2 Hz; n=12 cells from four mice; Figure 5.2D-F). Analysis of membrane properties of CA1 neurons revealed significant increases in upstroke velocity, spike amplitude, and input resistance as well as decreased rheobase in the mutant CA1 neurons (Table 5.1)

Expression of R1872W in forebrain excitatory neurons leads to seizures and lethality

To obtain restricted neural expression of the R1872W mutant channel, we crossed *Scn8a*$^{cond/cond}$ mice with mice expressing a Nestin-Cre transgene. *Scn8a*$^{cond/+}$, Nes-Cre mice developed spontaneous seizures at three to four weeks of age, leading rapidly to lethality with a median age at death of 21 postnatal days (Figure 5.3). These results indicate that, as expected, neural expression of the R1872W variant is sufficient for the seizure phenotype.

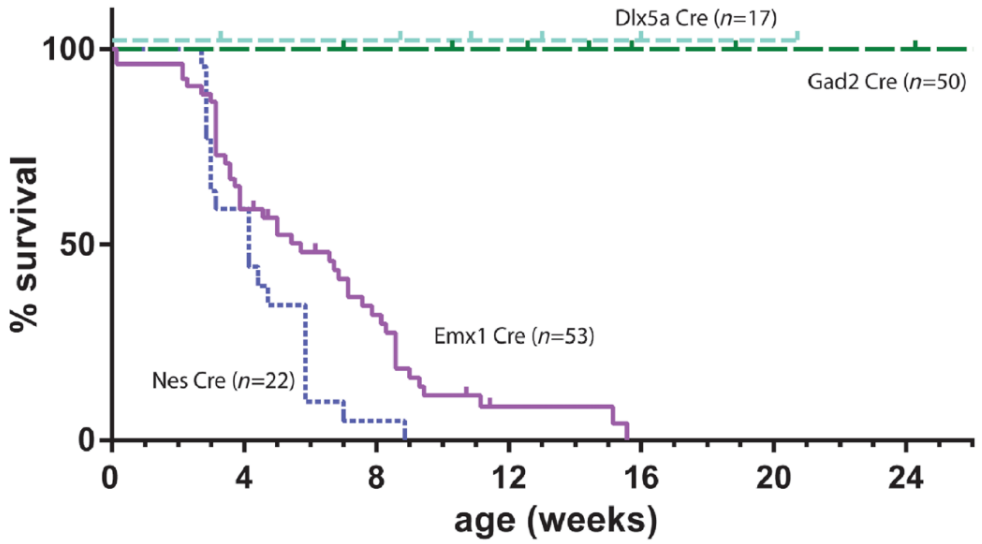

Figure 5.3: Expression of R1872W in forebrain excitatory neurons is causes premature lethality. Survival of conditional mice expressing cell-specific Cre constructs. Nestin-Cre is broadly expressed in neural cells; median survival 21 days. Emx1-Cre is expressed in excitatory neurons of the forebrain; median survival 46 days. Gad2-Cre and Dlx5a-Cre is expressed in inhibitory neurons.

To dissect the contributions of neuronal subpopulations, we compared the effect of activating the R1872W mutation in excitatory versus inhibitory neurons. *Scn8a*$^{cond/cond}$ mice were crossed heterozygous mice carrying Emx1-Cre from an endogenous Emx1 locus that is expressed in forebrain excitatory neurons. All of the *Scn8a*$^{cond/+}$, Emx1-Cre mice experienced lethal seizures, beginning at 1 month of age, with median survival to 6 weeks (Figure 5.3). Many mice exhibited multiple seizures types that included facial spasms, mouth clicking, opisthotonos (head rearing), circular running with tonic extension of the tail, retropulsion with clonic movements of the hindlimbs, rearing, falling, clonic limb seizures, and tonic-clonic seizures. Interestingly, no spontaneous behavioral seizures were observed in *Scn8a*$^{cond/+}$, Gad2-Cre or Dlx5a-Cre mice suggesting that inhibitory interneurons labeled by these particular Cre-drivers are insufficient *per se* for the development of spontaneous seizures.

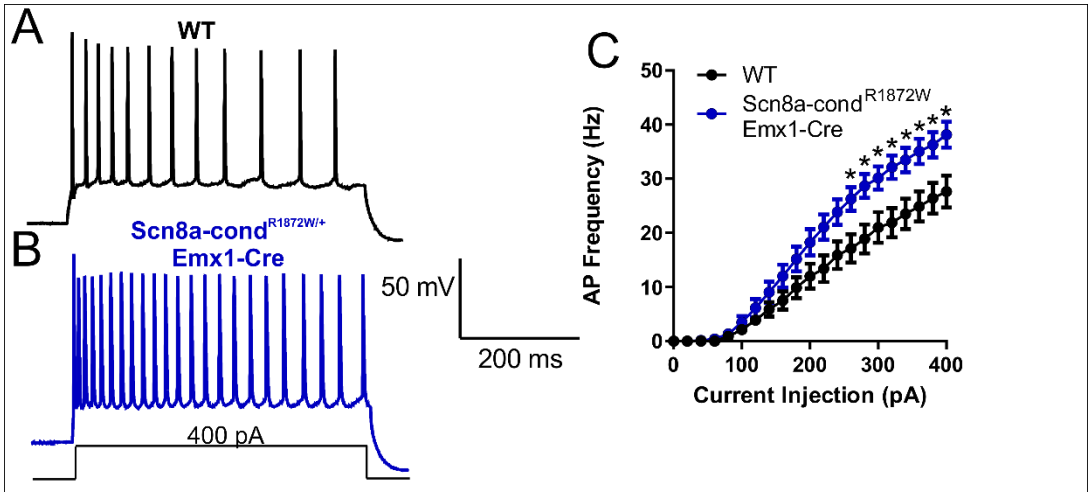

Figure 5.4. Neuronal hyperactivity in Scn8a$^{cond/+}$, EMX1-Cre mice. (A and B) Representative slice recordings from WT control (black; 16 cells from four mice) and Scn8a-EMX$^{1W/+}$ CA1 neurons (blue; 15 cells from three mice). (C) Action potential firing frequency at 400 pA current injection. Data shown represent means ± standard error of the mean (SEM) *P < 0.05.

Hyperexcitability of cortical neurons in Scn8a$^{cond/+}$*, Emx1-Cre mice*

To confirm hyperexcitability of neurons due to forebrain-restricted expression of R1872W, I recorded neuronal excitability in CA1 neurons from both WT and *Scn8a*$^{cond/+}$, Emx1-Cre at 4-6

weeks of age. As expected, AP firing frequencies were significantly (*P<0.05) elevated in Scn8a$^{cond/+}$, Emx1-Cre mice relative to WT controls (Figure 5.4A-C). This data further supports the notion that seizures are related to intrinsic hyperexcitability of forebrain cortical neurons due to mutant R1872W expression.

Prax330 inhibits the R1872W-derived persistent sodium current and extends survival of Scn8a$^{cond/+}$, EIIa-Cre mice.

As discussed in Chapter III, Prax330 is a novel sodium channel modulator that preferentially targets the persistent sodium current (Baker et al., 2018; Barbieri et al., 2019). To evaluate the effectiveness of the drug against our novel R1872W allele, we provided mothers of *Scn8a$^{cond/+}$*, EIIa-Cre mice with food containing the drug beginning 1 day after delivery (P1). In *Scn8a$^{cond/+}$*, EIIa-Cre offspring whose mothers received the drug, seizure onset and lethality were postponed for average of 6 days relative to mice whose mothers received regular chow (Figure 5.5A). In recordings of ND7/23 cells expressing the R1872W mutation, we found that Prax330 1 μM did not reduce the peak sodium current, while steady-state inactivation was facilitated and the persistent sodium current was significantly reduced (Figure 5.5B-E). Overall, our data indicate that the R1872W-derived persistent sodium current is pathogenic and that Prax330 is effectively able to inhibit development of seizures and prolong survival.

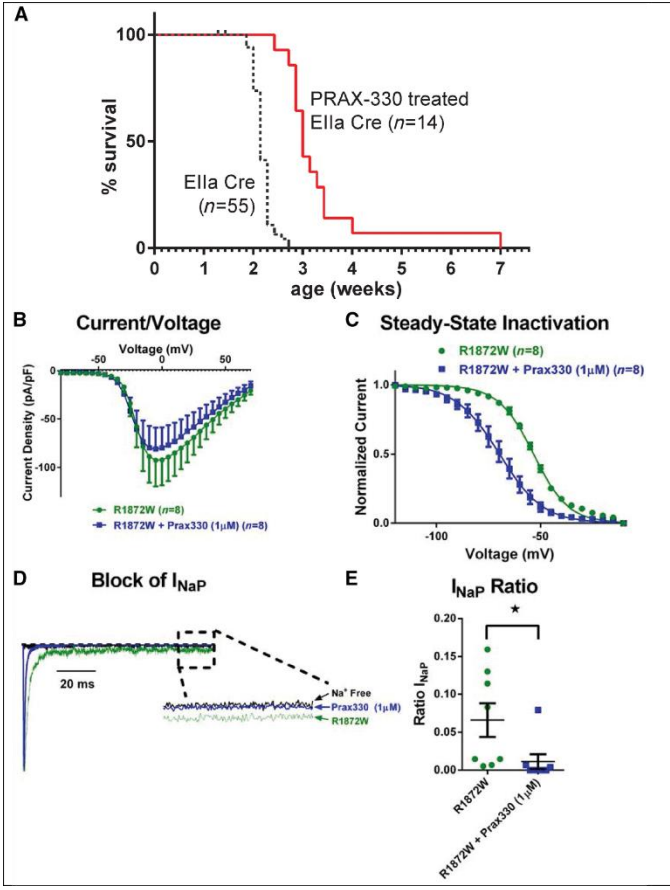

Figure 5.5: Prax330 extends the survival of Scn8acond/+,EIIa-Cre mice and reduces activity of the mutant channel in transfected cells. Prax330 was added to the mouse chow at 8 mg/kg beginning on P1. Untreated mice received normal chow. Mean survival was increased from 15 days for untreated mice (n = 55) to 21 days for treated mice (n = 14). Kaplan-Meier log-rank (Mantel-Cox) test, $\chi2(1) = 32$, $P < 0.0001$. (B–E) ND7/23 cells were transfected with Scn8aR1872W cDNA and incubated in the presence or absence of 1 μM Prax330. (B) Averaged current-voltage (I-V) relation for cells expressing mutant Nav1.6 ± Prax330. Peak currents were normalized to cell capacitance. (C) Voltage dependence of steady-state inactivation. Smooth lines correspond to the least squares fit when average data were fit to a single Boltzmann equation. (D) Representative normalized current traces recorded during a 100 ms depolarizing pulse from −120 mV to 0 mV illustrating the reduction of persistent sodium current for p.Arg1872Trp in the presence of Prax330. (E) Quantification of the ratio of peak to persistent sodium current. Data are means ± SEM statistical significance (*P < 0.05).

Discussion

In this chapter, my collaborators and I have utilized a novel mouse model of *SCN8A* encephalopathy in which the R1872W patient-derived point-mutation is conditionally expressed to uncover a prominent role of forebrain excitatory neurons in the driving seizures and lethality. Similar to the *Scn8a$^{D/+}$* mouse model of *SCN8A* encephalopathy, our data indicate that the R1872W mutation leads to significant hyperexcitability in excitatory neurons and that treatment with Prax330 reduces the abnormally large persistent sodium current and prolongs survival of the *Scn8a$^{cond/+}$*, EIIa-Cre mice.

Forebrain excitatory neuron expression of *Scn8a^{R1872W}* is sufficient to cause seizures and sudden death

In the conditional mouse model, activation of the R1872W patient mutation by Cre recombinase permits spatial and temporal regulation of expression. Global activation of R1872W resulted in seizures and early lethality between 2 and 3 weeks of age. Sudden death was frequently observed after a single seizure in these mice indicating the pronounced severity of this particular mutation. Restricted activation of R1872W by Nestin-Cre also resulted in seizures and sudden death, demonstrating neural origin of the major phenotypes of *SCN8A* encephalopathy. Further, activation of R1872W in forebrain excitatory neurons by Emx1-Cre was sufficient to cause seizures and sudden death in 100% of animals, demonstrating the important role of excitatory neurons in initiation of seizures in *SCN8A* encephalopathy. Electrophysiology recordings of neurons from both *Scn8a$^{cond/+}$*, EIIa-Cre and *Scn8a$^{cond/+}$*, Emx1-Cre revealed hyperexcitability of forebrain excitatory

neurons. Interestingly, activation of mutant channel in inhibitory neurons by Gad2-Cre or Dlx5a-Cre did not appear to be sufficient to cause spontaneous seizures. While this data does not rule out that inhibitory interneurons are affected by *SCN8A* mutations, it indicates a prominent role for forebrain excitatory neurons in driving the seizure behaviors and premature lethality. Using this mouse model enabling Cre-dependent expression of the R1872W variant, future studies will further refine the cell-type specific contribution to underlying pathology in *SCN8A* epileptic encephalopathy.

Distinct mechanisms underlying Dravet syndrome and *SCN8A* encephalopathy

This work taken alongside previous studies indicates fundamental differences between *SCN8A* encephalopathy and Dravet syndrome, a developmental and epileptic encephalopathy most typically caused by physiologically loss-of-function mutations in the voltage-gated sodium channel isoform *SCN1A*. Most *SCN8A* encephalopathy mutations have been characterized to have gain-of-function phenotypes in that they elevate channel opening either by premature activation or impaired inactivation. This framework is consistent with the notion that sodium channel blockers are clinically efficacious in many *SCN8A* encephalopathy patients, while this class of drugs is typically avoided in Dravet syndrome patients. In this chapter, my work suggested that forebrain excitatory neurons are important for seizures because they are sufficient to generate spontaneous seizures and premature death whereas expression of R1872W in inhibitory interneurons failed to produce seizures or death. This result is reminiscent of the converse scenario found in a mouse model of Dravet syndrome in which inhibitory interneuron expression is sufficient for spontaneous seizures while excitatory neuron expression is insufficient *per se* (Cheah et al., 2012; Dutton et al., 2013). However, the results provided in this chapter do not rule out an important contribution of inhibitory interneurons to pathology in *SCN8A* encephalopathy. The nuanced contribution of inhibitory interneurons to *SCN8A* encephalopathy is a topic of worthy investigation and is addressed directly in Chapter VI of this Thesis.

***SCN8A*^{R1872W} is more severe than *SCN8A*^{N1768D} in human and mouse**

Children with the *de novo* mutation R1872W in *SCN8A* are severely impaired, and do not develop the verbal and motor skills that were seen with the N1768D mutation (Veeramah et al., 2012). In the mouse, ubiquitous, global activation of *Scn8a*^{R1872W} by EIIa-Cre causes seizure onset and death at 2–3 weeks of age, while heterozygous *Scn8a*$^{N1768D/+}$ mice exhibit spontaneous seizures after 8 weeks of age (Wagnon et al., 2015). The penetrance of seizures is 100% for the R1872W heterozygotes but only 50% for N1768D heterozygotes. The seizures of R1872W mice are also more severe. A lethal, tonic seizure is often the first sign of disease in the R1872W mice, while N1768D mice often exhibit a brief tonic-clonic seizure followed by 30 seconds of immobility and relatively rapid recovery.

The biophysical abnormalities of the R1872W channel are also more extreme than the N1768D channel. Expression of N1768D in primary neurons or transfected cells results in delayed channel inactivation and elevated persistent current (Lopez-Santiago et al., 2017; Veeramah et al., 2012). A greater delay in decay of macroscopic current is seen in transfected cells expressing R1872W, as well as elevation of peak current density, which may contribute to the more severe phenotype (Wagnon et al., 2016). The sodium channel modulator Prax330/GS967, which preferentially inhibits persistent sodium current, confers complete protection to heterozygous N1768D mice but only delays seizure onset in homozygous N1768D mice and heterozygous R1872W mice (Baker et al., 2018). In addition to its direct effect on the mutant channel, the therapeutic effect of Prax330 is likely mediated by reduction of persistent current generated by the wild-type allele in heterozygous patients.

The early onset, rapid progression, temporal and conditional regulation and fully penetrant lethal phenotype of the *Scn8a*$^{cond/+}$ mouse make it a useful test system for therapeutic intervention, and will accelerate investigation of core mechanisms as well as spur preclinical evaluation of new therapies for *SCN8A* encephalopathy. The ability to regulate expression of a deleterious mutation of *Scn8a* will facilitate future studies of pathogenic mechanisms underlying epilepsy in general.

Chapter VI: Somatostatin-positive Interneurons Contribute to Seizures in *SCN8A* Epileptic Encephalopathy

Rationale

SCN8A epileptic encephalopathy is a devastating epilepsy syndrome caused by mutant *SCN8A* which encodes the voltage-gated sodium channel $Na_V1.6$. In the previous chapter, I demonstrated that forebrain excitatory neurons are important in driving pathology in *SCN8A* encephalopathy—expression of R1872W exclusively in forebrain excitatory neurons was sufficient for spontaneous seizures and premature lethality. While those studies suggested that expression of R1872W in inhibitory interneurons was insufficient *per se* to result in spontaneous seizures, it remains unclear if and how inhibitory interneurons, which express $Na_V1.6$, influence disease pathology. Using our novel test for audiogenic seizures (Chapter IV), I found that selective expression of the R1872W mutation in somatostatin-positive (SST) interneurons was sufficient to convey susceptibility to audiogenic seizures. Patch-clamp recordings revealed that SST interneurons from mutant mice were initially hyperexcitable but hypersensitive to action potential failure via depolarization block under normal and seizure-like conditions. Remarkably, GqDREADD-mediated induction of similar hyperexcitability and depolarization block of wild-type SST interneurons resulted in prolonged electrographic seizures indicative of status epilepticus. Aberrantly large persistent sodium currents, a hallmark of pathogenic *SCN8A* mutations, were observed and found to contribute directly to aberrant SST physiology in computational and pharmacological experiments. These novel findings demonstrate a critical and previously unidentified contribution of SST interneurons to seizure generation not only in *SCN8A* encephalopathy, but epilepsy in general.

Introduction

SCN8A encephalopathy is a severe genetic epilepsy syndrome caused by *de novo* mutations in the *SCN8A* gene which codes for the voltage-gated sodium channel isoform $Na_V1.6$ (Gardella et al., 2018; Larsen et al., 2015; Ohba et al., 2014; Veeramah et al., 2012). Patients exhibit a panoply of devastating symptoms including refractory epilepsy, cognitive impairment, motor dysfunction, sensorineural hearing loss, and have a substantial risk of sudden unexpected death in epilepsy (SUDEP) (Gardella et al., 2018; Larsen et al., 2015; Ohba et al., 2014; Veeramah et al., 2012).

Previous studies using patient-derived *SCN8A* mutations have sought to mechanistically understand how these *de novo* mutations alter biophysical properties of voltage-gated sodium channels, intrinsic excitability of single neurons, and network dynamics underlying behavioral seizures (Baker et al., 2018; Bunton-Stasyshyn et al., 2019; Estacion et al., 2014; de Kovel et al., 2014; Lopez-Santiago et al., 2017; Ottolini et al., 2017; Patel et al., 2016; Wagnon et al., 2016; Wengert et al., 2019b). Understanding the circuit-basis for *SCN8A* encephalopathy requires evaluation of the various cellular subpopulations which comprise neural circuits. Although $Na_V1.6$ is expressed in inhibitory interneurons (Li et al., 2014; Lorincz and Nusser, 2008; Makinson et al., 2017), the mechanisms of network dysfunction in *SCN8A* encephalopathy is greatly limited by the current lack of understanding how inhibitory interneuron function is affected by the expression of mutant $Na_V1.6$. Inhibitory interneuron function is critical for constraining overall network excitability and preventing seizures (Bernard et al., 2000; Kumar and Buckmaster, 2006; Markram et al., 2004). Dysfunction of inhibitory interneurons has therefore been proposed as an important mechanism of epilepsy (Bernard et al., 2000; Stafstrom, 2013). With respect to sodium channel epileptic encephalopathies, hypofunction of inhibitory interneurons has typically been associated with loss-of-function *SCN1A* mutations which result in Dravet Syndrome (Cheah et al., 2012; Escayg and Goldin, 2010; Rhodes et al., 2004; Tai et al., 2014). Previous studies utilizing mouse models of Dravet Syndrome have confirmed that expression of the mutant *SCN1A* allele in GABAergic interneurons is sufficient to recapitulate the key phenotypes of Dravet Syndrome (Cheah et al., 2012). Measurements of intrinsic excitability also revealed impaired excitability of parvalbumin-positive (PV) and somatostatin-positive (SST) inhibitory interneurons at certain key points in development (Favero et al., 2018; Tai et al., 2014). The phenotypic severity of Dravet Syndrome suggests that seemingly small changes to inhibitory interneuron excitability (reduction of max firing frequency by ~20%) may have profound effects for overall network excitability and seizure behavior (Tai et al., 2014).

In this chapter, I utilized both available mouse models of patient-derived *SCN8A* mutations; N1768D ($Scn8a^{D/+}$) which allows global heterozygous expression, and the conditional mouse in which the R1872W ($Scn8a^{w/+}$) mutation is expressed contingent on Cre recombinase. Mice globally expressing either mutation are susceptible to audiogenic seizures, providing a powerful experimental approach to assess seizure susceptibility. Using these two clinically relevant mouse models of epileptic encephalopathy, we report that specific expression of R1872W in SST interneurons ($Scn8a$-$SST^{W/+}$), but not expression in forebrain excitatory neurons ($Scn8a$-$EMX1^{W/+}$), results in audiogenic seizures, indicating that abnormal activity of SST interneurons uniquely contributes to seizures in *SCN8A* encephalopathy. Recordings from SST interneurons from both $Scn8a^{D/+}$ and $Scn8a$-$SST^{W/+}$ showed an initial steady-state hyperexcitability, followed by action potential failure via depolarization block. Dual-cell recordings revealed that mutant SST interneurons are particularly sensitive to

depolarization block under seizure-like conditions and that depolarization block occurs coincidently with pyramidal neuron ictal discharges. Counterintuitively, GqDREADD-mediated chemogenetic activation of wild-type control SST interneurons was sufficient to facilitate initial hyperexcitability followed by depolarization block and *status epilepticus* in the mice, directly demonstrating the proconvulsant effect of aberrant SST physiology. Recordings of voltage-gated sodium channel activity identified elevated persistent sodium currents (I_{NaP}) in mutant SST interneurons. Computational modelling revealed that elevating I_{NaP} was singly sufficient to induce initial hyperexcitability and premature entry into depolarization block. Lastly, we validated the model predictions by demonstrating that application of veratridine, a pharmacological activator of I_{NaP}, to wild-type SST interneurons induces premature depolarization block. Overall, our results reveal a previously unappreciated mechanism by which SST interneurons contribute to seizures in *SCN8A* encephalopathy and may potentially generate novel therapeutic intervention strategies through targeting this important neuronal subpopulation.

Methods

Ethics Approval

All procedures were conducted in accordance with University of Virginia's ACUC guidelines.

Mouse husbandry and genotyping

Scn8a$^{D/+}$ and *Scn8a*$^{W/+}$ were generated as previously described and maintained through crosses with C57BL/6J mice (Jax#: 000664) (Bunton-Stasyshyn et al., 2019; Wagnon et al., 2015). Cell-type specific expression of R1872W was achieved using males homozygous or heterozygous for the R1872W allele and females homozygous for EIIa-Cre (Jax#: 003724), EMX1-Cre (Jax#: 005628), or SST-Cre (Jax#:013044) to generate mutant mice (*Scn8a*-EIIa$^{W/+}$, *Scn8a*-EMX1$^{W/+}$, and *Scn8a*-SST$^{W/+}$ respectively) (Bunton-Stasyshyn et al., 2019). Control mice for audiogenic experiments in *Scn8a*-EIIa$^{W/+}$ and *Scn8a*-EMX1$^{W/+}$ were separate litters lacking the R1872W allele and for *Scn8a*-SST$^{W/+}$ they were littermate controls lacking the R1872W allele. Fluorescent labeling of SST interneurons was achieved by first crossing male *Scn8a*$^{D/+}$ or *Scn8a*$^{W/+}$ mice with a Cre-dependent tdTomato reporter (Jax#:007909) and then with female mice homozygous for SST-Cre. Experimental groups used roughly equal numbers of male and female mice to control for any potential sex differences. For chemogenetic experiments, male mice heterozygous for GqDREADD allele (Jax#: 026220) were crossed with female mice homozygous for SST-Cre. All genotyping was conducted through using Transnetyx automated genotyping PCR services.

Audiogenic seizure testing

To test for audiogenic seizures mice were taken from their home cage and transferred to a clean test cage where they were allowed to acclimate for ~20 seconds before the onset of the acoustic stimulus. Similar to a method described previously (Martin et al., 2020), a sonicator (Branson 200 ultrasonic cleaner) was used to produce the audiogenic stimulus directly adjacent to the test cage. The stimulus duration lasted for 50 seconds or until the animal had a behavioral seizure. *Scn8a*-EIIa$^{W/+}$ mice were tested between P13-P16. *Scn8a*-Emx1$^{W/+}$ were tested between 21-24 days. *Scn8a*-SST$^{W/+}$ mice were tested at 7-10 weeks. Videos of audiogenic seizure tests were recorded with a laptop webcam and the duration of seizure phases was analyzed by taking the time in seconds that the mouse spent in each of the phases: a wild-running phase characterized by fast circular running throughout the cage, a tonic phase characterized by hindlimb extension and muscle rigidity, a clonic phase typified by myoclonic jerking of the hindlimbs, and recovery exemplified when the mouse ceased myoclonic jerking and righted itself.

Brain slice preparation

Preparation of acute brain slices for patch-clamp electrophysiology experiments was modified from standard protocols previously described (Baker et al., 2018; Bunton-Stasyshyn et al., 2019; Wengert et al., 2019b). Mice were anesthetized with isoflurane and decapitated. The brains were rapidly removed and kept in chilled ACSF (0^{O}C) containing in mM: 125 NaCl, 2.5 KCl, 1.25 NaH_2PO_4, 2 $CaCl_2$, 1 $MgCl_2$, 0.5 L-Ascorbic acid, 10 glucose, 25 $NaHCO_3$, and 2 Na-pyruvate. The slices were constantly oxygenated with 95% O_2 and 5% CO_2 throughout the preparation. 300 μM coronal or horizontal brain sections were prepared using a Leica VT1200 vibratome. Slices were collected and placed in ACSF warmed to 37^{O}C for ~30 minutes then kept at room temperature for up to 6 hours.

Electrophysiology recordings

Brain slices were placed in a chamber continuously superfused (~2 mL/min) with continuously oxygenated recording solution warmed to 32 ± 1 ºC. Cortical layer V SST interneurons were identified as red fluorescent cells and pyramidal

neurons were identified based on absence of fluorescence and pyramidal morphology via video microscopy using a Zeiss Axioscope microscope. Whole-cell recordings were performed using a Multiclamp 700B amplifier with signals digitized by a Digidata 1322A digitizer. Currents were amplified, low-pass filtered at 2 kHz, and sampled at 100 kHz. Borosilicate electrodes were fabricated using a Brown-Flaming puller (Model P1000, Sutter Instruments) to have pipette resistances between 1.5-3.5 MΩ.

Intrinsic excitability recordings

Current-clamp recordings of neuronal excitability were collected in ACSF solution identical to that used for preparation of brain slices. The internal solution contained in mM: 120 K-gluconate, 10 NaCl, 2 $MgCl_2$, 0.5 K_2EGTA, 10 HEPES, 4 Na_2ATP, 0.3 NaGTP (pH 7.2; osmolarity 290 mOsm). Intrinsic excitability was assessed using methods adapted from those previously described (Ottolini et al., 2017; Wengert et al., 2019b). Briefly, resting membrane potential was manually recorded immediately going whole-cell and confirmed using a 1-min gap-free recording of the neuron at rest. Current ramps from 0 to 400 pA over 4 seconds were used to calculate passive membrane and AP properties including threshold as the point at which membrane potential slope reaches 5% of the maximum slope, upstroke and downstroke velocity which are the maximum and minimum slopes on the AP respectively, the amplitude which was defined as the voltage range between AP peak and threshold, the APD_{50} which is the duration of the AP at the midpoint between threshold and peak, input resistance which was calculated using a -20 pA pulse in current clamp recordings, and the rheobase which was operationally defined as the maximum amount of depolarizing current that could be injected into the neurons before eliciting APs. AP frequency-current relationships were determined using 500-ms current injections ranging from -140 to 600 pA. APs were counted only if the peak of the action potential was greater than 0 mV. Threshold for depolarization block was defined in this context as the current injection that resulted in the maximum number of APs, which for neurons that did not undergo depolarization block was the maximum current injection 600 pA.

Outside-out voltage-gated sodium channel recordings

Patch-clamp recordings in the outside-out configuration were collected using a protocol modified from an approach previously described (Ottolini et al., 2017). The recording solution was identical to that used for brain-slice preparation. The internal solution for all voltage-gated sodium channel recordings contained in mM: 140 CsF, 2 $MgCl_2$, 1 EGTA, 10 HEPES, 4 Na_2ATP, and 0.3 NaGTP with the pH adjusted to 7.3 and osmolality to 300 mOsm. Voltage-dependent activation and steady-state inactivation parameters were recorded using voltage protocols previously described (Wengert et al., 2019b).

Persistent sodium current recordings

The recording solution was modified with a reduced sodium concentration to allow for proper voltage control through the entire range of command voltages (Royeck et al., 2008; Wengert et al., 2019b). It contained in mM: 50 NaCl, 90 TEACl, 10 HEPES, 3.5 KCl, 2 $CaCl_2$, 2 $MgCl_2$, 0.2 $CdCl_2$, 4 4-AP, 25 D-glucose. Steady-state persistent sodium currents were elicited using a voltage ramp (20 mV/sec) from -80 to -20 mV. After collecting recordings at baseline, the procedure was repeated in the presence of 1uM tetrodotoxin (TTX) to completely isolate the sodium current. TTX-subtracted traces were analyzed by extracting the current at each mV from -80 mV to -20 mV. The half-maximal voltage for activation of the current was calculated as previously described (Wengert et al., 2019b). Any recordings in which the neuron escaped steady-state voltage control were discarded before TTX application.

Dual-cell recordings

Gap-free recordings of pairs of one pyramidal and one SST interneuron <200 μM away were used to examine cell interplay during seizure-like events. Seizure-like events were evoked using Mg^{2+}-free ACSF containing either 50 or 100 μM 4-aminopyridine (4-AP). Seizure-like depolarization block events were defined in this context as instances in which the membrane potential reached a stable value above action potential threshold which occurred simultaneously with burst of action potentials in the nearby pyramidal neuron.

Computational modeling

A single-compartment conductance-based neuronal model was modified based on one used previously (Nowacki et al., 2012). The dynamics of the neuronal voltage is described by:

$$C\dot{V} = I_{\mathrm{app}} - I_{\mathrm{NaT}} - I_{\mathrm{NaP}} - I_{\mathrm{KT}} - I_{\mathrm{KP}} - I_{\mathrm{L}}$$

where V is the transmembrane voltage, C is the membrane capacitance, I_{app} is the applied current density, $I_{NaT/NaP}$ are the transient and persistent sodium current densities, respectively, and $I_{KT/KP}$ are the transient and persistent potassium currents densities, respectively. These currents are specified by the functional forms:

$$I_{\mathrm{NaT}} = g_{\mathrm{NaT}} m_{\mathrm{NaT}}^3 h_{\mathrm{NaT}} (V - V_{\mathrm{Na}}),$$
$$I_{\mathrm{NaP}} = g_{\mathrm{NaP}} m_{\mathrm{NaP}} (V - V_{\mathrm{Na}}),$$
$$I_{\mathrm{KT}} = g_{\mathrm{KT}} m_{\mathrm{KT}} h_{\mathrm{KT}} (V - V_{\mathrm{K}}),$$
$$I_{\mathrm{KP}} = g_{\mathrm{KP}} m_{\mathrm{KP}} (V - V_{\mathrm{K}}),$$
$$I_{\mathrm{L}} = g_{\mathrm{L}} (V - V_{\mathrm{L}}),$$

where g_X represents the maximal conductance of channel type $X \in \{\mathrm{NaT}, \mathrm{NaP}, \mathrm{KT}, \mathrm{KP}\}$, m_X represents the fraction of open activation gates of channel type X, with h_X corresponding to the fraction of open inactivation gates, where appropriate, and V_Y is the reversal (Nernst) potential of ionic species $Y \in \{\mathrm{Na}, \mathrm{K}, \mathrm{L}\}$. The dynamics of the gating variables obey:

$$\tau_{m_X} \dot{m}_X = m_{X,\infty}(V) - m_X, \qquad \tau_{h_X} \dot{h}_X = h_{X,\infty}(V) - h_X,$$

where τ_{m_X, h_X} are the timescales of the activation and inactivation of channel type X, respectively; and $m_{X,\infty}(V)$ and $h_{X,\infty}(V)$ are its steady state activation and inactivation curves (e.g., Figure 3F-G), which are themselves described by Boltzmann functions of the form:

$$m_{X,\infty}(V) = (1 + \exp(-(V - V_{m_X})/k_{m_X})^{-1}, \qquad h_{X,\infty}(V) = (1 + \exp(-(V - V_{h_X})/k_{h_X})^{-1},$$

where V_{m_X, h_X} are the thresholds for activation and inactivation and k_{m_X, h_X} are the associated sensitivities around this threshold. The activation of both types of sodium channel is assumed to be instantaneous, meaning that $m_{\mathrm{NaT,NaP}} = m_{\mathrm{NaT,NaP},\infty}(V)$ always. The parameter units and values are as follows:

Parameter	Unit	Value	Parameter	Unit	Value
g_{NaT}	mmho/cm^2	130	V_{Na}	mV	60
g_{NaP}	mmho/cm^2	[0-0.4]	V_{K}	mV	-85
g_{KT}	mmho/cm^2	10	V_{L}	mV	-65
g_{KP}	mmho/cm^2	1.65	$\tau_{m_{\mathrm{KT}}}$	ms	1
g_{L}	mmho/cm^2	0.02	$\tau_{m_{\mathrm{KP}}}$	ms	75
$V_{m_{\mathrm{NaT}}}$	mV	-37	$\tau_{h_{\mathrm{NaT}}}$	ms	1
$V_{m_{\mathrm{NaP}}}$	mV	-47	$\tau_{h_{\mathrm{KT}}}$	ms	1400
$V_{m_{\mathrm{KT}}}$	mV	-5.8	$k_{m_{\mathrm{NaT}}}$	mV	5
$V_{m_{\mathrm{KP}}}$	mV	-30	$k_{m_{\mathrm{NaP}}}$	mV	3
$V_{h_{\mathrm{NaT}}}$	mV	-70	$k_{m_{\mathrm{KT}}}$	mV	11.4
$V_{h_{\mathrm{KT}}}$	mV	-68	$k_{m_{\mathrm{KP}}}$	mV	10
I_{app}	mA/cm^2	[0-0.4]	$k_{h_{\mathrm{NaT}}}$	mV	-7
C	μF/cm^2	1	$k_{h_{\mathrm{KT}}}$	mV	-9.7

All model simulations were performed in MATLAB R2020a. Code to replicate these simulations is available to download via Git from www.GitHub.com/kyle-wedgwood/DepolarizationBlock.

Bifurcation analysis

Bifurcation analysis was performed in DDE-BIFTOOL v3.1.1, which is a MATLAB-based numerical software package for numerical continuation and in AUTO-07P which is a Fortran-based numerical continuation program.

In-vivo seizure monitoring

Custom electrocorticogram (ECoG) headsets (PlasticsOne, Inc.) were implanted in 7–10-week-old SST-Cre$^{+/-}$; GqDREADD$^{+/-}$ or SST-Cre; GqDREADD$^{-/-}$ mice using standard aseptic surgical techniques. Anesthesia was induced with

5% and maintained with 0.5%–3% isoflurane. Adequacy of anesthesia was assessed by lack of toe-pinch reflex. A midline skin incision was made over the skull, and burr holes were made at the lateral/rostral end of both the left and right parietal bones to place ECoG leads, and at the interparietal bone for a reference and ground electrodes. A headset was attached to the skull with dental acrylic (Jet Acrylic; Lang Dental). Mice received postoperative analgesia with ketoprofen (5 mg/kg, i.p.) and 0.9 % saline (0.5 ml i.p.) and were allowed to recover a minimum of 2-5 days prior to seizure-monitoring experiments.

Mice were then individually housed in custom-fabricated chambers and monitored for the duration of the experiment. The headsets were attached to a custom low torque swivel cable, allowing mice to move freely in the chamber. ECoG signals were amplified at 2000x and bandpass filtered between 0.3 - 100 Hz, with an analogue amplifier (Neurodata Model 12, Grass Instruments Co.). Biosignals were digitized with a Powerlab 16/35 and recorded using LabChart 7 software (AD Instruments, Inc.) at 1 kS/s. Video acquisition was performed by multiplexing four miniature night vision-enabled cameras and then digitizing the video feed with a Dazzle Video Capture Device (Corel, Inc.) and recording at 30 fps with LabChart 7 software in tandem with biosignals.

In seizure monitoring experiments, ~30 minutes of baseline ECoG signal were recorded before the mice were injected with vehicle or CNO (0.2, 1, and 5 mg/kg). Video ECoG was continuously recorded until the ECoG and behavioral manifestations of status epilepticus ended (typically ~8 hours). Mice had access to food *ad libitum*, but were restricted from water to protect against headset damage and animal injury during status epilepticus. Power analysis was performed using Spike2 v7.17 (Cambridge Electronic Design, Limited), using FFT size of 1024 points (Hanning method), which provides a 0.9766 Hz resolution across intervals of 1.024 s. To obtain values for the CNO dose-response (Fig. 4D) the peak power in band 2-10 Hz after injection was normalized to pre-injection levels.

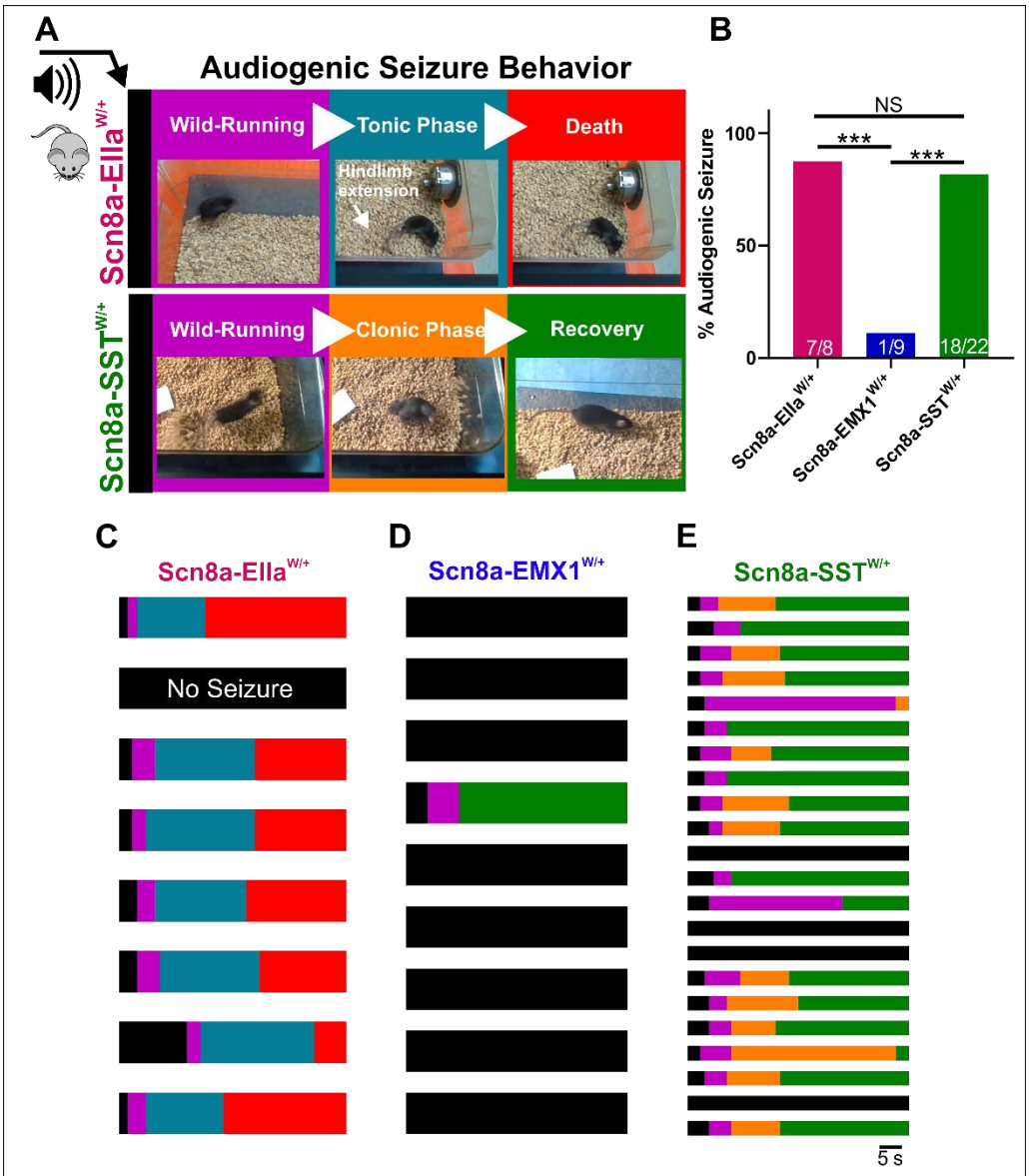

Figure 6.1. Somatostatin interneuron-specific expression of mutant Scn8a is sufficient for susceptibility to audiogenic seizures.
A. Audiogenic seizure behavior in mice with cell-type specific expression of R1872W Scn8a mutation. Upon high-intensity acoustic stimulation, Scn8a-EIIa$^{W/+}$ mice exhibit wild-running (purple) followed by a tonic phase characterized by hindlimb extension (blue) which is followed by collapse of breathing and death (red). Scn8a-SST$^{W/+}$ mice exhibit wild-running (purple) but progress to a convulsive clonic phase characterized by repetitive shaking and limb-jerking followed by recovery. B. 7 of 8 (87.5%) Scn8a-EIIa$^{W/+}$ mice (magenta) and 18 of 22 (~82%) Scn8a-SST$^{W/+}$ mice (green) had audiogenic seizures while only 1 of 9 (~11%) Scn8a-EMX1$^{W/+}$. Significance determined by Fisher's exact test (*P<0.01, ***P<0.001). C-E. Color-coded raster plots for seizure behavior of Scn8a-EIIa$^{W/+}$ (C), Scn8a-EMX1$^{W/+}$ (D), and Scn8a-SST$^{W/+}$ (E) mice.

Analysis

All patch-clamp electrophysiology data were analyzed using custom MATLAB scripts and/or ClampFit 10.7. All statistical comparisons were made using the appropriate test using GraphPad Prism 8. One-sided t-tests were only used in the CNO physiology experiments where a clear directional hypothesis was articulated. Data are presented as individual data points and/or mean ± standard error of the mean.

Results

Using a model of *SCN8A* encephalopathy in which the patient-derived mutation R1872W is expressed in a Cre-dependent manner, we sought to determine the cell-type specific contribution to audiogenic seizure susceptibility. Acoustic stimulation of mice globally-expressing the R1872W *Scn8a* mutation (*Scn8a*-EIIa$^{W/+}$) caused audiogenic seizures (7 of 8 mice; 87.5%; Figure 6.1A-C). Seizures were characterized by a period of wild-running, a tonic phase associated with hindlimb extension, and sudden death (Figure 6.1A; Video 6.1). To our surprise, expression of the R1872W *Scn8a* mutation in forebrain excitatory neurons (*Scn8a*-EMX1$^{W/+}$) did not reliably convey susceptibility to audiogenic seizures, with only 1 of 9 mice exhibiting a single brief bout of wild-running; (Video 6.2; ***P<0.01 Fisher's Exact test; Figure 6.1B, C, E). In contrast, expression of the R1872W *Scn8a* mutation selectively in somatostatin-positive (SST) inhibitory interneurons (*Scn8a*-

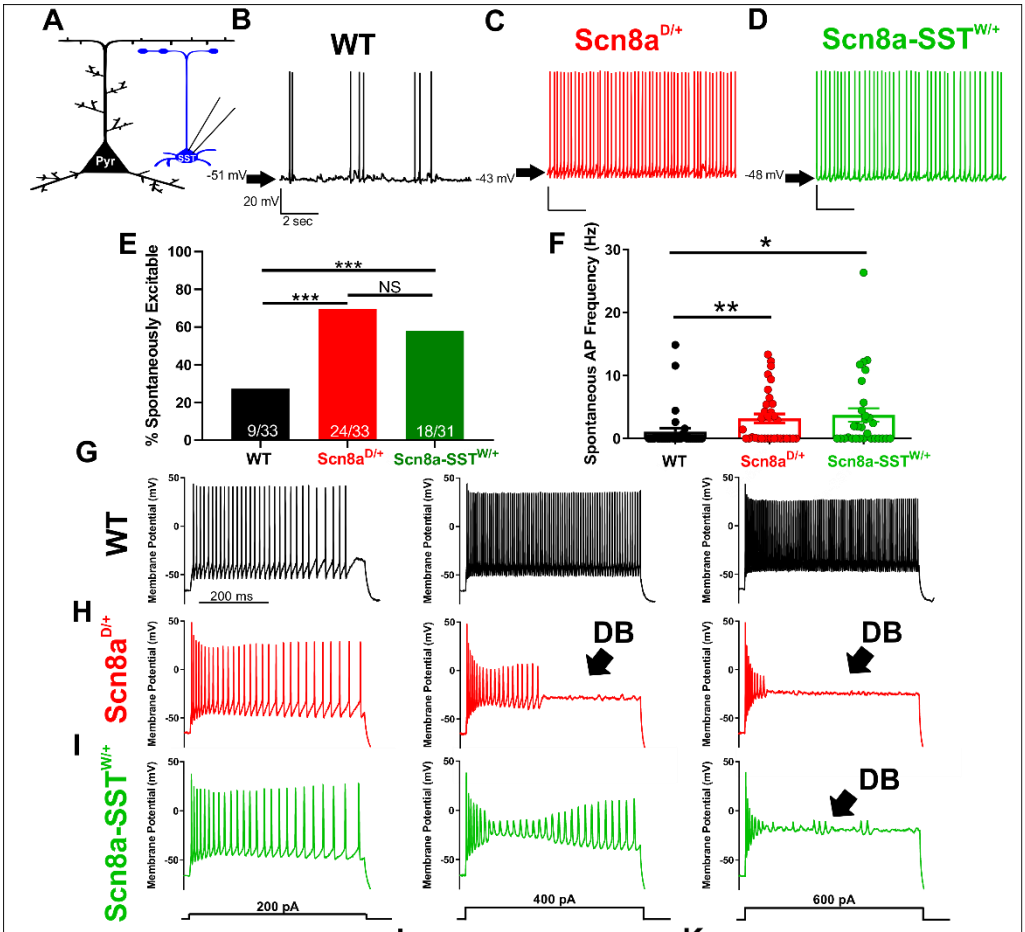

Figure 6.2: Scn8a$^{D/+}$ and Scn8a-SST$^{W/+}$ somatostatin interneurons are hyperexcitable and readily enter depolarization block. Whole-cell recordings collected from WT, Scn8a$^{D/+}$, and Scn8a-SST$^{W/+}$ somatosensory layer V SST interneurons (blue). B-D. Representative example traces of spontaneous excitability of WT (B; black), Scn8a$^{D/+}$ (C; red) and Scn8a-SST$^{W/+}$ (D; green) SST interneurons. Arrows indicate membrane potential between spontaneous APs. E. Only 9 of 33 (~27%) WT SST interneurons were spontaneously excitable, whereas 24 of 33 (~73%) Scn8a$^{D/+}$ and 18 of 31 (~58%) Scn8a-SST$^{W/+}$ spontaneously fired APs (***P<0.01 by Fisher's exact test). F. Average spontaneous firing frequencies for WT (black), Scn8a$^{D/+}$ (red), and Scn8a-SST$^{W/+}$ (green) SST interneurons. Statistical significance calculated by Kruskal-Wallis test followed by Dunn's multiple comparisons (*P<0.05; **P<0.01). G-I. Representative traces for WT (G; black), Scn8a$^{D/+}$ (H; red), and Scn8a-SST$^{W/+}$ (I; green) SST interneurons eliciting APs in response to 500-ms current injections of 200, 400, and 600 pA. Depolarization block is indicated (arrow; DB) in the Scn8a$^{D/+}$ (H; red) and Scn8a-SST$^{W/+}$ (I; green) interneurons. J. Average number of APs elicited relative to current injection magnitude for WT (black; n=33, 7 mice), Scn8a$^{D/+}$ (red; n=33, 6 mice), and Scn8a-SST$^{W/+}$ (green; n=31, 4 mice). At current injections >400 pA, both Scn8a$^{D/+}$ and Scn8a-SST$^{W/+}$ AP frequencies were reduced relative to WT (*P<0.05; Two-way ANOVA followed by Tukey's correction for multiple comparisons). K. Cumulative distribution of SST interneuron entry into depolarization block relative to current injection magnitude for WT (black), Scn8a$^{D/+}$ (red), and Scn8a-SST$^{W/+}$ (green) mice. Curve comparison by Log-rank Mantel-Cox test (**P<0.01).

SST$^{W/+}$) was sufficient to induce an audiogenic seizure in 18 of 22 (~82%), typified by a wild-running phase, a clonic phase characterized by convulsions and jerking of limbs, followed by recovery (Video 6.3; Figure 6.1A-C). Audiogenic seizures were never observed in WT littermate control mice (n=26: Video 6.4). These results indicate that expression of R1872W specifically in SST interneurons is sufficient to induce audiogenic seizures.

We next sought to determine the impact of N1768D and R1872W patient-derived *SCN8A* mutations on SST interneuron function with a goal to better understand how alterations in SST interneuron excitability could lead to seizure susceptibility. We conducted whole-cell patch-clamp electrophysiology recordings of SST interneurons from layer V somatosensory cortex from adult *Scn8a*$^{D/+}$, *Scn8a*-SST$^{W/+}$ and littermate WT mice (Figure 6.2A). Relative to WT controls, a greater proportion of SST interneurons from *Scn8a*$^{D/+}$ and *Scn8a*-SST$^{W/+}$ were spontaneously active (***P<0.01; Fisher's Exact test; Figure 6.2B-E) each with significantly greater frequency of spontaneous action potentials (APs) (*P<0.05 and **P<0.01 relative to WT; Kruskal-Wallis test followed by Dunn's test; Figure 6.2F). Analysis of membrane and AP properties revealed that, relative to WT, both *Scn8a*$^{D/+}$ and *Scn8a*-SST$^{W/+}$ SST interneurons had depolarized resting membrane potentials and decreased rheobases likely contributing to their steady-state hyperexcitability (Table 6.1). Additionally, *Scn8a*$^{D/+}$ SST interneurons had an elevated input resistance and *Scn8a*-SST$^{W/+}$ interneurons had hyperpolarized AP thresholds and increased AP duration (APD_{50}; Table 6.1).

	V_m (mV)	AP Threshold (mV)	Upstroke Velocity (mV/ms)	Downstroke Velocity (mV/ms)	AP Amplitude (mV)	APD50 (ms)	Input Resistance (MΩ)	Rheobase (pA)
WT (n=32)	-60.7 ± 1.7	-36.8 ± 0.8	323 ± 16	-157 ± 13	74.0 ± 2.0	0.62 ± 0.03	215 ± 18	82 ± 12
Scn8a$^{D/+}$ (n=33)	**-52.9 ± 1.5****	-38.4 ± 0.8	290 ± 18	-131 ± 7	76.7 ± 1.4	0.69 ± 0.03	**298 ± 20***	**37 ± 7***
Scn8a-SST$^{W/+}$ (n=31)	**-54.4 ± 1.6***	**-40.84 ± 1.2****	**231 ± 12.8*****	**-87 ± 5.7*****	73.9 ± 2.0	**1.0 ± 0.06*****	250 ± 15	**37 ± 5***

*P<0.05, **P<0.01, ***P<0.001. Data shown as mean ± SEM.

Table 6.1: Membrane and action potential properties of WT, Scn8a$^{D/+}$, and Scn8a-SST$^{W/+}$ somatostatin inhibitory interneurons.

We subjected each neuron to a range of depolarizing current injections to characterize intrinsic excitability. Relative to WT controls (n=33, 7 mice), SST interneurons from both *Scn8a*$^{D/+}$ (n=33, 6 mice) and *Scn8a*-SST$^{W/+}$ mice (n=31, 4 mice) exhibited progressive AP failure at current injections above 400 pA as the interneurons entered depolarization block: At 600 pA, WT SST interneurons fired 47 ± 6 APs/500 ms (94 Hz), *Scn8a*$^{D/+}$ fired 25 ± 5 APs/500 ms (50 Hz), and *Scn8a*-SST$^{W/+}$ fired 23 ± 4 APs/500 ms (46 Hz; ***P<0.001 Two-way ANOVA with Tukey's correction for multiple comparisons; Figure 6.2G-J). Over the range of current injection magnitudes, both *Scn8a*$^{D/+}$ and *Scn8a*-SST$^{W/+}$ interneurons were significantly more prone to depolarization block than WT counterparts (**P<0.01; Log-rank Mantel-Cox test; Figure 6.2K).

Prior studies have described cellular interplay between excitatory pyramidal neurons and fast-spiking interneurons during brain-slice seizure-like activity and *in vivo* seizures in which interneuron depolarization block occurs coincidentally with pyramidal neuron ictal discharges (Cammarota et al., 2013; Jayant et al., 2019; Parrish et al., 2019; Swadlow, 2003; Ziburkus et al., 2006). To test whether SST interneurons expressing *Scn8a* mutations also exhibit depolarization block seizure-like events coincident with pyramidal ictal discharges, we simultaneously recorded from a SST interneuron and a nearby pyramidal neuron and induced seizure-like activity by applying a bath solution with 0 Mg^{2+} and 4-AP (50 μM) (Ziburkus et al., 2006). Under these conditions, although neurons in all groups increased their excitability, we observed a significantly greater propensity for *Scn8a*$^{D/+}$ (n= 12, 3 mice; Figure 6.3B) and *Scn8a*-SST$^{W/+}$ (n=10, 3 mice; Figure 6.3C) SST interneurons to spontaneously exhibit depolarization block events compared with WT SST interneurons (n=9, 3 mice; Figure 6.3A) supporting our findings that expression of mutant *SCN8A* renders SST interneurons prone to depolarization block (**P<0.01 Log-rank Mantel-Cox test; Figure 6.3A-C, E). Consistent with previous reports in fast-spiking interneurons (Cammarota et al., 2013; Jayant et al., 2019; Parrish et al., 2019; Swadlow, 2003; Ziburkus et al., 2006), instances of SST interneuron depolarization block were entirely concomitant with seizure-like ictal discharges of nearby layer V pyramidal neurons (Figure 6.3B-D). Only when the bath concentration of the proconvulsant 4-AP was increased to 100 μM did we observe similar ictal-discharges of pyramidal neurons and depolarization block events in WT SST interneurons (Figure 6.3D-E). These results demonstrate not only that mutant SST interneurons are hypersensitive to depolarization block in the

seizure-like context, but also that simultaneous SST depolarization block is coincident with pyramidal neuron bursting activity, a hallmark of seizure-like activity.

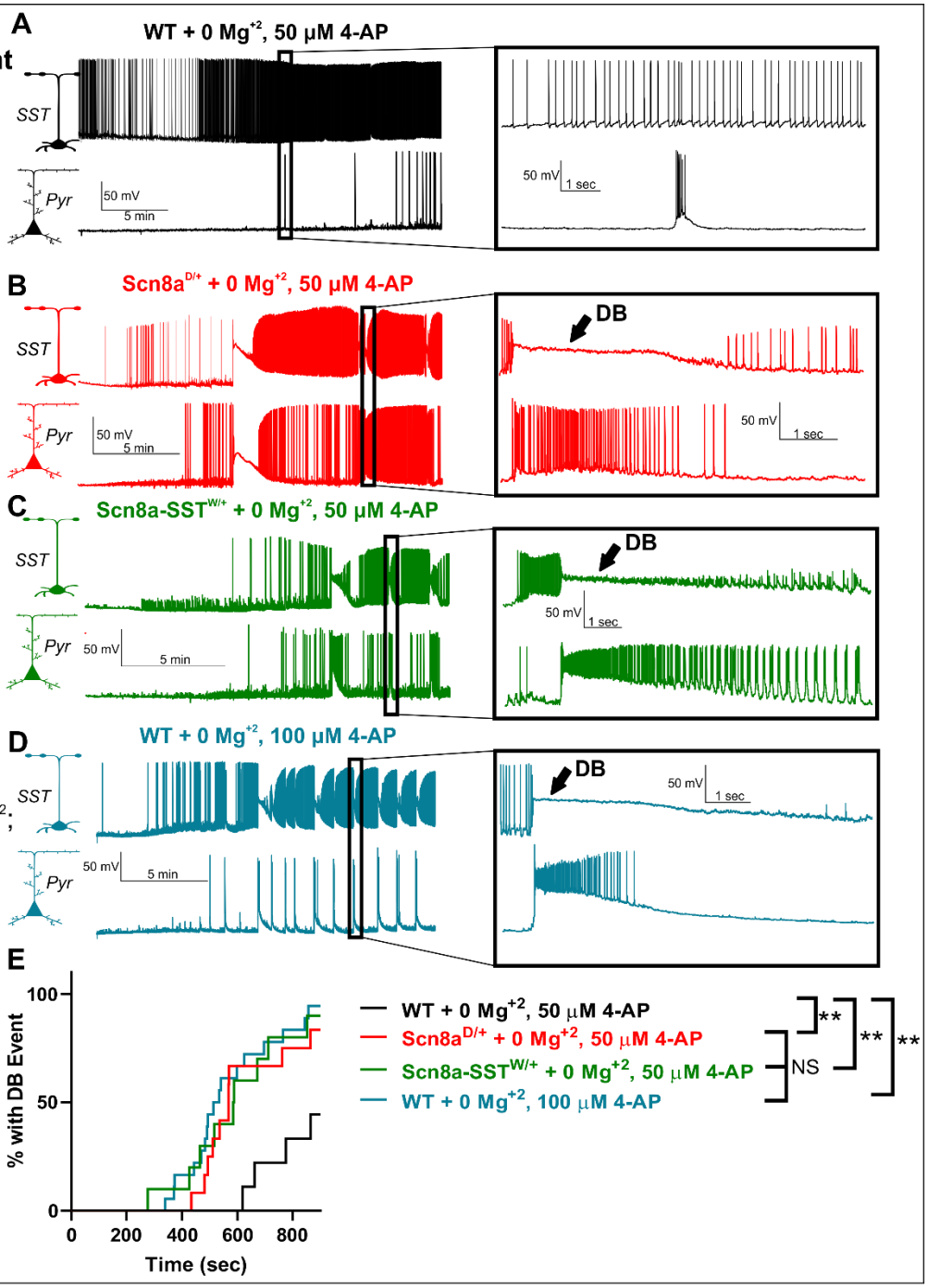

Figure 6.3: Hypersensitive depolarization block of mutant somatostatin interneurons in seizure-like conditions. A-D. Representative example traces of WT (A; black), Scn8a$^{D/+}$ (B; red), and Scn8a-SST$^{W/+}$ (C; green) SST-pyramidal neuron pairs exposed to bath solution containing 0 Mg^{2+}, 50 µM 4-AP (A-C) and WT SST-pyramidal neuron pairs exposed to 0 Mg^{2+}, 100 µM 4-AP (D). Expanded views indicate example synchronous SST interneuron depolarization block and pyramidal neuron ictal discharge events (B-D) which were not present in most neuronal pairs in the control group (A). E. Cumulative distribution plot of seizure-like events over time reveals that Scn8a$^{D/+}$ + 0 Mg^{+2}; 50 µM (red), Scn8a-SST$^{W/+}$ + 0 Mg^{+2}; 50 µM (green), and WT + 0 Mg^{+2}; 100 µM (blue) were hypersensitive to depolarization block-mediated seizure-like events relative to WT + 0 Mg^{+2}; 50 µM neuron pairs (black; **P<0.01; Log-rank Mantel-Cox test).

To test whether depolarization block of SST interneurons directly contributes to behavioral seizures, we generated mice in which the GqDREADD excitatory chemogenetic receptor was specifically expressed in SST interneurons (SST-Cre; GqDREADD$^{+/-}$, Figure 6.4A). GqDREADD receptors were activated using CNO (i.p.) at 0.2, 1, and 5 mg/kg and changes in ECoG activity monitored (Figure 6.4A). In control mice (SST-Cre; GqDREADD$^{-/-}$), CNO administration at 5 mg/kg did not alter the ECoG or induce seizure behavior (Figure 6.4B). In contrast, SST-Cre; GqDREADD$^{+/-}$ mice exhibited a robust hypersynchronization of ECoG activity characterized by an increase in low-frequency (2-10Hz) power and displayed behavioral manifestations associated with *status epilepticus* including loss of balance, and clonic jerks (Figure 6.4C; Video 6.5). The fact that the effect of CNO administration in SST-Cre; GqDREADD$^{+/-}$ mice was dose-dependent (*P<0.05 comparing SST-Cre;GqDREADD$^{-/-}$; black; n=4 and SST-Cre;GqDREADD$^{+/-}$; red; n=8; unpaired t-test; Figure 6.4D) taken

alongside the absence of effect of CNO in SST-Cre;GqDREADD$^{-/-}$ mice supports our notion that GqDREADD-mediated activation of SST interneurons is sufficient to induce prolonged seizures (i.e. *status epilepticus*) in mice expressing wild-type sodium channels. In support of our hypothesis, recordings from SST interneurons in SST-Cre;GqDREADD$^{+/-}$ mice

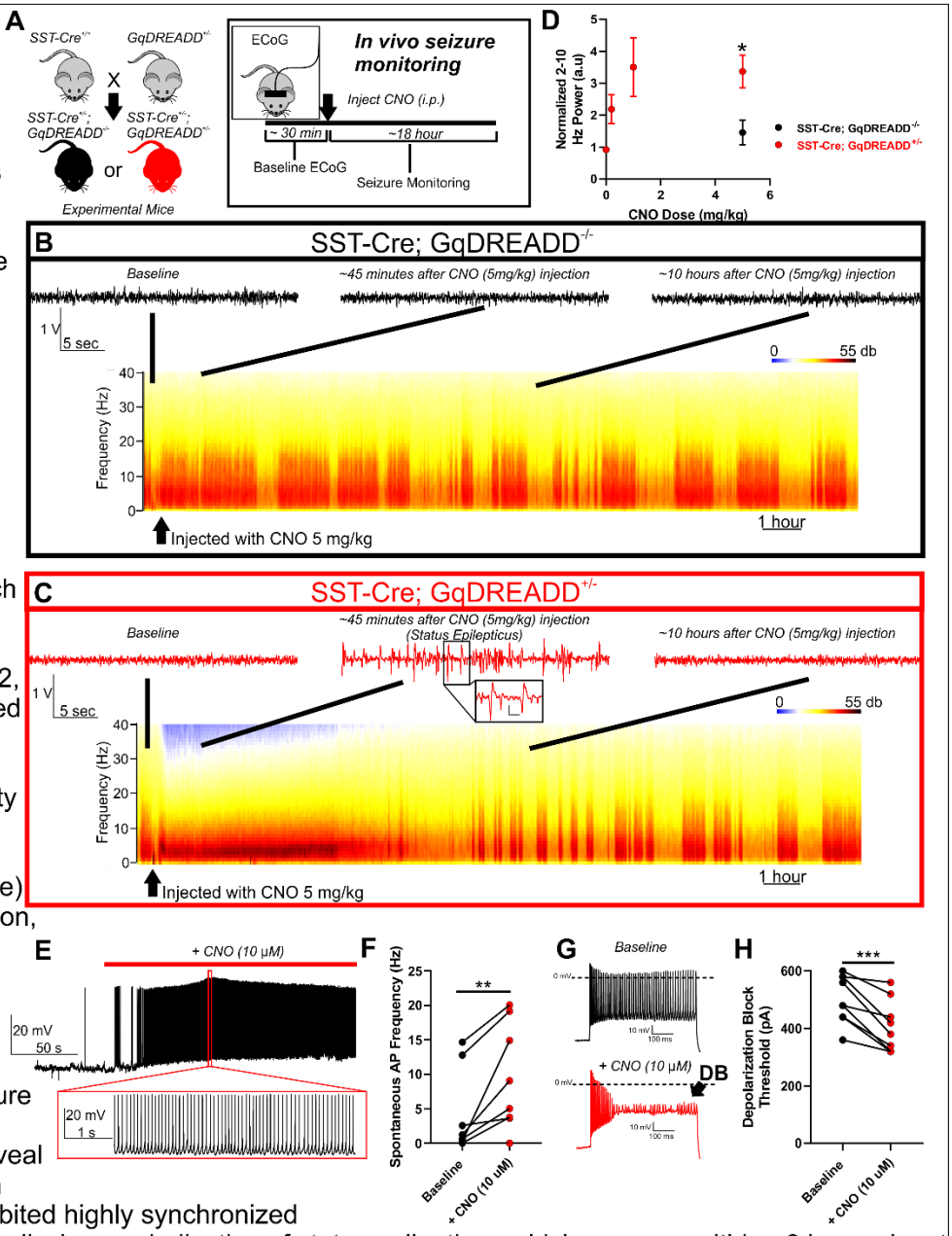

Figure 6.4: Chemogenetic activation of somatostatin interneurons induces hyperexcitability and depolarization block, and results in status epilepticus in wild-type mice.
A. Breeding strategy: Female mice homozygous for SST-cre (SST-cre$^{+/+}$) were bred with male mice heterozygous for a floxed GqDREADD allele (GqDREADD$^{+/-}$) to produce offspring that were either SST-Cre$^{+/-}$; GqDREADD$^{-/-}$ control mice (black) or SST-Cre$^{+/-}$; GqDREADD$^{+/-}$ experimental mice (red). For *in vivo* seizure monitoring, ECoG was recorded from each mouse for ~30 minutes of baseline activity, then treated with vehicle or CNO (i.p. at 0.2, 1, and 5 mg/kg), and monitored for seizure activity for ~18 hours. B-C. Example relative power spectra of ECoG activity for ~18 hours with representative ECoG traces before CNO injection (baseline) ~45 minutes after CNO injection, and ~10 hours after CNO injection. B. Example traces indicating that in mice lacking the GqDREADD receptor (black), CNO treatment (5 mg/kg) did not lead to seizure behavior or changes in ECoG activity. C. Example traces reveal that upon CNO administration GqDREADD$^{+/-}$ mice (red) exhibited highly synchronized ECoG activity and spike-wave discharges indicative of status epilepticus which recovers within ~8 hours. Inset shows expanded view of example spike-wave discharges. Scale bar is 0.25 volts and 0.2 sec. D. Normalized 2-10 Hz power relative to pre-injection baseline observed in response to vehicle and CNO (0.2, 1, and 5 mg/kg). SST-Cre; GqDREADD$^{+/-}$ mice (n=5 for vehicle, 0.2, and 1 mg/kg, n=8 for 5 mg/kg; red) experienced a robust and dose-dependent increase in 2-10 Hz power. SST-Cre; GqDREADD$^{-/-}$ control mice (black) did not show a significant increase in 2-10 Hz power upon administration of 5 mg/kg CNO (N=4). E. Representative example trace of an SST-Cre; GqDREADD$^{+/-}$ SST interneuron showing spontaneous increase in excitability in response to bath application of CNO (10 µM; red bar). Expanded view illustrates the high firing frequency during CNO exposure. F. Spontaneous firing frequencies of SST interneurons from SST-Cre; GqDREADD$^{+/-}$ mice before (black) and after (red) treatment with CNO (10 µM; n=8, 4 mice; **P<0.01; paired t-test). G. Example traces of SST interneuron excitability from an SST-Cre; GqDREADD$^{+/-}$ mouse in response to a 600 pA current injection before (black), and after (red) CNO (10 µM) bath application. Premature depolarization block (DB, arrow) is observed after CNO treatment. H. Depolarization block threshold for each SST-Cre; GqDREADD$^{+/-}$ SST interneuron before (black) and after (red) treatment with CNO (10 µM; n=8, 4 mice; ***P<0.001; paired t-test).

demonstrated an increase in spontaneous excitability (**P<0.01; n=8,4 mice; paired t-test; Figure 6.4E-F) and premature depolarization block in response to depolarizing current injections (***P<0.001; n=8,4 mice; paired t-test; Figure 6.4G-H) after bath application of CNO (10 μM). These findings thus resembled the physiological phenotype observed in mutant *SCN8A*-expressing SST interneurons (Figure 6.2).

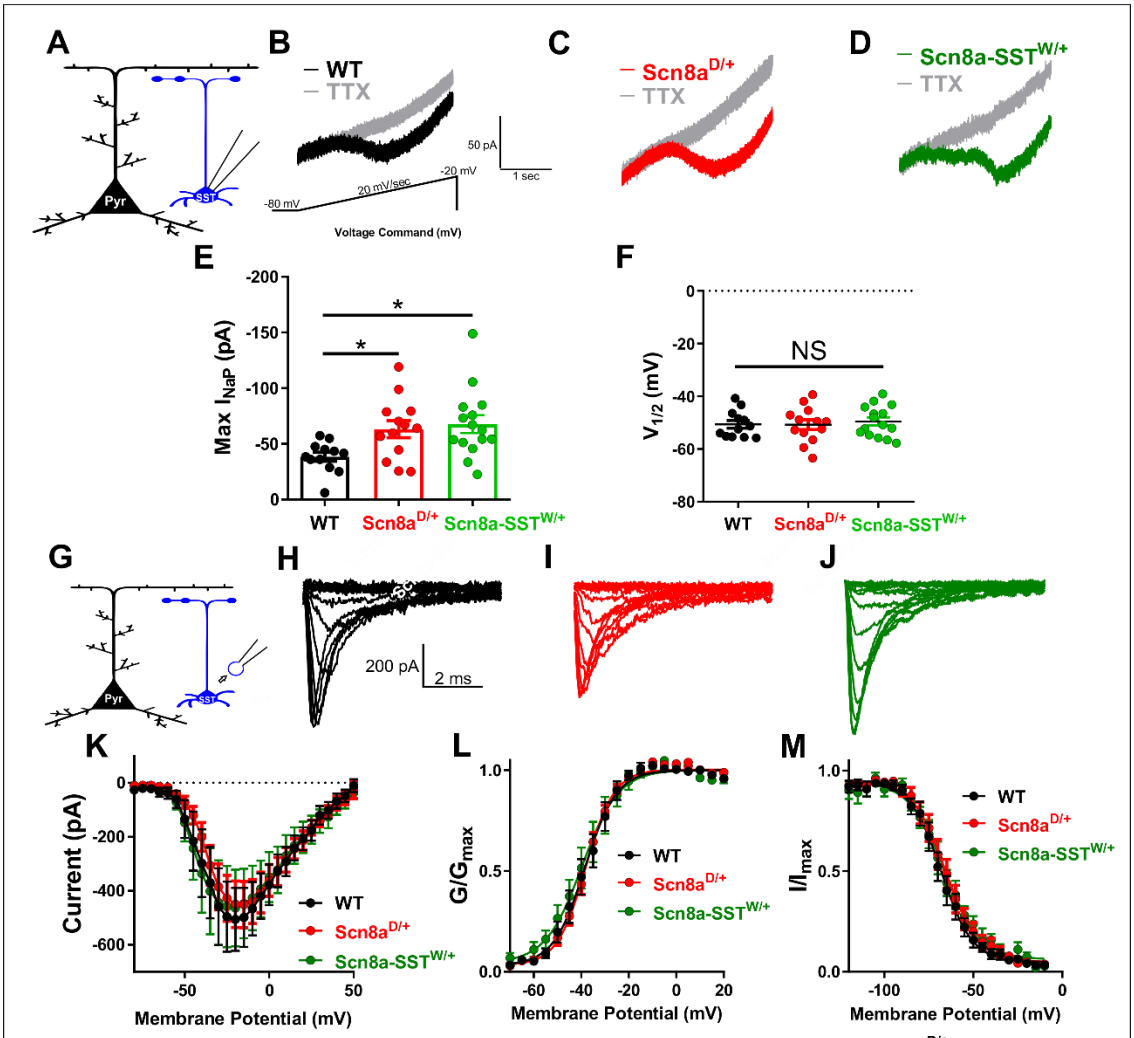

Figure 6.5: Elevated steady-state persistent sodium currents in Scn8a$^{D/+}$ and Scn8a-SST$^{W/+}$ somatostatin interneurons. A. Whole-cell recordings were collected from SST interneurons (blue) to measure whole-cell persistent sodium currents. B-D. Example traces of steady-state persistent sodium currents evoked by slow voltage ramps (-80 mV to -20 mV at 20 mV/sec) before (black, red, or green) and after addition of TTX (500 nM; gray) for WT (B; black), Scn8a$^{D/+}$ (C; red), and Scn8a-SST$^{W/+}$ (D; green) SST interneurons. E. Elevated maximum persistent sodium current (I_{NaP}) in Scn8a$^{D/+}$ SST interneurons (red; n=13, 4; *P<0.05) and Scn8a-SST$^{W/+}$ (green; n=14, 3; *P<0.05) compared to WT SST interneurons (black; n=12, 4; One-way ANOVA followed by Dunnett's multiple comparisons test). F. Half-maximal voltage of activation between WT, Scn8a$^{D/+}$, and Scn8a-SST$^{W/+}$ SST interneurons was not significantly different between groups (NS; P>0.05). G. Somatic transient sodium current was assessed in SST interneurons (blue) using patch-clamp recordings in the outside-out configuration. H-J. Example traces for family of voltage-dependent sodium currents recorded from outside-out excised patches from either WT (H; black), Scn8a$^{D/+}$ (I; red), and Scn8a-SST$^{W/+}$ (J; green) SST interneurons. K. Current-voltage relationship for WT (black; n=9, 4 mice), Scn8a$^{D/+}$ (red; n=13, 5 mice), and Scn8a-SST$^{W/+}$ (green; n=8, 3 mice) SST interneurons. L-M. Voltage-dependent conductance and steady-state inactivation curves for WT (black), Scn8a$^{D/+}$ (red), and Scn8a-SST$^{W/+}$ (green) SST interneurons.

The most prominent biophysical impairment of both the N1768D and R1872W voltage-gated sodium channel variants is an elevated steady-state persistent sodium current (I_{NaP}) (Baker et al., 2018; Bunton-Stasyshyn et al., 2019; Lopez-Santiago et al., 2017; Ottolini et al., 2017; Veeramah et al., 2012; Wengert et al., 2019b). We recorded I_{NaP} in SST interneurons using slow voltage-ramps (Figure 6.5A). I_{NaP} from *Scn8a*$^{D/+}$ (63 ± 8 pA; n=13, 4 mice) and *Scn8a*-SST$^{W/+}$ (68 ± 8 pA; n=15, 3 mice) SST interneurons were augmented relative to WT interneurons (38 ± 4 pA; n=12, 4 mice; *P<0.05 ANOVA followed by Dunnett's multiple comparisons test; Figure 6.5B-E). Half-maximal voltages ($V_{1/2}$) were not different between groups (Figure 6.5F). The transient sodium current was recorded in excised somatic patches in order to assess activation and steady-state inactivation properties under proper voltage-control (Figure 6.5G). No differences in current density, voltage-dependent activation, or steady-state inactivation between WT (n=9,4 mice), *Scn8a*$^{D/+}$ (n=13,5 mice) and *Scn8a*-SST$^{W/+}$ (n=8, 3 mice) SST interneurons were detected (Figure 6.5H-M; Table 2). Together, these results suggest that an increased I_{NaP} current

magnitude is likely the primary cause for the altered excitability observed in the mutant SST interneurons and subsequent entry into depolarization block.

To test our hypothesis, we utilized a single-compartment conductance-based computational neuron model to examine neuronal frequency-current relationships as we varied the magnitude of the persistent sodium conductance (g_{NaP}). At low levels of g_{NaP}, neuronal firing frequency increased with the injected current magnitude over a large range of depolarizing current injections, reaching a maximum of 96 APs/500-ms (Figure 6.6A-C). In support of our hypothesis, we found that increasing the magnitude of the g_{NaP} led to a decrease in rheobase current and a corresponding facilitation of AP firing at low magnitude current injections, followed by premature AP failure via entry into depolarization block as the current injection magnitude was increased (Figure 6.6A-C). Although the neuronal model used is overly simple in both geometric and ionic terms relative to SST interneurons *in vivo*, the sufficiency of the model to reproduce both features of mutant SST interneuron excitability is strong evidence that an elevated I_{NaP} is directly sufficient for initial hyperexcitability followed by premature entry into depolarization block.

	Peak Current (pA)	Activation $V_{1/2}$ (mV)	Activation Boltzmann Slope Factor	Inactivation $V_{1/2}$ (mV)	Inactivation Boltzmann Slope Factor	Decay Tau (ms)
WT (n=13)	-505 ± 117	-38.7 ± 2.2	5.1 ± 0.4	-67.9 ± 2.7	9.6 ± 0.9	0.54 ± 0.04
$Scn8a^{D/+}$ (n=9)	-451 ± 87	-37.7 ± 1.6	5.9 ± 0.6	-65.0 ± 3.1	10.1 ± 0.7	0.66 ± 0.05
Scn8a-$SST^{W/+}$ (n=8)	-498 ± 153	-40.4 ± 2.9	5.9 ± 0.8	-65.8 ± 2.8	11.2 ± 1.0	0.68 ± 0.05

Data shown as mean ± SEM.

Table 6.2: Voltage-gated sodium channel parameters from somatic outside-out recordings WT, $Scn8a^{D/+}$, and Scn8a-$SST^{W/+}$ somatostatin inhibitory interneurons.

Transitions in dynamical states, such as the entry into depolarization block can be understood through the application of bifurcation theory. This approach allowed for tracking of the number and properties of steady states (corresponding to the neuron being at rest or in depolarization block) and periodic orbits (corresponding to spiking behavior) as model parameters are varied. Providing further evidence for our hypothesis, we observed that, as g_{NaP} was increased, the depolarization block boundary shifted leftwards to lower current magnitudes, corroborating our simulation results and providing a more detailed theoretical underpinning for them (Figure 6.6D). Of note, our results indicate that the dynamical transition into depolarization block results from the interplay between the persistent sodium current and slow potassium currents.

To test predictions from the computational model regarding the effect of increasing persistent sodium conductance, we collected recordings of WT SST interneurons before and after application of veratridine. Veratridine is a plant-derived toxin that increases the magnitude of the I_{NaP} (Alkadhi and Tian, 1996; Bikson et al., 2003; Mantegazza et al., 1998; Otoom and Alkadhi, 2000; Tazerart et al., 2008; Tsuruyama et al., 2013). In agreement with our hypothesis, veratridine (1 μM) increased the SST interneuron I_{NaP} by 68 ± 20 pA (n=6, 2 mice; *P<0.05; Paired t-test; Figure 6.6F). In current-clamp recordings, we compared the depolarization block threshold before and after treatment with veratridine at 100 nM, 500 nM, and 1 μM. We observed a dose-dependent reduction in depolarization block threshold in response to veratridine at 500 nM (**P<0.01; Paired t-test; n=8, 3 mice) and 1 μM (***P<0.01; Paired t-test; n=7, 3 mice), but not at 100 nM (n=8, 3 mice; Paired t-test; Figure 6.6G-I). Taken together, our computational and pharmacological evidence demonstrate that the magnitude of the I_{NaP} current strongly influences the threshold for depolarization block in SST interneurons.

Discussion

In this final chapter, my colleagues and I have identified a mechanism by which SST interneurons are impaired and contribute to seizures in *SCN8A* encephalopathy. We show that 1) expression of the *SCN8A* mutation R1872W selectively in SST interneurons is sufficient to induce audiogenic seizures, implicating a previously unidentified role for SST interneurons in *SCN8A* encephalopathy, 2) gain-of-function *SCN8A* mutations facilitate SST interneuron intrinsic hyperexcitability and AP failure via depolarization block, 3) rhythmic instances of depolarization block of mutant SST interneurons are coincident with cortical pyramidal neuron ictal discharge under seizure-like conditions, 4) chemogenetic activation and induction of depolarization block of WT SST interneurons induces prolonged seizures, further supporting a critical role for SST interneurons in maintaining balanced neuronal network excitation, and 5) the I_{NaP} is elevated in SST interneurons expressing gain-of–function *SCN8A* mutations, and it directly facilitates depolarization block. These findings

provide novel insight into a previously unappreciated role for SST interneurons in seizure initiation, not only in the context of *SCN8A* encephalopathy, but to epilepsy more generally.

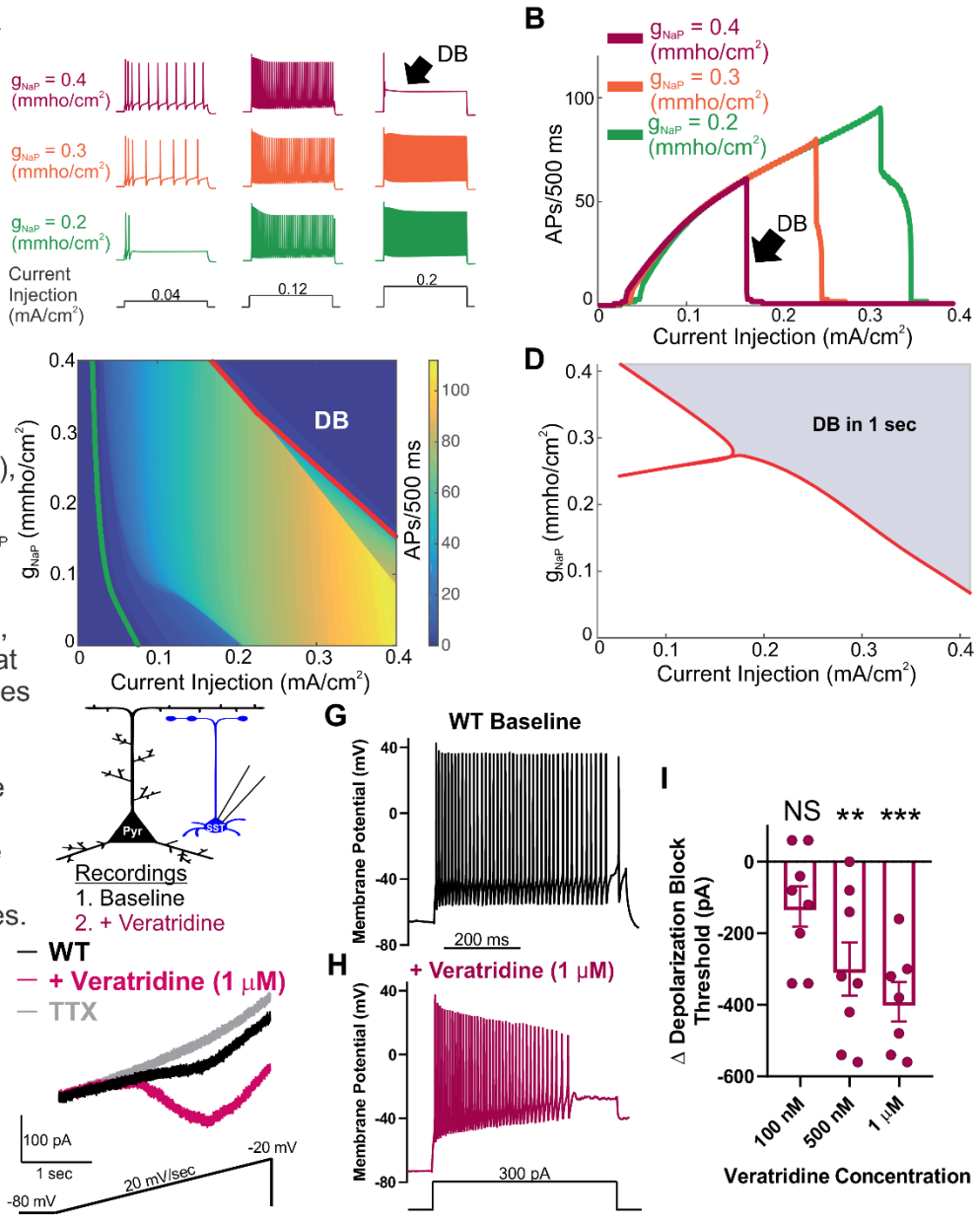

Figure 6.6: Augmentation in the persistent sodium current induces depolarization block. **A.** Example traces of action potentials elicited in response to 500 ms current injections in an *in silico* neuronal model. The maximal persistent sodium conductance was varied from g_{NaP} = 0.2 mmho/cm^2 (green), through g_{NaP} = 0.3 mmho/cm^2 (orange) to g_{NaP} = 0.4 mmho/cm^2 (magenta), whilst the magnitude of the current injection was increased from 0.04 mA/cm^2 (left), through 0.12 mA/cm^2 (middle) to 0.2 mA/cm^2 (right). Increasing g_{NaP} increased the number of APs observed over the stimulation period at low current magnitudes, and led to failure of AP initiation at higher current injection magnitudes (black arrow, DB). **B.** Number of action potentials observed over the 500-ms stimulus relative to the current magnitude. As g_{NaP} increases, the current magnitude required to induce depolarization block (black arrow, DB) decreases. **C.** Heat map showing the number of APs as both g_{NaP} and the current injection magnitude are varied. Also shown is the rheobase current required to induce at least one AP (green line) and the curve at which the neuron ceases to generate repetitive APs as it enters depolarization block (red line, DB). **D.** Two parameter bifurcation showing the location of dynamic transitions leading to depolarization block as the g_{NaP} and the current magnitude are varied. The red line demarcates the shaded region of parameter space in which depolarization block occurs (over a 1s current pulse) from the unshaded region in which it does not. Further information about the bifurcations can be found in the Supplementary Information. **E.** Experimental design: Whole-cell recordings were made from an SST interneuron (blue) before (baseline) and after bath application of the I_{NaP} current activator, veratridine (magenta). **F.** Example trace of I_{NaP} current before (black) and after application of veratridine (1 μM; magenta). **G-H.** Example traces of a WT SST interneuron before (G; black) and after (H; magenta) bath application of I_{NaP} current-activator veratridine (1 μM). **I.** Shift in depolarization block threshold in response to bath-applied veratridine at 100 nM (n=8, 3 mice), 500 nM (n=8, 3 mice), and 1 μM (n=7, 3 mice). Significance determined by paired t-test (**P<0.01; ***P<0.001).

Previous studies using transgenic mice models of *SCN8A* encephalopathy have focused primarily on the impact of gain-of-function *SCN8A* mutations on excitatory neurons and how pro-excitatory alterations in sodium channel properties render these neurons hyperexcitable and corresponding networks seizure prone (Baker et al., 2018; Bunton-Stasyshyn et al., 2019; Lopez-Santiago et al., 2017; Ottolini et al., 2017; Wengert et al., 2019). Our finding that cell-type-specific expression of a

patient-derived gain-of-function *SCN8A* mutation (R1872W) in SST interneurons, but not forebrain excitatory neurons, resulted in audiogenic seizures indicates that this neuronal population contributes to seizures in *SCN8A* encephalopathy.

A proconvulsant impact of inhibitory interneuron hypofunction has been reported previously in the context of Dravet syndrome in which expression of loss-of-function *SCN1A* results in reduced intrinsic excitability of inhibitory interneurons (Cheah et al., 2012; Escayg and Goldin, 2010; Rhodes et al., 2004; Tai et al., 2014). In contrast, our recordings in SST interneurons expressing gain-of-function *SCN8A* mutations exhibited an initial hyperexcitability followed by progressive AP failure due to depolarization block. Interestingly, our results were similar to those found in a recent study examining the gain-of-function *SCN1A* point-mutation T226M which leads to hypofunction through depolarization block and clinically results in a distinct epileptic encephalopathy more severe than traditional Dravet Syndrome (Berecki et al., 2019; Sadleir et al., 2017). Our findings support their interpretation that gain-of-function voltage-gated sodium channel variants can produce functionally dominant-negative effects through depolarization block-mediated AP failure.

Making up 5-10% of cortical neurons, SST inhibitory interneurons are critical components of cortical microcircuits (Nigro et al., 2018; Rudy et al., 2011). In cortical layer V, SST interneurons have been shown to provide lateral inhibition to local pyramidal neurons upon high-frequency AP firing (Silberberg and Markram, 2007). This disynaptic inhibitory mechanism has been suggested to regulate the overall excitability of the cortical column, preventing simultaneous excitability in many pyramidal neurons at one time (Silberberg and Markram, 2007). In our dual-recording experiments, in which an SST interneuron and a nearby pyramidal neuron were recorded simultaneously under seizure-like conditions, we observed that SST interneuron depolarization block events and pyramidal neuron ictal discharges were coincident. Depolarization block of SST interneurons could alter the excitability of nearby pyramidal neurons by transiently silencing synaptic inhibition from SST interneurons which have been shown to act in concert to strongly constrain the excitability of cortical pyramidal neurons (Safari et al., 2017). An additional, non-mutually exclusive mechanism, is that depolarization block in SST interneurons could change the local extracellular ionic environment in a manner that elevates pyramidal neuron excitability. In a previous modeling study of interplay between interneurons and pyramidal neurons during *in vitro* seizure-like events, elevations in external potassium concentration due to interneuron depolarization block was a critical parameter in achieving good agreement between the model and experimental results (Ullah and Schiff, 2010).

An interplay between inhibitory and excitatory neurons via depolarization block of inhibitory interneurons and network seizure-like activity has been previously proposed (Cammarota et al., 2013; Parrish et al., 2019; Swadlow, 2003; Ziburkus et al., 2006). In the study by Parrish *et al*, depolarization block of PV, but not SST interneurons occurred during seizure-like events *in vitro*, although recording in the cell-attached configuration might prohibit one to definitively detect the brief instances of depolarization block in SST interneurons observed in our study (Parrish et al., 2019). To our knowledge, this study is the first to show that cortical SST-interneurons, similar to other fast-spiking interneurons, have coordinated activity with nearby pyramidal neurons characterized by coincident depolarization block events during pyramidal ictal discharges.

Our chemogenetic experiments further support our hypothesis that hypersensitivity to depolarization block of SST interneurons directly contributes to seizures *in vivo*. GqDREADD-mediated hyperactivation of WT SST interneurons increased spontaneous excitability and increased susceptibility to depolarization block (similar to the effects of mutant *SCN8A* expression) and remarkably, led to prolonged seizure activity and behavior (i.e., *status epilepticus*). These surprising results indicate that aberrant SST physiology, namely increased propensity for depolarization block, is sufficient to induce hypersynchronous ECoG activity and seizures in otherwise normal mice. Further experiments are warranted to continue to clarify the role that SST interneurons have in various types of epilepsy and whether SST depolarization block is pathogenic in other contexts.

I observed a profound increase in the magnitude of the I_{NaP} in both *Scn8a*$^{D/+}$ and *Scn8a*-SST$^{W/+}$ SST interneurons. The I_{NaP} has been intensely investigated since its discovery (French et al., 1990; Stafstrom, 2007; Stafstrom et al., 1985; Wengert and Patel, 2021). It has been ascribed a variety of important physiological and neurocomputational functions including spike timing (Osorio et al., 2010; Vervaeke et al., 2006), amplification of synaptic inputs (Schwindt and Crill, 1995; Stuart, 1999; Stuart and Sakmann, 1995), and pacemaking (Del Negro et al., 2002; Yamada-Hanff and Bean, 2013; Yamanishi et al., 2018; Zhong et al., 2007). An aberrantly large I_{NaP} has also been implicated in various epilepsy syndromes (Hargus et al., 2011, 2013; Lossin et al., 2003; Ottolini et al., 2017; Rhodes et al., 2004; Stafstrom, 2007; Veeramah et al., 2012; Wengert and Patel, 2021). In our recordings of mutant SST interneurons, we found higher rates of spontaneous activity, depolarized resting membrane potential, decreased rheobase, hyperpolarized AP threshold, altered upstroke and downstroke velocity, and elevated input resistance, each of which has been previously associated with an augmented I_{NaP} (Ceballos et al., 2017; Herzog et al., 2001; Stafstrom et al., 1982; Yamada-Hanff and Bean, 2013). Moreover, by modifying the magnitude of the

I_{NaP} alone, our computational model recapitulated both of the primary physiological features of the mutant interneurons, that of initial hyperexcitability at low current injections followed by premature depolarization block at higher current injections. Our findings that veratridine, a toxin previously utilized to interrogate the mechanism of the I_{NaP} (Alkadhi and Tian, 1996; Bikson et al., 2003; Mantegazza et al., 1998; Otoom and Alkadhi, 2000; Tazerart et al., 2008; Tsuruyama et al., 2013) increased the I_{NaP} and induced premature depolarization block in WT SST interneurons, support our computational modeling. Further, our bifurcation analysis revealed that the dynamic transitions from resting to spiking to depolarization block were each dependent upon the I_{NaP} magnitude, indicating that the I_{NaP} magnitude is of general importance for determining neuronal spiking dynamics. Thus, an increased I_{NaP}, regardless of particular mechanism, would be predicted to induce hypersensitivity to depolarization block.

Within the class of SST interneurons there is a great deal of diversity with respect to morphology, gene-expression, synaptic input and output, and physiology. In our recordings of cortical layer V SST interneurons we likely recorded from numerous distinct subpopulations of inhibitory interneurons including Martinotti cells, basket cells, bitufted, horizontal, and multipolar cells (Yavorska and Wehr, 2016). Ongoing efforts to distinguish subcellular populations within somatostatin-positive interneurons will further refine the interpretation of the results presented here.

Conclusion

Previous studies have contributed significant evidence to the notion that *SCN8A* epileptic encephalopathy is caused by gain-of-function *SCN8A* mutations which result in hyperexcitability of excitatory neurons and renders the network hyperexcitable and seizure-prone. In this report, we have demonstrated that dysfunctional SST inhibitory interneurons also contribute to *SCN8A* epileptic encephalopathy: An elevated I_{NaP} in SST inhibitory interneurons results in hyperexcitability and AP failure due to depolarization block. Gain-of-function *SCN8A* mutations render SST interneurons more sensitive to depolarization block, and under seizure conditions, these instances of SST depolarization block are coincident to pyramidal neuron ictal discharges. Induction of SST interneuron hyperexcitability and depolarization block, even in the absence of an *SCN8A* mutation, paradoxically leads to *status epilepticus* illustrating the critical contribution of SST interneurons to seizures. Restoration of normal physiological function in SST inhibitory interneurons may provide a novel therapeutic strategy for patients with *SCN8A* encephalopathy.

Chapter VIII: Conclusions and Future Directions

SCN8A encephalopathy is a severe developmental and epileptic syndrome in which patients suffer many symptoms including seizures, cognitive and motor impairment, in addition to a substantial risk for SUDEP. In accordance with the operating framework articulated in Chapter I, a theoretical complete mechanistic understanding of *SCN8A* encephalopathy requires a depth of knowledge into how specific patient-derived mutations alter the biophysics of voltage-gated sodium channel function, how the altered sodium channels influence neuronal excitability of various neuronal populations, how these changes in neuronal excitability effect neuronal circuits, and ultimately how these circuit disruptions lead to behavioral seizures. In this Thesis, my experimental results have provided critical insight into the mechanisms of *SCN8A* encephalopathy at each level of investigation from gene to SUDEP. While there is still much to be learned, I am confident that the body of work described in this thesis will contribute not only to a deeper understanding *SCN8A* epilepsy, but will also help to fuel efforts to develop better treatment approaches.

In Chapter II, I presented evidence for the first time that biallelically inherited loss-of-function *SCN8A* mutations are able to cause developmental and epileptic encephalopathy. Because of this work, I have demonstrated that the heuristic that only gain-of-function *SCN8A* causes epilepsy is an oversimplification. In contrast, due to my data, I suggest that *SCN8A* levels must be maintained at a proper level to achieve balanced excitability in the brain to prevent hypersynchrony and seizures: Too little or too much *SCN8A* function can both be pathogenic and pro-epileptic. Ongoing and future research in the characterization of patient-derived *SCN8A* variants will likely yield a more nuanced understanding of how *SCN8A* channel biophysics relates to clinical features and hopefully will fuel precision medicine approaches in which individual mutations are considered when selecting a clinical treatment approach.

In Chapter III, my results demonstrated that Prax330 is an efficacious treatment for *SCN8A* encephalopathy and that its primary mechanism is through preferential inhibition of the persistent and resurgent sodium currents. For one, this data is important and has contributed to efforts to develop Prax330 (and other related sodium channel modulators) as a clinically available drug for *SCN8A* encephalopathy patients. Secondly, Prax330 has been a useful new tool for examining how the persistent sodium current affects neuronal function in the both the normal and epileptic context. Future studies using Prax330 and other preferential inhibitors of persistent and/or resurgent sodium currents will continue to provide understanding regarding the physiological role and potential pathogenicity of these currents.

Chapter IV focused on the novel discovery of audiogenic seizures and sudden death in the *Scn8a*$^{D/+}$ mouse model of *SCN8A* encephalopathy. In testing the developmentally-determined susceptibility to the seizures, I fortunately found that *Scn8a*$^{D/+}$ mice at P20-21 experienced seizure-induced sudden death which served as a tool for investigating the mechanisms of seizure-induced sudden death. My colleagues and I demonstrated that *Scn8a*$^{D/+}$ mice die from seizure-induced respiratory arrest and that stimulation of breathing with mechanical ventilation or through exogenous activation of alpha-1 adrenergic receptors is sufficient for the prevention of sudden death. The importance of adrenergic receptor function for breathing recovery after seizures was further indicated by our results showing that pharmacological blockade of adrenergic receptors induced respiratory arrest and sudden death in adult *Scn8a*$^{D/+}$ mice which typically experience only non-fatal seizures. Overall, these results highlight a useful new model for exploring mechanisms of seizures and SUDEP in *SCN8A* encephalopathy and provide some promising new strategies for SUDEP prevention through augmentation of alpha-1 adrenergic receptor activity. The research described in this chapter specifically calls for future studies examining augmentation of adrenergic signaling as an interventional approach to prevent SUDEP.

For Chapters V and VI, I described the results of my efforts to understand the contribution of particular neuronal populations to seizures in *SCN8A* encephalopathy. Using a novel transgenic mouse model of *SCN8A* encephalopathy in which an *SCN8A* mutation is expressed in a cell-type specific manner (determined by expression of Cre recombinase), my work revealed that cortical and hippocampal neurons from mice expressing the mutation R1872W are hyperexcitable. Further, we found that mice with forebrain excitatory neuron expression of R1872W exhibited spontaneous seizures and premature lethality, a phenotype that was not observed in mice in which the R1872W mutation was introduced into inhibitory interneurons (specified by Gad2-Cre and Dlx5a-Cre). This work initially suggested that excitatory neurons, but not inhibitory interneurons were primarily responsible for the network hyperexcitability and hypersynchrony underlying seizures.

However, my results from Chapter VI challenged the paradigm that inhibitory interneurons do not actively contribute to seizures in *SCN8A* encephalopathy: Indeed, my data surprisingly demonstrated that somatostatin-positive inhibitory interneurons have aberrant physiological function caused by mutant *SCN8A*. Elevated persistent sodium currents drive SST interneurons into depolarization block, which contributes to seizure activity both *in vitro* and *in vivo*. My evidence suggests that inhibitory interneurons, particularly somatostatin-positive, while not sufficient to generate spontaneous seizures in response to *SCN8A* mutations, are major contributors to the pathology of *SCN8A* encephalopathy in a manner that must be taken into account when developing new and better treatment approaches. Thus, these results call for continued investigation into how *SCN8A* variants impact the physiology of neuronal populations beyond excitatory neurons of the forebrain including various inhibitory interneuron populations, and neurons of subcortical regions.

The future of *SCN8A* research will benefit from emerging technologies including new mouse models of *SCN8A* encephalopathy, *in vivo* monitoring of neuronal activity with optical physiology approaches, *in vivo* manipulation of neuronal circuits with both optogenetic and chemogenetic tools, computational modeling of the impact of mutations on currents and single neuronal excitability, human patient-derived induced pluripotent stem cells and cerebral organoids, and others. Investigation into the mechanisms of *SCN8A* encephalopathy, while worthy in its own right, will yield insight not only into this particular rare form of epilepsy, but epilepsy and brain function in general. Thus, studying *SCN8A* encephalopathy is a powerful entry point into understanding voltage-gated sodium channel function, the bedrock of cellular excitability, and ultimately how they relate to complex brain functions, behavior, and pathology.

References

Agrawal, N., Alonso, A., and Ragsdale, D.S. (2003). Increased Persistent Sodium Currents in Rat Entorhinal Cortex Layer V Neurons in a Post-Status Epilepticus Model of Temporal Lobe Epilepsy. Epilepsia *44*, 1601–1604.

Aiba, I., and Noebels, J.L. (2015). Spreading depolarization in the brainstem mediates sudden cardiorespiratory arrest in mouse SUDEP models. Sci. Transl. Med. *7*.

Aiba, I., Wehrens, X.H.T., and Noebels, J.L. (2016). Leaky RyR2 channels unleash a brainstem spreading depolarization mechanism of sudden cardiac death. Proc. Natl. Acad. Sci. U. S. A. *113*, 4895–4903.

Alexander, A., and Huguenard, J. (2014). Lamotrigine suppresses thalamic epileptiform oscillations via a blockade of the persistent sodium current. Epilepsy Curr. *14*, 97–98.

Alkadhi, K.A., and Tian, L.M. (1996). Veratridine-enhanced persistent sodium current induces bursting in CA1 pyramidal neurons. Neuroscience *71*, 625–632.

Anand, G., Collett-White, F., Orsini, A., Thomas, S., Jayapal, S., Trump, N., Zaiwalla, Z., and Jayawant, S. (2016). Autosomal dominant SCN8A mutation with an unusually mild phenotype. Eur. J. Paediatr. Neurol. *20*, 761–765.

Anderson, L.L., Thompson, C.H., Hawkins, N.A., Nath, R.D., Petersohn, A.A., Rajamani, S., Bush, W.S., Frankel, W.N., Vanoye, C.G., Kearney, J.A., et al. (2014). Antiepileptic activity of preferential inhibitors of persistent sodium current. Epilepsia *55*, 1274–1283.

Anderson, L.L., Hawkins, N.A., Thompson, C.H., Kearney, J.A., and George, A.L. (2017). Unexpected Efficacy of a Novel Sodium Channel Modulator in Dravet Syndrome. Sci. Rep. *7*.

Auerbach, D.S., Jones, J., Clawson, B.C., Offord, J., Lenk, G.M., Ogiwara, I., Yamakawa, K., Meisler, M.H., Parent, J.M., and Isom, L.L. (2013). Altered Cardiac Electrophysiology and SUDEP in a Model of Dravet Syndrome. PLoS One *8*, e77843.

Baker, E.M., Thompson, C.H., Hawkins, N.A., Wagnon, J.L., Wengert, E.R., Patel, M.K., George, A.L., Meisler, M.H., and Kearney, J.A. (2018). The novel sodium channel modulator GS-458967 (GS967) is an effective treatment in a mouse model of SCN8A encephalopathy. Epilepsia *59*, 1166–1176.

Barbieri, R., Bertelli, S., Pusch, M., and Gavazzo, P. (2019). Late sodium current blocker GS967 inhibits persistent currents induced by familial hemiplegic migraine type 3 mutations of the SCN1A gene. J. Headache Pain *20*, 107.

Barker, B.S., Ottolini, M., Wagnon, J.L., Hollander, R.M., Meisler, M.H., and Patel, M.K. (2016). The SCN8A encephalopathy mutation p.Ile1327Val displays elevated sensitivity to the anticonvulsant phenytoin. Epilepsia *57*, 1458–1466.

Barker, B.S., Nigam, A., Ottolini, M., Gaykema, R.P., Hargus, N.J., and Patel, M.K. (2017). Pro-excitatory alterations in sodium channel activity facilitate subiculum neuron hyperexcitability in temporal lobe epilepsy. Neurobiol. Dis. *108*, 183–194.

Bartoo, A.C., Sprunger, L.K., and Schneider, D.A. (2005). Expression and distribution of TTX-sensitive sodium channel alpha subunits in the enteric nervous system. J. Comp. Neurol. *486*, 117–131.

Bateman, L.M., Li, C.-S., and Seyal, M. (2008). Ictal hypoxemia in localization-related epilepsy: analysis of incidence, severity and risk factors. Brain *131*, 3239–3245.

Bayat, A., Hjalgrim, H., and Møller, R.S. (2015). The incidence of SCN1A-related Dravet syndrome in Denmark is 1:22,000: A population-based study from 2004 to 2009. Epilepsia *56*, e36–e39.

Bean, B.P. (2007). The action potential in mammalian central neurons. Nat. Rev. Neurosci. *8*, 451–465.

Belardinelli, L., Liu, G., Smith-Maxwell, C., Wang, W.Q., El-Bizri, N., Hirakawa, R., Karpinski, S., Li, C.H., Hu, L., Li, X.J., et al. (2013). A novel, potent, and selective inhibitor of cardiac late sodium current suppresses experimental

arrhythmias. J. Pharmacol. Exp. Ther. *344*, 23–32.

Beneski, D.A., and Catterall, W.A. (1980). Covalent labeling of protein components of the sodium channel with a photoactivable derivative of scorpion toxin. Proc. Natl. Acad. Sci. *77*, 639.

Berecki, G., Bryson, A., Terhag, J., Maljevic, S., Gazina, E. V, Hill, S.L., and Petrou, S. (2019). SCN1A gain of function in early infantile encephalopathy. Ann. Neurol. *85*, 514–525.

Berg, A.T., Berkovic, S.F., Brodie, M.J., Buchhalter, J., Cross, J.H., Van Emde Boas, W., Engel, J., French, J., Glauser, T.A., Mathern, G.W., et al. (2010). Revised terminology and concepts for organization of seizures and epilepsies: Report of the ILAE Commission on Classification and Terminology, 2005–2009. Epilepsia *51*, 676–685.

Berghuis, B., de Kovel, C.G.F., van Iterson, L., Lamberts, R.J., Sander, J.W., Lindhout, D., and Koeleman, B.P.C. (2015). Complex SCN8A DNA-abnormalities in an individual with therapy resistant absence epilepsy. Epilepsy Res. *115*, 141–144.

Bernard, C., Cossart, R., Hirsch, J.C., Esclapez, M., and Ben-Ari, Y. (2000). What is GABAergic Inhibition? How Is it Modified in Epilepsy? Epilepsia *41*, S90–S95.

Bikson, M., Hahn, P.J., Fox, J.E., and Jefferys, J.G.R. (2003). Depolarization block of neurons during maintenance of electrographic seizures. J. Neurophysiol. *90*, 2402–2408.

Bird, J.M., Dembny, K.A.T., Sandeman, D., and Butler, S. (1997). Sudden Unexplained Death in Epilepsy: An Intracranially Monitored Case. Epilepsia *38*, S52–S56.

Blanchard, M.G., Willemsen, M.H., Walker, J.B., Dib-Hajj, S.D., Waxman, S.G., Jongmans, M.C.J., Kleefstra, T., van de Warrenburg, B.P., Praamstra, P., Nicolai, J., et al. (2015). De novo gain-of-function and loss-of-function mutations of SCN8A in patients with intellectual disabilities and epilepsy. J. Med. Genet. *52*, 330–337.

Bond, R.F. (1985). Vascular adrenergic interactions during hemorrhagic shock. Fed. Proc. *44*, 281–289.

Broese, M., Riemann, D., Hein, L., and Nissen, C. (2012). α-Adrenergic Receptor Function, Arousal and Sleep: Mechanisms and Therapeutic Implications. Pharmacopsychiatry *45*, 209–216.

Buchanan, G.F., Murray, N.M., Hajek, M.A., and Richerson, G.B. (2014a). Serotonin neurones have anti-convulsant effects and reduce seizure-induced mortality. J. Physiol. *592*, 4395–4410.

Buchanan, G.F., Murray, N.M., Hajek, M.A., and Richerson, G.B. (2014b). Serotonin neurones have anti-convulsant effects and reduce seizure-induced mortality. J. Physiol. *592*, 4395–4410.

Bunton-Stasyshyn, R.K.A., Wagnon, J.L., Wengert, E.R., Barker, B.S., Faulkner, A., Wagley, P.K., Bhatia, K., Jones, J.M., Maniaci, M.R., Parent, J.M., et al. (2019). Prominent role of forebrain excitatory neurons in SCN8A encephalopathy. Brain *142*, 362–375.

Butler, K.M., da Silva, C., Shafir, Y., Weisfeld-Adams, J.D., Alexander, J.J., Hegde, M., and Escayg, A. (2017). De novo and inherited SCN8A epilepsy mutations detected by gene panel analysis. Epilepsy Res. *129*, 17–25.

Caldwell, J.H., Schaller, K.L., Lasher, R.S., Peles, E., and Levinson, S.R. (2000). Sodium channel Nav1.6 is localized at nodes of Ranvier, dendrites, and synapses. Proc. Natl. Acad. Sci. U. S. A. *97*, 5616–5620.

Cammarota, M., Losi, G., Chiavegato, A., Zonta, M., and Carmignoto, G. (2013). Fast spiking interneuron control of seizure propagation in a cortical slice model of focal epilepsy. J. Physiol. *591*, 807–822.

Catterall, W.A. (2000). From ionic currents to molecular mechanisms: The structure and function of voltage-gated sodium channels. Neuron *26*.

Catterall, W.A. (2012). Voltage-gated sodium channels at 60: Structure, function and pathophysiology. J. Physiol. *590*, 2577–2589.

Cavazos, J.E., Jones, S.M., and Cross, D.J. (2004). Sprouting and synaptic reorganization in the subiculum and CA1 region of the hippocampus in acute and chronic models of partial-onset epilepsy. Neuroscience *126*, 677–688.

Ceballos, C.C., Roque, A.C., and Leão, R.M. (2017). A Negative Slope Conductance of the Persistent Sodium Current Prolongs Subthreshold Depolarizations. Biophys. J. *113*, 2207–2217.

Cheah, C.S., Yu, F.H., Westenbroek, R.E., Kalume, F.K., Oakley, J.C., Potter, G.B., Rubenstein, J.L., and Catterall, W.A. (2012). Specific deletion of NaV1.1 sodium channels in inhibitory interneurons causes seizures and premature death in a mouse model of Dravet syndrome. Proc. Natl. Acad. Sci. U. S. A. *109*, 14646–14651.

Chen, S., Su, H., Yue, C., Remy, S., Royeck, M., Sochivko, D., Opitz, T., Beck, H., and Yaari, Y. (2011). An increase in persistent sodium current contributes to intrinsic neuronal bursting after status epilepticus. J. Neurophysiol. *105*, 117–129.

Clatot, J., Hoshi, M., Wan, X., Liu, H., Jain, A., Shinlapawittayatorn, K., Marionneau, C., Ficker, E., Ha, T., and Deschênes, I. (2017). Voltage-gated sodium channels assemble and gate as dimers. Nat. Commun. *8*.

Coffey, L.L., Reith, M.E.A., Chen, N.H., Mishra, P.K., and Jobe, P.C. (1996). Amygdala kindling of forebrain seizures and the occurrence of brainstem seizures in genetically epilepsy-prone rats. Epilepsia *37*, 188–197.

Colombo, E., Franceschetti, S., Avanzini, G., and Mantegazza, M. (2013). Phenytoin Inhibits the Persistent Sodium Current in Neocortical Neurons by Modifying Its Inactivation Properties. PLoS One *8*, 55329.

Council, N.R. (2011). Guide for the Care and Use of Laboratory Animals: Eighth Edition (Washington, DC: The National Academies Press).

Dasheiff, R.M., and Dickinson, L.J. (1986). Sudden Unexpected Death of Epileptic Patient due to Cardiac Arrhythmia After Seizure. Arch. Neurol. *43*, 194–196.

Deng, P.Y., and Klyachko, V.A. (2016). Increased Persistent Sodium Current Causes Neuronal Hyperexcitability in the Entorhinal Cortex of Fmr1 Knockout Mice. Cell Rep. *16*, 3157–3166.

Devinsky, O., Marsh, E., Friedman, D., Thiele, E., Laux, L., Sullivan, J., Miller, I., Flamini, R., Wilfong, A., Filloux, F., et al. (2016a). Cannabidiol in patients with treatment-resistant epilepsy: an open-label interventional trial. Lancet Neurol. *15*, 270–278.

Devinsky, O., Hesdorffer, D.C., Thurman, D.J., Lhatoo, S., and Richerson, G. (2016b). Sudden unexpected death in epilepsy: epidemiology, mechanisms, and prevention. Lancet Neurol. *15*, 1075–1088.

Devinsky, O., Cross, J.H., Laux, L., Marsh, E., Miller, I., Nabbout, R., Scheffer, I.E., Thiele, E.A., and Wright, S. (2017). Trial of Cannabidiol for Drug-Resistant Seizures in the Dravet Syndrome. N. Engl. J. Med. *376*, 2011–2020.

Dlouhy, B.J., Gehlbach, B.K., Kreple, C.J., Kawasaki, H., Oya, H., Buzza, C., Granner, M.A., Welsh, M.J., Howard, M.A., Wemmie, J.A., et al. (2015). Breathing inhibited when seizures spread to the amygdala and upon amygdala stimulation. J. Neurosci. *35*, 10281–10289.

Dong, H.W., and Ennis, M. (2014). Activation of group I metabotropic glutamate receptors enhances persistent sodium current and rhythmic bursting in main olfactory bulb external tufted cells. J. Neurophysiol. *111*, 641–647.

Dutton, S.B., Makinson, C.D., Papale, L.A., Shankar, A., Balakrishnan, B., Nakazawa, K., and Escayg, A. (2013). Preferential inactivation of Scn1a in parvalbumin interneurons increases seizure susceptibility. Neurobiol. Dis. *49*, 211–220.

Escayg, A., and Goldin, A.L. (2010). Sodium channel SCN1A and epilepsy: Mutations and mechanisms. Epilepsia *51*, 1650–1658.

Estacion, M., O'Brien, J.E., Conravey, A., Hammer, M.F., Waxman, S.G., Dib-Hajj, S.D., and Meisler, M.H. (2014). A novel de novo mutation of SCN8A (Nav1.6) with enhanced channel activation in a child with epileptic encephalopathy. Neurobiol. Dis. *69*, 117–123.

Faingold, C., Tupal, S., and N'Gouemo, P. (2017). Genetic Models of Reflex Epilepsy and SUDEP in Rats and Mice. In Models of Seizures and Epilepsy: Second Edition, (Academic Press), pp. 441–453.

Faingold, C.L., Naritoku a, D.K., Copley, C.A., Randall, M.E., Riaz, A., Anderson, C.A.B., and Arneric, S.P. (1992). Glutamate in the inferior colliculus plays a critical role in audiogenic seizure initiation. Epilepsy Res. *13*, 95–105.

Faingold, C.L., Randall, M., and Tupal, S. (2010). DBA/1 mice exhibit chronic susceptibility to audiogenic seizures followed by sudden death associated with respiratory arrest. Epilepsy Behav. *17*, 436–440.

Faingold, C.L., Tupal, S., and Randall, M. (2011). Prevention of seizure-induced sudden death in a chronic SUDEP model by semichronic administration of a selective serotonin reuptake inhibitor. Epilepsy Behav. *22*, 186–190.

Faingold, C.L., Randall, M., and Kommajosyula, S.P. (2016). Susceptibility to seizure-induced sudden death in DBA/2 mice is altered by adenosine. Epilepsy Res. *124*, 49–54.

Favero, M., Sotuyo, N.P., Lopez, E., Kearney, J.A., and Goldberg, E.M. (2018). A Transient Developmental Window of Fast-Spiking Interneuron Dysfunction in a Mouse Model of Dravet Syndrome. J. Neurosci. *38*, 7912.

Feng, H.-J., and Faingold, C.L. (2017). Abnormalities of serotonergic neurotransmission in animal models of SUDEP. Epilepsy Behav. *71*, 174–180.

Fleming, S.M., Jordan, M.C., Mulligan, C.K., Masliah, E., Holden, J.G., Millard, R.W., Chesselet, M.-F., and Roos, K.P. (2013). Impaired baroreflex function in mice overexpressing alpha-synuclein. Front. Neurol. *4*, 103.

Frasier, C.R., Wagnon, J.L., Bao, Y.O., McVeigh, L.G., Lopez-Santiago, L.F., Meisler, M.H., and Isom, L.L. (2016). Cardiac arrhythmia in a mouse model of sodium channel SCN8A epileptic encephalopathy. Proc. Natl. Acad. Sci. U. S. A. *113*, 12838–12843.

French, C.R., Sah, P., Bucketr, K.J., and Gage, P.W. (1990). A Voltage-dependent persistent sodium current in mammalian hippocampal neurons. J. Gen. Physiol. *95*, 1139–1157.

Fujita, S., Toyoda, I., Thamattoor, A.K., and Buckmaster, P.S. (2014). Preictal Activity of Subicular, CA1, and Dentate Gyrus Principal Neurons in the Dorsal Hippocampus before Spontaneous Seizures in a Rat Model of Temporal Lobe Epilepsy. J. Neurosci. *34*, 16671.

Gardella, E., Becker, F., Møller, R.S., Schubert, J., Lemke, J.R., Larsen, L.H.G., Eiberg, H., Nothnagel, M., Thiele, H., Altmüller, J., et al. (2016). Benign infantile seizures and paroxysmal dyskinesia caused by an SCN8A mutation. Ann. Neurol. *79*, 428–436.

Gardella, E., Marini, C., Trivisano, M., Fitzgerald, M.P., Alber, M., Howell, K.B., Darra, F., Siliquini, S., Bölsterli, B.K., Masnada, S., et al. (2018). The phenotype of SCN8A developmental and epileptic encephalopathy. Neurology *91*, E1112–E1124.

Gastaut, H., Roger, J., Ouahchi, S., Timsit, M., and Broughton, R. (1963). An Electro-clinical Study of Generalized Epileptic Seizures of Tonic Expression. Epilepsia *4*, 15–44.

Gehrmann, J., Hammer, P.E., Maguire, C.T., Wakimoto, H., Triedman, J.K., and Berul, C.I. (2000). Phenotypic screening for heart rate variability in the mouse. Am. J. Physiol. Circ. Physiol. *279*, H733–H740.

Ghovanloo, M.-R., Shuart, N.G., Mezeyova, J., Dean, R.A., Ruben, P.C., and Goodchild, S.J. (2018). Inhibitory effects of cannabidiol on voltage-dependent sodium currents. J. Biol. Chem. *293*, 16546–16558.

Glasscock, E., Yoo, J.W., Chen, T.T., Klassen, T.L., and Noebels, J.L. (2010). Kv1.1 potassium channel deficiency reveals brain-driven cardiac dysfunction as a candidate mechanism for sudden unexplained death in epilepsy. J. Neurosci. *30*, 5167–5175.

Goldin, A.L. (1999). Diversity of mammalian voltage-gated sodium channels. In Annals of the New York Academy of Sciences, pp. 38–50.

Goldin, A.L., Snutch, T., Lubbert, H., Dowsett, A., Marshall, J., Auld, V., Downey, W., Fritz, L.C., Lester, H.A., and Dunn, R. (1986). Messenger RNA coding for only the α subunit of the rat brain Na channel is sufficient for expression of functional channels in Xenopus oocytes. Proc. Natl. Acad. Sci. U. S. A. *83*, 7503–7507.

de Guzman, P., Inaba, Y., Biagini, G., Baldelli, E., Mollinari, C., Merlo, D., and Avoli, M. (2006). Subiculum network excitability is increased in a rodent model of temporal lobe epilepsy. Hippocampus *16*, 843–860.

Hampl, M., Eberhardt, E., O'Reilly, A.O., and Lampert, A. (2016). Sodium channel slow inactivation interferes with open

channel block. Sci. Rep. *6*.

Han, J.Y., Jang, J.H., Lee, I.G., Shin, S., and Park, J. (2017). A Novel Inherited Mutation of SCN8A in a Korean Family with Benign Familial Infantile Epilepsy Using Diagnostic Exome Sequencing. Ann. Clin. Lab. Sci. *47*, 747–753.

Hardebo, J.E., and Owman, C. (1980). Barrier mechanisms for neurotransmitter monoamines and their precursors at the blood-brain interface. Ann. Neurol. *8*, 1–11.

Hardie, J.B., and Pearce, R.A. (2006). Active and passive membrane properties and intrinsic kinetics shape synaptic inhibition in hippocampal CA1 pyramidal neurons. J. Neurosci. *26*, 8559–8569.

Hargus, N.J., Merrick, E.C., Nigam, A., Kalmar, C.L., Baheti, A.R., Bertram 3rd, E.H., and Patel, M.K. (2011). Temporal lobe epilepsy induces intrinsic alterations in Na channel gating in layer II medial entorhinal cortex neurons. Neurobiol. Dis. *41*, 361–376.

Hargus, N.J., Nigam, A., Bertram, E.H., and Patel, M.K. (2013). Evidence for a role of Nav1.6 in facilitating increases in neuronal hyperexcitability during epileptogenesis. J. Neurophysiol. *110*, 1144–1157.

Harvey, P.J., Li, Y., Li, X., and Bennett, D.J. (2006). Persistent Sodium Currents and Repetitive Firing in Motoneurons of the Sacrocaudal Spinal Cord of Adult Rats. J. Neurophysiol. *96*, 1141–1157.

Heffner, R.S., Koay, G., and Heffner, H.E. (2019). Normal audiogram but poor sensitivity to brief sounds in mice with compromised voltage-gated sodium channels (Scn8a medJ). Hear. Res. *374*, 1–4.

Herzog, R.I., Cummins, T.R., and Waxman, S.G. (2001). Persistent TTX-Resistant Na+ Current Affects Resting Potential and Response to Depolarization in Simulated Spinal Sensory Neurons. J. Neurophysiol. *86*, 1351–1364.

Hesdorffer, D.C., Tomson, T., Benn, E., Sander, J.W., Nilsson, L., Langan, Y., Walczak, T.S., Beghi, E., Brodie, M.J., Hauser, A., et al. (2011). Combined analysis of risk factors for SUDEP. Epilepsia *52*, 1150–1159.

Hodgkin, A.L., and Huxley, A.F. A Quantitative Description of Membrane Current and its Application to Conduction and Excitation in Nerve. J. Physiol. I *7*, 500–544.

Holland, K.D., Kearney, J.A., Glauser, T.A., Buck, G., Keddache, M., Blankston, J.R., Glaaser, I.W., Kass, R.S., and Meisler, M.H. (2008). Mutation of sodium channel SCN3A in a patient with cryptogenic pediatric partial epilepsy. Neurosci. Lett. *433*, 65–70.

Im, Y.B., Won, J.S., Suh, H.W., Huh, S.O., Kim, Y.H., and Song, D.K. (1998). Differential effects of adrenaline and noradrenaline on the hepatic expression of immediate early genes in mice. J. Auton. Pharmacol. *18*, 149–155.

Irizarry, R., Sukato, D., Kollmar, R., Schild, S., Silverman, J., Sundaram, K., Stephenson, S., and Stewart, M. (2020). Seizures induce obstructive apnea in DBA/2J audiogenic seizure-prone mice: Lifesaving impact of tracheal implants. Epilepsia *61*, e13–e16.

Isom, L.L., De Jongh, K.S., Patton, D.E., Reber, B.F., Offord, J., Charbonneau, H., Walsh, K., Goldin, A.L., and Catterall, W.A. (1992). Primary structure and functional expression of the beta 1 subunit of the rat brain sodium channel. Science (80-.). *256*, 839.

Jansen, N.A., Schenke, M., Voskuyl, R.A., Thijs, R.D., van den Maagdenberg, A.M.J.M., and Tolner, E.A. (2019). Apnea Associated with Brainstem Seizures in Cacna1aS218L Mice Is Caused by Medullary Spreading Depolarization. J. Neurosci. *39*, 9633–9644.

Jarecki, B.W., Piekarz, A.D., Jackson II, J.O., and Cummins, T.R. (2010). Human voltage-gated sodium channel mutations that cause inherited neuronal and muscle channelopathies increase resurgent sodium currents. J. Clin. Invest. *120*, 369–378.

Jayant, K., Wenzel, M., Bando, Y., Hamm, J.P., Mandriota, N., Rabinowitz, J.H., Plante, I.J. La, Owen, J.S., Sahin, O., Shepard, K.L., et al. (2019). Flexible Nanopipettes for Minimally Invasive Intracellular Electrophysiology In Vivo. Cell Rep. *26*.

Johannesen, K.M., Gardella, E., Scheffer, I., Howell, K., Smith, D.M., Helbig, I., Møller, R.S., and Rubboli, G. (2018).

Early mortality in SCN8A-related epilepsies. Epilepsy Res. *143*, 79–81.

Johannesen, K.M., Gardella, E., Encinas, A.C., Lehesjoki, A.E., Linnankivi, T., Petersen, M.B., Lund, I.C.B., Blichfeldt, S., Miranda, M.J., Pal, D.K., et al. (2019). The spectrum of intermediate SCN8A-related epilepsy. Epilepsia *60*, 830–844.

Jones, J.M., and Meisler, M.H. (2014). Modeling human epilepsy by TALEN targeting of mouse sodium channel Scn8a. Genesis *52*, 141–148.

Kalume, F., Westenbroek, R.E., Cheah, C.S., Yu, F.H., Oakley, J.C., Scheuer, T., and Catterall, W.A. (2013). Sudden unexpected death in a mouse model of Dravet syndrome. J. Clin. Invest. *123*, 1798–1808.

Kaplan, J.S., Stella, N., Catterall, W.A., and Westenbroek, R.E. (2017). Cannabidiol attenuates seizures and social deficits in a mouse model of Dravet syndrome. Proc. Natl. Acad. Sci. *114*, 11229.

Kearney, J.A., Buchner, D.A., de Haan, G., Adamska, M., Levin, S.I., Furay, A.R., Albin, R.L., Jones, J.M., Montal, M., Stevens, M.J., et al. (2002). Molecular and pathological effects of a modifier gene on deficiency of the sodium channel Scn8a (Nav1.6). Hum. Mol. Genet. *11*, 2765–2775.

Khaliq, Z.M., and Bean, B.P. (2010). Pacemaking in dopaminergic ventral tegmental area neurons: Depolarizing drive from background and voltage-dependent sodium conductances. J. Neurosci. *30*, 7401–7413.

Khaliq, Z.M., Gouwens, N.W., and Raman, I.M. (2003). The Contribution of Resurgent Sodium Current to High-Frequency Firing in Purkinje Neurons: An Experimental and Modeling Study. J. Neurosci. *23*, 4899.

Khan, A.A., Shekh-Ahmad, T., Khalil, A., Walker, M.C., and Ali, A.B. (2018). Cannabidiol exerts antiepileptic effects by restoring hippocampal interneuron functions in a temporal lobe epilepsy model. Br. J. Pharmacol. *175*, 2097–2115.

Kim, Y., Bravo, E., Thirnbeck, C.K., Smith-Mellecker, L.A., Kim, S.H., Gehlbach, B.K., Laux, L.C., Zhou, X., Nordli, D.R., and Richerson, G.B. (2018). Severe peri-ictal respiratory dysfunction is common in Dravet syndrome. J. Clin. Invest. *128*, 1141–1153.

Koay, G., Heffner, R.S., and Heffner, H.E. (2002). Behavioral audiograms of homozygous medJ mutant mice with sodium channel deficiency and unaffected controls. Hear. Res. *171*, 111–118.

Koltun, D.O., Parkhill, E.Q., Elzein, E., Kobayashi, T., Notte, G.T., Kalla, R., Jiang, R.H., Li, X., Perry, T.D., Avila, B., et al. (2016). Discovery of triazolopyridine GS-458967, a late sodium current inhibitor (Late INai) of the cardiac NaV 1.5 channel with improved efficacy and potency relative to ranolazine. Bioorganic Med. Chem. Lett. *26*, 3202–3206.

Kommajosyula, S.P., Randall, M.E., Brozoski, T.J., Odintsov, B.M., and Faingold, C.L. (2017). Specific subcortical structures are activated during seizure-induced death in a model of sudden unexpected death in epilepsy (SUDEP): A manganese-enhanced magnetic resonance imaging study. Epilepsy Res. *135*, 87–94.

de Kovel, C.G.F., Meisler, M.H., Brilstra, E.H., van Berkestijn, F.M.C., Slot, R. van t., van Lieshout, S., Nijman, I.J., O'Brien, J.E., Hammer, M.F., Estacion, M., et al. (2014). Characterization of a de novo SCN8A mutation in a patient with epileptic encephalopathy. Epilepsy Res. *108*, 1511–1518.

Kruse, S.W., Dayton, K.G., Purnell, B.S., Rosner, J.I., and Buchanan, G.F. (2019). Effect of monoamine reuptake inhibition and α1 blockade on respiratory arrest and death following electroshock-induced seizures in mice. Epilepsia *60*, 495–507.

Kumar, S.S., and Buckmaster, P.S. (2006). Hyperexcitability, Interneurons, and Loss of GABAergic Synapses in Entorhinal Cortex in a Model of Temporal Lobe Epilepsy. J. Neurosci. *26*, 4613.

Kuo, C.C., and Bean, B.P. (1994). Na+ channels must deactivate to recover from inactivation. Neuron *12*, 819–829.

Lacuey, N., Zonjy, B., Hampson, J.P., Rani, M.R.S., Zaremba, A., Sainju, R.K., Gehlbach, B.K., Schuele, S., Friedman, D., Devinsky, O., et al. (2018). The incidence and significance of periictal apnea in epileptic seizures. Epilepsia *59*, 573–582.

Larsen, J., Carvill, G.L., Gardella, E., Kluger, G., Schmiedel, G., Barisic, N., Depienne, C., Brilstra, E., Mang, Y., Nielsen, J.E.K., et al. (2015). The phenotypic spectrum of SCN8A encephalopathy. Neurology *84*, 480–489.

Li, T., Tian, C., Scalmani, P., Frassoni, C., Mantegazza, M., Wang, Y., Yang, M., Wu, S., and Shu, Y. (2014). Action Potential Initiation in Neocortical Inhibitory Interneurons. PLoS Biol. *12*, e1001944.

Li, Y., Steven Evans, M., and Faingold, C.L. (1994). Inferior colliculus neuronal membrane and synaptic properties in genetically epilepsy-prone rats. Brain Res. *660*, 232–240.

Liao, Y., Anttonen, A.K., Liukkonen, E., Gaily, E., Maljevic, S., Schubert, S., Bellan-Koch, A., Petrou, S., Ahonen, V.E., Lerche, H., et al. (2010). SCN2A mutation associated with neonatal epilepsy, late-onset episodic ataxia, myoclonus, and pain. Neurology *75*, 1454–1458.

Liu, Y., Schubert, J., Sonnenberg, L., Helbig, K.L., Hoei-Hansen, C.E., Koko, M., Rannap, M., Lauxmann, S., Huq, M., Schneider, M.C., et al. (2019). Neuronal mechanisms of mutations in SCN8A causing epilepsy or intellectual disability. Brain *142*, 376–390.

Loonen, I.C.M., Jansen, N.A., Cain, S.M., Schenke, M., Voskuyl, R.A., Yung, A.C., Bohnet, B., Kozlowski, P., Thijs, R.D., Ferrari, M.D., et al. (2019). Brainstem spreading depolarization and cortical dynamics during fatal seizures in Cacna1a S218L mice. Brain *142*, 412–425.

Lopez-Santiago, L.F., Yuan, Y., Wagnon, J.L., Hull, J.M., Frasier, C.R., O'Malley, H.A., Meisler, M.H., and Isom, L.L. (2017). Neuronal hyperexcitability in a mouse model of SCN8A epileptic encephalopathy. Proc. Natl. Acad. Sci. U. S. A. *114*, 2383–2388.

Lorincz, A., and Nusser, Z. (2008). Cell-type-dependent molecular composition of the axon initial segment. J. Neurosci. *28*, 14329–14340.

Lossin, C., Wang, D.W., Rhodes, T.H., Vanoye, C.G., and George, A.L. (2002). Molecular basis of an inherited epilepsy. Neuron *34*, 877–884.

Lossin, C., Rhodes, T.H., Desai, R.R., Vanoye, C.G., Wang, D., Carniciu, S., Devinsky, O., and George, A.L. (2003). Epilepsy-Associated Dysfunction in the Voltage-Gated Neuronal Sodium Channel SCN1A. J. Neurosci. *23*, 11289–11295.

Mackenzie, F.E., Parker, A., Parkinson, N.J., Oliver, P.L., Brooker, D., Underhill, P., Lukashkina, V.A., Lukashkin, A.N., Holmes, C., and Brown, S.D.M. (2009). Analysis of the mouse mutant Cloth-ears shows a role for the voltage-gated sodium channel Scn8a in peripheral neural hearing loss. Genes, Brain Behav. *8*, 699–713.

Makinson, C.D., Dutt, K., Lin, F., Papale, L.A., Shankar, A., Barela, A.J., Liu, R., Goldin, A.L., and Escayg, A. (2016). An Scn1a epilepsy mutation in Scn8a alters seizure susceptibility and behavior. Exp. Neurol. *275*, 46–58.

Makinson, C.D., Tanaka, B.S., Sorokin, J.M., Wong, J.C., Christian, C.A., Goldin, A.L., Escayg, A., and Huguenard, J.R. (2017). Regulation of Thalamic and Cortical Network Synchrony by Scn8a. Neuron *93*, 1165-1179.e6.

Mantegazza, M., Franceschetti, S., and Avanzini, G. (1998). Anemone toxin (ATX II)-induced increase in persistent sodium current: Effects on the firing properties of rat neocortical pyramidal neurones. J. Physiol. *507*, 105–116.

Marincovich, A., Bravo, E., Dlouhy, B., and Richerson, G.B. (2019). Amygdala lesions reduce seizure-induced respiratory arrest in DBA/1 mice. Epilepsy Behav. 106440.

Markram, H., Toledo-Rodriguez, M., Wang, Y., Gupta, A., Silberberg, G., and Wu, C. (2004). Interneurons of the neocortical inhibitory system. Nat. Rev. Neurosci. *5*, 793–807.

Martin, B., Dieuset, G., Pawluski, J.L., Costet, N., and Biraben, A. (2020). Audiogenic seizure as a model of sudden death in epilepsy: A comparative study between four inbred mouse strains from early life to adulthood. Epilepsia *61*, 342–349.

Martin, M.S., Tang, B., Papale, L.A., Yu, F.H., Catterall, W.A., and Escayg, A. (2007). The voltage-gated sodium channel Scn8a is a genetic modifier of severe myoclonic epilepsy of infancy. Hum. Mol. Genet. *16*, 2892–2899.

Massey, C.A., Sowers, L.P., Dlouhy, B.J., and Richerson, G.B. (2014). Mechanisms of sudden unexpected death in epilepsy: The pathway to prevention. Nat. Rev. Neurol. *10*, 271–282.

Meisler, M.H., Helman, G., Hammer, M.F., Fureman, B.E., Gaillard, W.D., Goldin, A.L., Hirose, S., Ishii, A., Kroner,

B.L., Lossin, C., et al. (2016). SCN8A encephalopathy: Research progress and prospects. Epilepsia *57*, 1027–1035.

Millan, M.H., Meldrum, B.S., and Faingold, C.L. (1986). Induction of audiogenic seizure susceptibility by focal infusion of excitant amino acid or bicuculline into the inferior colliculus of normal rats. Exp. Neurol. *91*, 634–639.

Møller, R.S., Wuttke, T. V, Helbig, I., Marini, C., Johannesen, K.M., Brilstra, E.H., Vaher, U., Borggraefe, I., Talvik, I., Talvik, T., et al. (2017). Mutations in GABRB3 From febrile seizures to epileptic encephalopathies. Neurology *88*, 483–492.

Motiejunaite, J., Amar, L., and Vidal-Petiot, E. (2020). Adrenergic receptors and cardiovascular effects of catecholamines. Ann. Endocrinol. (Paris).

Nakase, K., Kollmar, R., Lazar, J., Arjomandi, H., Sundaram, K., Silverman, J., Orman, R., Weedon, J., Stefanov, D., Savoca, E., et al. (2016). Laryngospasm, central and obstructive apnea during seizures: Defining pathophysiology for sudden death in a rat model. Epilepsy Res. *128*, 126–139.

Nashef, L., So, E.L., Ryvlin, P., and Tomson, T. (2012). Unifying the definitions of sudden unexpected death in epilepsy. Epilepsia *53*, 227–233.

Del Negro, C.A., Koshiya, N., Butera, R.J., and Smith, J.C. (2002). Persistent sodium current, membrane properties and bursting behavior of pre-Bötzinger complex inspiratory neurons in vitro. J. Neurophysiol. *88*, 2242–2250.

Nguyen, H.M., and Goldin, A.L. (2010). Sodium Channel Carboxyl-terminal Residue Regulates Fast Inactivation. J. Biol. Chem. *285*, 9077–9089.

Nigro, M.J., Hashikawa-Yamasaki, Y., and Rudy, B. (2018). Diversity and Connectivity of Layer 5 Somatostatin-Expressing Interneurons in the Mouse Barrel Cortex. J. Neurosci. *38*, 1622.

Nilsson, L., Farahmand, B.Y., Persson, P.-G., Thiblin, I., and Tomson, T. (1999). Risk factors for sudden unexpected death in epilepsy: a case control study. Lancet *353*, 888–893.

Nobis, W.P., Otárula, K.A.G., Templer, J.W., Gerard, E.E., VanHaerents, S., Lane, G., Zhou, G., Rosenow, J.M., Zelano, C., and Schuele, S. (2019). The effect of seizure spread to the amygdala on respiration and onset of ictal central apnea. J. Neurosurg. JNS 1–11.

Nowacki, J., Osinga, H.M., and Tsaneva-Atanasova, K. (2012). Dynamical systems analysis of spike-adding mechanisms in transient bursts. J. Math. Neurosci. *2*, 7.

O'Brien, J.E., and Meisler, M.H. (2013). Sodium channel SCN8A (Nav1.6): properties and de novo mutations in epileptic encephalopathy and intellectual disability. Front. Genet. *4*.

Ohba, C., Kato, M., Takahashi, S., Lerman-Sagie, T., Lev, D., Terashima, H., Kubota, M., Kawawaki, H., Matsufuji, M., Kojima, Y., et al. (2014). Early onset epileptic encephalopathy caused by de novo SCN8A mutations. Epilepsia *55*, 994–1000.

Olesen, J. (1972). The effect of intracarotid epinephrine, norepinephrine, and angiotensin on the regional cerebral blood flow in man. Neurology *22*, 978–987.

Osorio, N., Cathala, L., Meisler, M.H., Crest, M., Magistretti, J., and Delmas, P. (2010). Persistent Nav1.6 current at axon initial segments tunes spike timing of cerebellar granule cells. J. Physiol. *588*, 651–670.

Otoom, S.A., and Alkadhi, K.A. (2000). Epileptiform activity of veratridine model in rat brain slices: Effects of antiepileptic drugs. Epilepsy Res. *38*, 161–170.

Otoom, S.A., Handu, S.S., Wazir, J.F., James, H., Sharma, P.R., Hasan, Z.A., and Sequeira, R.P. (2006). Veratridine-induced wet dog shake behaviour and apoptosis in rat hippocampus. Basic Clin. Pharmacol. Toxicol. *98*, 423–426.

Ottolini, M., Barker, B.S., Gaykema, R.P., Meisler, M.H., and Patel, M.K. (2017). Aberrant sodium channel currents and hyperexcitability of medial entorhinal cortex neurons in a mouse model of SCN8A encephalopathy. J. Neurosci. *37*, 7643–7655.

Pan, Y., and Cummins, T.R. (2020). Distinct functional alterations in SCN8A epilepsy mutant channels. J. Physiol. *598*, 381–401.

Parrish, R.R., Codadu, N.K., Mackenzie-Gray Scott, C., and Trevelyan, A.J. (2019). Feedforward inhibition ahead of ictal wavefronts is provided by both parvalbumin- and somatostatin-expressing interneurons. J. Physiol. *597*, 2297–2314.

Patel, R.R., Barbosa, C., Brustovetsky, T., Brustovetsky, N., and Cummins, T.R. (2016). Aberrant epilepsy-associated mutant Nav1.6 sodium channel activity can be targeted with cannabidiol. Brain *139*, 2164–2181.

Patodia, S., Somani, A., O'Hare, M., Venkateswaran, R., Liu, J., Michalak, Z., Ellis, M., Scheffer, I.E., Diehl, B., Sisodiya, S.M., et al. (2018). The ventrolateral medulla and medullary raphe in sudden unexpected death in epilepsy. Brain *141*, 1719–1733.

Paton, J.F.R., Abdala, A.P.L., Koizumi, H., Smith, J.C., and St-John, W.M. (2006). Respiratory rhythm generation during gasping depends on persistent sodium current. Nat. Neurosci. *9*, 311–313.

Potet, F., Vanoye, C.G., and George, A.L. (2016). Use-dependent block of human cardiac sodium channels by GS967. Mol. Pharmacol. *90*, 52–60.

Raman, I.M., and Bean, B.P. (1997). Resurgent sodium current and action potential formation in dissociated cerebellar Purkinje neurons. J. Neurosci. *17*, 4517–4526.

Raman, I.M., Sprunger, L.K., Meisler, M.H., and Bean, B.P. (1997). Altered subthreshold sodium currents and disrupted firing patterns in Purkinje neurons of Scn8a mutant mice. Neuron *19*, 881–891.

Reinson, K., Õiglane-Shlik, E., Talvik, I., Vaher, U., Õunapuu, A., Ennok, M., Teek, R., Pajusalu, S., Murumets, Ü., Tomberg, T., et al. (2016). Biallelic CACNA1A mutations cause early onset epileptic encephalopathy with progressive cerebral, cerebellar, and optic nerve atrophy. Am. J. Med. Genet. Part A *170*, 2173–2176.

Rhodes, T.H., Lossin, C., Vanoye, C.G., Wang, D.W., and George, A.L. (2004). Noninactivating voltage-gated sodium channels in severe myoclonic epilepsy of infancy. Proc. Natl. Acad. Sci. U. S. A. *101*, 11147–11152.

Ribak, C.E. (2017). An abnormal GABAergic system in the inferior colliculus provides a basis for audiogenic seizures in genetically epilepsy-prone rats. Epilepsy Behav. *71*, 160–164.

Richards, S., Aziz, N., Bale, S., Bick, D., Das, S., Gastier-Foster, J., Grody, W.W., Hegde, M., Lyon, E., Spector, E., et al. (2015). Standards and guidelines for the interpretation of sequence variants: a joint consensus recommendation of the American College of Medical Genetics and Genomics and the Association for Molecular Pathology. Genet. Med. *17*, 405–423.

Romettino, S., Lazdunski, M., and Gottesmann, C. (1991). ee ar. Eur. J. Pharmacol. *199*, 371–373.

Royeck, M., Horstmann, M.T., Remy, S., Reitze, M., Yaari, Y., and Beck, H. (2008). Role of axonal NaV1.6 sodium channels in action potential initiation of CA1 pyramidal neurons. J. Neurophysiol. *100*, 2361–2380.

Rudy, B., Fishell, G., Lee, S.H., and Hjerling-Leffler, J. (2011). Three groups of interneurons account for nearly 100% of neocortical GABAergic neurons. Dev. Neurobiol. *71*, 45–61.

Ryvlin, P., Nashef, L., Lhatoo, S.D., Bateman, L.M., Bird, J., Bleasel, A., Boon, P., Crespel, A., Dworetzky, B.A., Høgenhaven, H., et al. (2013). Incidence and mechanisms of cardiorespiratory arrests in epilepsy monitoring units (MORTEMUS): a retrospective study. Lancet Neurol. *12*, 966–977.

Sadleir, L.G., Mountier, E.I., Gill, D., Davis, S., Joshi, C., Devile, C., Kurian, M.A., Mandelstam, S., Wirrell, E., Nickels, K.C., et al. (2017). Not all SCN1A epileptic encephalopathies are Dravet syndrome. Neurology *89*, 1035–1042.

Safari, M.S., Mirnajafi-Zadeh, J., Hioki, H., and Tsumoto, T. (2017). Parvalbumin-expressing interneurons can act solo while somatostatin-expressing interneurons act in chorus in most cases on cortical pyramidal cells. Sci. Rep. *7*.

Salam, M.T., Montandon, G., Genov, R., Devinsky, O., Del Campo, M., and Carlen, P.L. (2017). Mortality with brainstem seizures from focal 4-aminopyridine–induced recurrent hippocampal seizures. Epilepsia *58*, 1637–1644.

Schaller, K.L., Krzemien, D.M., Yarowsky, P.J., Krueger, B.K., and Caldwell, J.H. (1995). A novel, abundant sodium channel expressed in neurons and glia. J. Neurosci. *15*, 3231.

Schultz, H.D., Li, Y.L., and Ding, Y. (2007). Arterial chemoreceptors and sympathetic nerve activity: Implications for hypertension and heart failure. Hypertension *50*, 6–13.

Schwindt, P.C., and Crill, W.E. (1995). Amplification of synaptic current by persistent sodium conductance in apical dendrite of neocortical neurons. J. Neurophysiol. *74*, 2220–2224.

Segal, M.M., and Douglas, A.F. (1997). Late Sodium Channel Openings Underlying Epileptiform Activity Are Preferentially Diminished by the Anticonvulsant Phenytoin. J. Neurophysiol. *77*, 3021–3034.

Sicouri, S., Belardinelli, L., and Antzelevitch, C. (2013). Antiarrhythmic effects of the highly selective late sodium channel current blocker GS-458967. Hear. Rhythm *10*, 1036–1043.

Silberberg, G., and Markram, H. (2007). Disynaptic Inhibition between Neocortical Pyramidal Cells Mediated by Martinotti Cells. Neuron *53*, 735–746.

Sintas, C., Carreño, O., Fernàndez-Castillo, N., Corominas, R., Vila Pueyo, M., Toma, C., Cuenca-León, E., Barroeta, I., Roig, C., Volpini, V., et al. (2017). Mutation Spectrum in the CACNA1A Gene in 49 Patients with Episodic Ataxia. Sci. Rep. *7*.

So, E.L., Sam, M.C., and Lagerlund, T.L. (2000). Postictal Central Apnea as a Cause of SUDEP: Evidence From Near-SUDEP Incident. Epilepsia *41*, 1494–1497.

Spadoni, F., Hainsworth, A.H., Mercuri, N.B., Caputi, L., Martella, G., Lavaroni, F., Bernardi, G., and Stefani, A. (2002). Lamotrigine derivatives and riluzole inhibit INa,P in cortical neurons. Neuroreport.

Sprissler, R.S., Wagnon, J.L., Bunton-Stasyshyn, R.K., Meisler, M.H., and Hammer, M.F. (2017). Altered gene expression profile in a mouse model of SCN8A encephalopathy. Exp. Neurol. *288*, 134–141.

Stafstrom, C.E. (2005). The Role of the Subiculum in Epilepsy and Epileptogenesis. Epilepsy Curr. *5*, 121–129.

Stafstrom, C.E. (2007). Persistent Sodium Current and Its Role in Epilepsy. Epilepsy Curr. *7*, 15–22.

Stafstrom, C.E. (2013). Jasper's Basic Mechanisms of the Epilepsies, 4th Edition. Neurology *81*, 1883–1884.

Stafstrom, C.E., Schwindt, P.C., and Crill, W.E. (1982). Negative slope conductance due to a persistent subthreshold sodium current in cat neocortical neurons in vitro. Brain Res. *236*, 221–226.

Stafstrom, C.E., Schwindt, P.C., Chubb, M.C., and Crill, W.E. (1985). Properties of persistent sodium conductance and calcium conductance of layer V neurons from cat sensorimotor cortex in vitro. J. Neurophysiol. *53*, 153–170.

Stuart, G. (1999). Voltage-activated sodium channels amplify inhibition in neocortical pyramidal neurons. Nat. Neurosci. *2*, 144–150.

Stuart, G., and Sakmann, B. (1995). Amplification of EPSPs by axosomatic sodium channels in neocortical pyramidal neurons. Neuron *15*, 1065–1076.

Su, H., Alroy, G., Kirson, E.D., and Yaari, Y. (2001). Extracellular Calcium Modulates Persistent Sodium Current-Dependent Burst-Firing in Hippocampal Pyramidal Neurons. J. Neurosci. *21*, 4173.

Suita, K., Fujita, T., Hasegawa, N., Cai, W., Jin, H., Hidaka, Y., Prajapati, R., Umemura, M., Yokoyama, U., Sato, M., et al. (2015). Norepinephrine-Induced Adrenergic Activation Strikingly Increased the Atrial Fibrillation Duration through β1- and α1-Adrenergic Receptor-Mediated Signaling in Mice. PLoS One *10*, e0133664-.

Sun, G.C., Werkman, T.R., Battefeld, A., Clare, J.J., and Wadman, W.J. (2007). Carbamazepine and topiramate modulation of transient and persistent sodium currents studied in HEK293 cells expressing the Nav1.3 α-subunit. Epilepsia *48*, 774–782.

Swadlow, H.A. (2003). Fast-spike Interneurons and Feedforward Inhibition in Awake Sensory Neocortex. Cereb. Cortex *13*, 25–32.

Tai, C., Abe, Y., Westenbroek, R.E., Scheuer, T., and Catterall, W.A. (2014). Impaired excitability of somatostatin- and parvalbumin-expressing cortical interneurons in a mouse model of Dravet syndrome. Proc. Natl. Acad. Sci. U. S. A. *111*.

Tazerart, S., Vinay, L., and Brocard, F. (2008). The persistent sodium current generates pacemaker activities in the central pattern generator for locomotion and regulates the locomotor rhythm. J. Neurosci. *28*, 8577–8589.

Toyoda, I., Bower, M.R., Leyva, F., and Buckmaster, P.S. (2013). Early Activation of Ventral Hippocampus and Subiculum during Spontaneous Seizures in a Rat Model of Temporal Lobe Epilepsy. J. Neurosci. *33*, 11100.

Trudeau, M.M., Dalton, J.C., Day, J.W., Ranum, L.P.W., and Meisler, M.H. (2006). Heterozygosity for a protein truncation mutation of sodium channel SCN8A in a patient with cerebellar atrophy, ataxia, and mental retardation. J. Med. Genet. *43*, 527–530.

Tryba, A.K., Kaczorowski, C.C., Ben-Mabrouk, F., Elsen, F.P., Lew, S.M., and Marcuccilli, C.J. (2011). Rhythmic intrinsic bursting neurons in human neocortex obtained from pediatric patients with epilepsy. Eur. J. Neurosci. *34*.

Tsuruyama, K., Hsiao, C.F., and Chandler, S.H. (2013). Participation of a persistent sodium current and calcium-activated nonspecific cationic current to burst generation in trigeminal principal sensory neurons. J. Neurophysiol. *110*, 1903–1914.

Ullah, G., and Schiff, S.J. (2010). Assimilating seizure dynamics. PLoS Comput. Biol. *6*, 1–12.

Urbani, A., and Belluzzi, O. (2000). Riluzole inhibits the persistent sodium current in mammalian CNS neurons. Eur. J. Neurosci. *12*, 3567–3574.

Veeramah, K.R., O'Brien, J.E., Meisler, M.H., Cheng, X., Dib-Hajj, S.D., Waxman, S.G., Talwar, D., Girirajan, S., Eichler, E.E., Restifo, L.L., et al. (2012). De novo pathogenic SCN8A mutation identified by whole-genome sequencing of a family quartet affected by infantile epileptic encephalopathy and SUDEP. Am. J. Hum. Genet. *90*, 502–510.

Vervaeke, K., Hu, H., Graham, L.J., and Storm, J.F. (2006). Contrasting effects of the persistent Na+ current on neuronal excitability and spike timing. Neuron *49*, 257–270.

Vilella, L., Lacuey, N., Hampson, J.P., Rani, M.R.S., Loparo, K., Sainju, R.K., Friedman, D., Nei, M., Strohl, K., Allen, L., et al. (2019a). Incidence, Recurrence, and Risk Factors for Peri-ictal Central Apnea and Sudden Unexpected Death in Epilepsy. Front. Neurol. *10*, 166.

Vilella, L., Lacuey, N., Hampson, J.P., Rani, M.R.S., Sainju, R.K., Friedman, D., Nei, M., Strohl, K., Scott, C., Gehlbach, B.K., et al. (2019b). Postconvulsive central apnea as a biomarker for sudden unexpected death in epilepsy (SUDEP). Neurology *92*, E171–E182.

Villiere, S.M., Nakase, K., Kollmar, R., Silverman, J., Sundaram, K., and Stewart, M. (2017). Seizure-associated central apnea in a rat model: Evidence for resetting the respiratory rhythm and activation of the diving reflex. Neurobiol. Dis. *101*, 8–15.

Vreugdenhil, M., Hoogland, G., Van Veelen, C.W.M., and Wadman, W.J. (2004). Persistent sodium current in subicular neurons isolated from patients with temporal lobe epilepsy. Eur. J. Neurosci. *19*, 2769–2778.

Wada, J.A., Terao, A., White, B., and Jung, E. (1970). Inferior colliculus lesion and audiogenic seizure susceptibility. Exp. Neurol. *28*, 326–332.

Wagnon, J.L., and Meisler, M.H. (2015). Recurrent and non-recurrent mutations of SCN8A in epileptic encephalopathy. Front. Neurol. *6*.

Wagnon, J.L., Korn, M.J., Parent, R., Tarpey, T.A., Jones, J.M., Hammer, M.F., Murphy, G.G., Parent, J.M., and Meisler, M.H. (2015). Convulsive seizures and SUDEP in a mouse model of SCN8A epileptic encephalopathy. Hum. Mol. Genet. *24*, 506–515.

Wagnon, J.L., Barker, B.S., Hounshell, J.A., Haaxma, C.A., Shealy, A., Moss, T., Parikh, S., Messer, R.D., Patel, M.K., and Meisler, M.H. (2016). Pathogenic mechanism of recurrent mutations of SCN8A in epileptic encephalopathy. Ann. Clin. Transl. Neurol. *3*, 114–123.

Wagnon, J.L., Barker, B.S., Ottolini, M., Park, Y., Volkheimer, A., Valdez, P., Swinkels, M.E., Patel, M.K., and Meisler,

M.H. (2017a). Loss-of-function variants of SCN8A in intellectual disability without seizures. Neurol. Genet. *3*.

Wagnon, J.L., Barker, B.S., Ottolini, M., Park, Y., Volkheimer, A., Valdez, P., Swinkels, M.E.M., Patel, M.K., and Meisler, M.H. (2017b). Loss-of-function variants of SCN8A in intellectual disability without seizures. Neurol. Genet. *3*, e170–e170.

Wagnon, J.L., Mencacci, N.E., Barker, B.S., Wengert, E.R., Bhatia, K.P., Balint, B., Carecchio, M., Wood, N.W., Patel, M.K., and Meisler, M.H. (2018). Partial loss-of-function of sodium channel SCN8A in familial isolated myoclonus. Hum. Mutat. *39*, 965–969.

Weissbrod, P., Pitman, M.J., Sharma, S., Bender, A., and Schaefer, S.D. (2011). Quantity and Three-Dimensional Position of the Recurrent and Superior Laryngeal Nerve Lower Motor Neurons in a Rat Model. Ann. Otol. Rhinol. Laryngol. *120*, 761–768.

Wellmer, J., Su, H., Beck, H., and Yaari, Y. (2002). Long-lasting modification of intrinsic discharge properties in subicular neurons following status epilepticus. Eur. J. Neurosci. *16*, 259–266.

Wengert, E.R., and Patel, M.K. (2021). The Role of the Persistent Sodium Current in Epilepsy. Epilepsy Curr. *21*, 40–47.

Wengert, E.R., Tronhjem, C.E., Wagnon, J.L., Johannesen, K.M., Petit, H., Krey, I., Saga, A.U., Panchal, P.S., Strohm, S.M., Lange, J., et al. (2019a). Biallelic inherited SCN8A variants, a rare cause of SCN8A-related developmental and epileptic encephalopathy. Epilepsia *60*, 2277–2285.

Wengert, E.R., Saga, A.U., Panchal, P.S., Barker, B.S., and Patel, M.K. (2019b). Prax330 reduces persistent and resurgent sodium channel currents and neuronal hyperexcitability of subiculum neurons in a mouse model of SCN8A epileptic encephalopathy. Neuropharmacology *158*, 107699.

Whelan, R.F., and Young, I.M. (1953). The effect of adrenaline and noradrenaline infusions on respiration in man. Br. J. Pharmacol. Chemother. *8*, 98–102.

Willott, J.F., and Bross, L.S. (1996). Morphological changes in the anteroventral cochlear nucleus that accompany sensorineural hearing loss in DBA/2J and C57BL/6J mice. Dev. Brain Res. *91*, 218–226.

Willott, J.F., Erway, L.C., Archer, J.R., and Harrison, D.E. (1995). Genetics of age-related hearing loss in mice. II. Strain differences and effects of caloric restriction on cochlear pathology and evoked response thresholds. Hear. Res. *88*, 143–155.

Wolff, M., Johannesen, K.M., Hedrich, U.B.S., Masnada, S., Rubboli, G., Gardella, E., Lesca, G., Ville, D., Milh, M., Villard, L., et al. (2017). Genetic and phenotypic heterogeneity suggest therapeutic implications in SCN2A-related disorders. Brain *140*, 1316–1336.

Wyllie, E. (2015). Wyllie's Treatment of Epilepsy (Wolters Kluwer).

Yamada-Hanff, J., and Bean, B.P. (2013). Persistent sodium current drives conditional pacemaking in CA1 pyramidal neurons under muscarinic stimulation. J. Neurosci. *33*, 15011–15021.

Yamanishi, T., Koizumi, H., Navarro, M.A., Milescu, L.S., and Smith, J.C. (2018). Kinetic properties of persistent Na+ current orchestrate oscillatory bursting in respiratory neurons. J. Gen. Physiol. *150*, 1523–1540.

Yarov-Yarovoy, V., DeCaen, P.G., Westenbroek, R.E., Pan, C.Y., Scheuer, T., Baker, D., and Catterall, W.A. (2012). Structural basis for gating charge movement in the voltage sensor of a sodium channel. Proc. Natl. Acad. Sci. U. S. A. *109*.

Yavorska, I., and Wehr, M. (2016). Somatostatin-Expressing Inhibitory Interneurons in Cortical Circuits. Front. Neural Circuits *10*, 76.

Zaman, T., Helbig, I., Božović, I.B., DeBrosse, S.D., Bergqvist, A.C., Wallis, K., Medne, L., Maver, A., Peterlin, B., Helbig, K.L., et al. (2018). Mutations in SCN3A cause early infantile epileptic encephalopathy. Ann. Neurol. *83*, 703–717.

Zaman, T., Abou Tayoun, A., and Goldberg, E.M. (2019). A single-center SCN8A-related epilepsy cohort: clinical,

genetic, and physiologic characterization. Ann. Clin. Transl. Neurol. *6*, 1445–1455.

Zanelli, S., Goodkin, H.P., Kowalski, S., and Kapur, J. (2014). Impact of transient acute hypoxia on the developing mouse EEG. Neurobiol. Dis. *68*, 37–46.

Zeng, C., Long, X., Cotten, J.F., Forman, S.A., Solt, K., Faingold, C.L., and Feng, H.J. (2015). Fluoxetine prevents respiratory arrest without enhancing ventilation in DBA/1 mice. Epilepsy Behav. *45*, 1–7.

Zhan, Q., Buchanan, G.F., Motelow, J.E., Andrews, J., Vitkovskiy, P., Chen, W.C., Serout, F., Gummadavelli, A., Kundishora, A., Furman, M., et al. (2016). Impaired serotonergic brainstem function during and after seizures. J. Neurosci. *36*, 2711–2722.

Zhang, H., Zhao, H., and Feng, H.-J. (2017). Atomoxetine, a norepinephrine reuptake inhibitor, reduces seizure-induced respiratory arrest. Epilepsy Behav. *73*, 6–9.

Zhang, H., Zhao, H., Zeng, C., Van Dort, C., Faingold, C.L., Taylor, N.E., Solt, K., and Feng, H.-J. (2018). Optogenetic activation of 5-HT neurons in the dorsal raphe suppresses seizure-induced respiratory arrest and produces anticonvulsant effect in the DBA/1 mouse SUDEP model. Neurobiol. Dis. *110*, 47–58.

Zhao, H., Cotten, J.F., Long, X., and Feng, H.J. (2017). The effect of atomoxetine, a selective norepinephrine reuptake inhibitor, on respiratory arrest and cardiorespiratory function in the DBA/1 mouse model of SUDEP. Epilepsy Res. *137*, 139–144.

Zhong, G., Masino, M.A., and Harris-Warrick, R.M. (2007). Persistent sodium currents participate in fictive locomotion generation in neonatal mouse spinal cord. J. Neurosci. *27*, 4507–4518.

Ziburkus, J., Cressman, J.R., Barreto, E., and Schiff, S.J. (2006). Interneuron and pyramidal cell interplay during in vitro seizure-like events. J. Neurophysiol. *95*, 3948–3954.

Appendix: Notes on Figures/Tables

Chapter I: Figure 1.1 was created by me and is unpublished.

Chapter II: All figures and tables were adapted from (Wengert et al., 2019a). Data provided includes patient descriptions collected by co-authors.

Chapter III: All figures and tables were adapted from (Wengert et al., 2019b) and (Baker et al., 2018). I contributed experimental data to each of the figures with the exception of the results shown in Figure 3.9 which were collected by my coauthors.

Chapter IV: All figures were adapted from (Wengert et al., 2021 *in press*). Each of the figures include data that was collected by me and my coauthors.

Chapter V: All figures were adapted from (Bunton-Stasyshyn et al., 2019) with the exception of Figure 5.4 which was created by me from my own data (unpublished). I contributed experimental data to each of the figures shown with the exception of Figure 5.1 and Figure 5.3 which were collected by our collaborators/coauthors. My own unpublished data support the results shown in Figure 5.1 that *Scn8a*$^{cond/+}$, EIIa-Cre and *Scn8a*$^{cond/+}$, Emx1-Cre mice exhibit seizures and premature sudden death, but I have not independently replicated the results shown using *Scn8a*$^{cond/+}$, Gad2-Cre; *Scn8a*$^{cond/+}$, Dlx5a-Cre; or *Scn8a*$^{cond/+}$, Nestin-Cre mice.

Chapter VI: All figures were adapted from a manuscript of which I am the sole lead author that is currently in peer-review, but is available on biorxiv: https://www.biorxiv.org/content/10.1101/2021.02.05.429987v1. Each of the figures include data that were collected by me and my coauthors.